MULTIDISCIPLINARY DESIGN OPTIMIZATION OF STAMPED AND WELDED STRUCTURES

by

Michael Mang,
B. Eng (Aerospace Engineering),
Ryerson University,
Toronto, Ontario, Canada, 2004

A Thesis Presented to
Ryerson University
In partial fulfillment of the
Requirements for the degree of
Master of Applied Science
In the Program of
Mechanical Engineering

Toronto, Ontario, Canada, 2006

Author's Declaration

I hereby declare that I am the sole author of this thesis.

I authorize Ryerson University to lend this thesis to other institutions or individuals for the purpose of scholarly research.

I further authorize Ryerson University to reproduce this thesis by photocopying or by other means, in total or in part, at the request of other institutions or individuals for the purpose of scholarly research.

MULTIDISCIPLINARY DESIGN OPTIMIZATION OF STAMPED AND WELD STRUCTURES

Michael Mang
Master of Applied Science
Department of Mechanical Engineering
Ryerson University
Toronto, 2006

Abstract

Multidisciplinary design optimization (MDO) is very useful in present day engineering. The aim of this thesis is to develop and utilize an MDO procedure that can be applied to stamped and welded structures. This procedure involves new techniques such as material selection, weld constraint, and cost optimizations. The MDO is developed through five design iterations starting with a simple finite element model. As more techniques are added, the procedure progresses towards using a real life radiator support structure in a static loading case. Three trials were completed to optimize the cost of the structure; the final result is that the total cost was minimized by 20%. The MDO procedure was also applied to a real life wheel chair ramp model from a modified minivan. This structure was subject to a rear crash situation and the total mass, after the procedure was applied, was reduced by 19%.

Acknowledgements

I would like to thank my supervisor Dr. Kamran Behdinan, and co-supervisor Dr. Zouheir Fawaz for their continuous help throughout the course of my degree.

I would like to thank the OCE/MMO (Materials and Manufacturing Ontario) who provided the funding for this project.

I would also like to thank Van-Rob Stampings Inc. and Dr. Kornel Farkas for their time and the use of their facilities.

Special thanks are extended to those of the Ryerson University administration, specifically: Mr. Gerald Bootes, Ms. Kim Gallo, and Ms. Leah Stanwyck.

Also, very special thanks are extended to Mr. Sacheen Bekah of Van-Rob.

Finally, I would like to thank my parents, family, and girlfriend for all the help that they have given me over the last many years.

Table of Contents

List of Tables

List of Figures

List of Appendices

Nomenclature

$A_{rear,ramp}$ – rear area of the wheel chair ramp

$A_{rear,van}$ – rear area of the van

CO – collaborative optimization

E – Young's Modulus

F – vector of objective functions

FEM – finite element method

F_w – force exerted on the wall by the van

f_m – an objective function

f_{ext} – external force vector

f_{int} – internal force vector

g – any constraint in an optimization

HDD – hard dish drive

k^e – element stiffness matrix

k^0 – global stiffness matrix

LAN – local area network

M – mass matrix

MDF – multidisciplinary feasible

MDO – multidisciplinary design optimization

$NGST$ – next generation space telescope

NVH – noise, vibration, and harshness

p – penalty factor

P_i – initial momentum of the wall

P_f – final momentum of the wall

th_i – gauge thickness of component i

$\ddot{u}$ – nodal acceleration vector

X – vector of design variables

x_n – a design variable

x^e – fraction of total density

Ω – a design domain

υ – Poisson's Ratio

ρ^0 – density of a material

ρ^e – the relative density of an element

σ_{max} – component maximum stress

σ_{yield} – material yield strength

Chapter 1

Introduction

1.1 Introduction

Between 1970 and 1990, engineering design saw some major changes occurring with the introduction of computer-aided design (CAD). Designers could now make changes to their designs almost instantly compared to before, and they could also analyze their new design quicker and with far better accuracy [1]. Within the aerospace domain, computer models of manufacturability, cost, maintainability and other life cycle functions could now be added to the early design stages of an aircraft. These functions were usually done after the plane design was finalized. Eventually, all these disciplines were able to be integrated into a design optimization procedure called Multidisciplinary Design Optimization (MDO).

In Barthelemy et al. [2], MDO is defined as: *a methodology for the design of complex engineering systems and subsystems that coherently exploits the synergism of mutually interacting phenomenon.* This provides the engineer with a collection of tools and methods that allow him/her to perform trade-offs between the different disciplines involved in the design process. Another definition from Pan et al. [3] includes the human aspect of design: *MDO is a methodology where the interaction of several disciplines is considered and the designer is free to affect system performance significantly.* Both of these definitions are valid; however, the inclusion of the human aspect in the latter is very important. MDO is not a push button design procedure, the human interface is important to enable the engineer to control the process and inject their judgment and creativity into

it [4]. Design viewed as decision making implies the need to plan the decision making process; this is called meta-design [5].

Every system that is designed is different, whether it is for aerospace or automotive, there are always different constraints that need to be met, as well as different costs and standards. There are also different disciplines to consider, different manufacturing needs, and also different economical and life issues. All this must be taken into account during the meta-design phase. Although each system may be different in terms of disciplines, it is almost a given that the diverse disciplines and design parameters are coupled into a closed loop numerical procedure where the engineer is a part of that loop [6]. MDO has made optimization faster, cheaper, and more reliable; and progress in optimization in the last thirty years has been enormous.

1.2 MDO in the Aerospace Industry

As was mentioned above, the aerospace industry played a major part in advancing MDO and bringing it to where it is today on a global scale. There are many studies on the uses of MDO in the aerospace industry [8 – 15]. The next few paragraphs briefly explain some of these real life examples.

In Chattopadyay et al. [7], the MDO of a gas cooled turbine blade is investigated. This optimization includes various disciplines such as aerodynamics, aeroelasticity, thermodynamics, and heat transfer. In this study, they were able to improve the efficiency of the blade by changing the geometry of the blade and cooling areas to meet all the constraints set forth by the many disciplines involved.

In Wakayama et al. [8], a blended wing body optimization is examined. This optimization includes everything about a plane from the shape up to the mission, fuel/payload, and even trim schedule. There are 134 design variables, and 20 design flight conditions. Tarzanin et al. [9] describes the optimization of how to reduce helicopter blade hub forces. In Radovcich et al. [10], the structural and aeroelastic components of an F-22 are redesigned using MDO. The objective was to reduce the weight of the aircraft after all the safety margins, flutter margins, and fatigue life requirements were already set. Some disciplines included were geometry, loads, stiffness, and flight control laws. In Love [11], the F-16 was also redesigned to be more agile using MDO practices. This process was done in two steps, first the wing planform was selected and tested at 6 discrete design points, then the twist and camber distribution in the second step tested at the same points. A ranking table was used to select the best design. Furthermore, the F/A-18 was also redesigned by use of MDO in Anderson et al [12]. The plane was extended to include missions that were not originally intended to be flown by the F/A-18. Some of these include fighter mission (range – minimize weight), strike mission (maximize payload), survivability and others. Another study by Fineegan et al. [13] includes the MDA (Multidisciplinary Design Analysis) of a turbine engine MDO process. It discusses the meta-design of the turbine optimization process.

Adimurthy [7] discusses MDO and space applications. MDO is used for launch vehicle trajectory optimization, orbit determination, and lunar and interplanetary mission design. Some disciplines such as the life and economics of the missions are mathematical models, as opposed to the previous examples which are based on the fundamentals of engineering (fluids, mechanics of material, dynamics and so on). In

Fitzgerald et al. [14] another application of MDO to space is investigated; it is the design of the NGST (Next Generation Space Telescope). There are five main parts to the design of the NGST: 1) Optical Telescope Assembly, 2) Science module (instruments), 3) Spacecraft systems (power, propulsion, and vibrations), 4) Operations Systems (ground systems, data handling) and 5) Systems Engineering. This is one of the most complicated MDO procedures because each of the five parts has their own design variables and objective. However, all the parts must work together for the NGST to be a success.

As can be seen, MDO plays an important role in the design of aerospace systems.

1.3 MDO in the Automotive Industry

The use of MDO in the automotive industry began in the late 1980's after it was proven to work magnificently in the aerospace industry. However, the uses in the automotive industry are not as widespread as in the aerospace industry. One of the main objectives is to always try and reduce the weight of the vehicle. But some of the most important objectives have to do with crash analysis and meeting government standards, while reducing mass. These analyses can include front and side impact, roof crush, interior head impact, rear impact, and rollover [15].

There are many studies which describe the MDO of an automobile [17 – 18]. Sometimes the optimization is of just one component of the car. In Marklund et al. [16], the car component being optimized is subject to a side impact. The B-pillar of a SAAB 9^5 is chosen as an example. A full car model is used, as well as many design variables for the pillar. In the end, the pillar's mass can be reduced by 25% without compromising the crashworthiness of the entire vehicle.

Furthermore, in Craig et al. [17] crashworthiness, as well as the inclusion of noise, vibration, and harshness testing (NVH) is included. NVH refers to the testing of the noises that the vehicle makes, the vibrations the driver and passengers feel in different situations, and the effect or harshness that this has upon them. Vehicle with low grade NVH will usually get a reputation for being poorly made. The main objective was again to reduce the mass while keeping the original crashworthiness of the car. A full car model was used and a full frontal crash into a wall was simulated. Some disciplines that were included are: structural, NVH, and crush energies. Many components were used as design variables and the final mass of the car was reduced by 4.7%. This will obviously benefit the design of the car making it lighter, and cheaper.

1.4 How MDO is Implemented

One way that MDO is implemented is a centralized format, and the simplest centralized version is using one computer. In this investigation, the MDO is implemented using this format, and the optimizations of the radiator support are run on a UNIX based HP platform that has dual Intel Itanium processors that are 64-bit. The optimization of the wheel chair ramp is run in the Ryerson Advanced Computation Lab on a Sun Microsystems PC which has a single 500 MHz 64-bit processor. For both situations, massive amounts of memory are needed to store the results. Some researchers use more powerful PC's that have 256 processors and are able to run many different versions of the same MDO process at once (21 executions, each using 12 processors) [18]. This is called parallel processing and it maximizes the gathering of results for the engineer. Some experts anticipate as many as 512 processors in one massive machine in

the near future. However, the key problem is to understand how to set up the optimizations to take advantage of this super processing speed [5].

A second way to have a centralized optimization is to have many computers working on the same problem connected by a local area network (LAN) [19]. This would be the most cost effective way for a company that can not afford a super computer to achieve fast computing speeds.

The last way to implement an optimization is to decentralize it. Globalization has connected us to the rest of the world in a way that has never before been seen. Companies today span many countries and even several continents. However, by way of the internet, all parties can work on the same MDO and design process at the same time [19]. Computing power can still be shared just like in the above LAN case; it is just that the computers may be several thousand kilometers away from each other!

Future advances in the field of MDO lie in a code developed by General Electric, Engineous [20]. This code uses numerical methods along with artificial intelligence (AI). However, it does not eliminate the user. It actively engages the user into the process, so he/she is able to monitor how the design is progressing.

1.5 Motivation and Contribution

The motivation behind this thesis is to make the engineer's job simpler, and more efficient. By combining various important optimization techniques into one procedure, the engineer can create a design that saves money and meets constraints in a shorter amount of time - this also saves money.

The contribution from this thesis is an MDO procedure that can be applied to any stamped and welded structure. A procedure is developed and applied to a radiator support structure from an automobile. Furthermore, the developed procedure is applied to another welded structure, namely a wheel chair ramp. The solution procedure for the radiator support involves linear finite element method (FEM) stress analysis using MSC-NASTRAN [21], and the non-linear crash situation involving the wheel chair ramp is inspected using LS-DYNA [22].

1.6 Upcoming Chapters

Chapter 2 will discuss the theory behind MDO, and some of the techniques, such as topology and size optimization, that are used in this thesis. Also, Chapter 3 begins the iterative process of the meta-design of the MDO procedure that is developed. In this chapter, smaller models are used to understand and develop the techniques that are used in the MDO procedure. In Chapter 4, these techniques are applied to a larger model of a radiator support structure. The optimization problems are explained, formulated, and the results are discussed. The MDO procedure is finalized in Chapter 4. Furthermore in Chapter 5, the MDO procedure is applied to a wheel chair ramp rear crash situation. Again, the problem and results are discussed. Chapter 6 discusses what can be added to this MDO procedure in the future and how it might be done. Chapter 6 also includes a conclusion of the entire thesis.

Chapter 2

Thesis Background Theory

2.1 MDO Theory

In Osyczka [23] MDO is defined as the process of finding a vector of design variables that satisfies the constraints and gives optimal values to all objective functions. Mathematically this can be defined as a vector, X, of design variables, x_n:

$$X = [x_1, x_2, ..., x_n]^T \tag{2.1}$$

These design variables have to optimize the objective function(s), f_m, which can also be represented by a vector F:

$$F(X) = [f_1(x), f_2(x), ..., f_m(x)] \tag{2.2}$$

The design variables are subject to l inequality constraints:

$$\begin{aligned} &\pm g_i(x_1, x_2, ..., x_n) \leq 0 \\ &i = 1, ..., e \end{aligned} \tag{2.3}$$

where g is any constraint; this is a very general optimization problem layout [24]. It assumes that there is more than one objective function $f_m(x)$ and e inequality constraints. The objective functions can either be minimized or maximized.

MDO is a methodology for the design of complex engineering systems that coherently exploits the synergism of mutually interacting phenomenon [2]. There are many different methods when dealing with MDO.

One conventional approach is multidisciplinary feasible (MDF), also called fully integrated optimization (FIO) [25]. This is the standard approach to MDO where all the

disciplines are evaluated simultaneously in one integrated objective function and constraint set. Some disciplines that might be included are topology, topography; size, shape, and cost optimization (see Figure 2.1a).

Another approach is structural decomposition, or a hierarchical approach called collaborative optimization (CO). CO is suited for problems where the degree of interdisciplinary coupling is small and the number of discipline specific constraints is large [26]. For this approach, a complex problem is divided along disciplinary or other user-defined boundaries, into a series of sub-problems [27]. By decomposing a large design problem into smaller problems, efficiency is increased [28]. Each sub-problem is solved following an organized structure. Figure 2.1b shows an example of the CO approach to MDO.

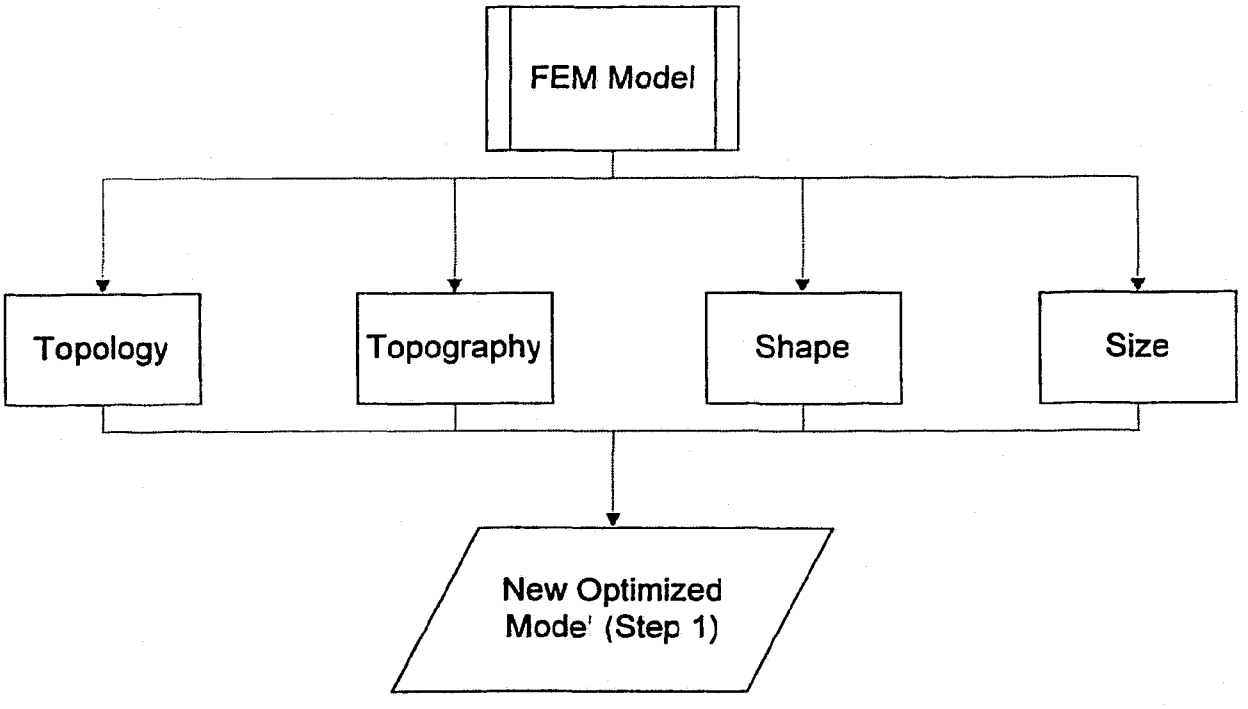

Figure 2.1a - MDF Approach to MDO

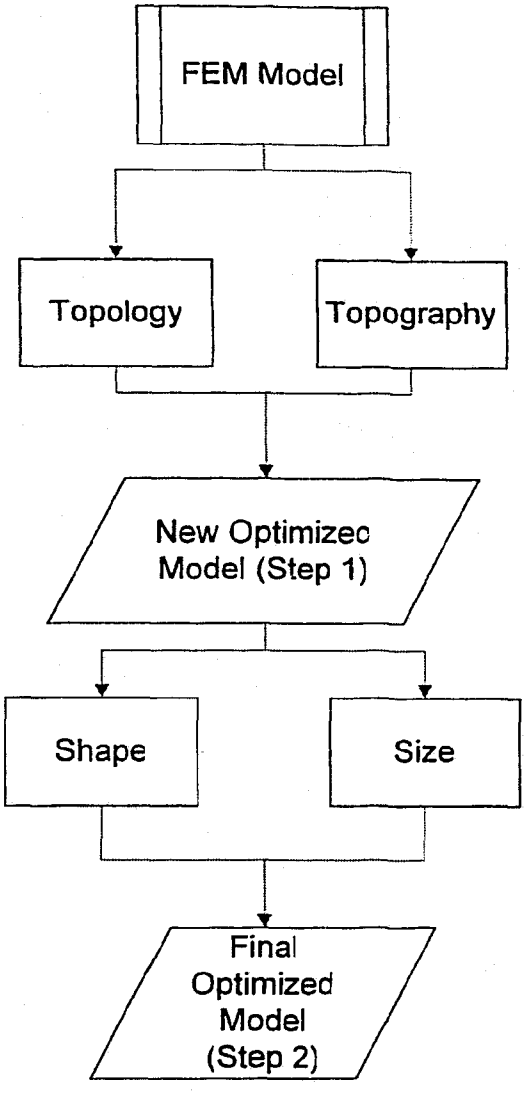

Figure 2.1b - CO Approach to MDO

2.2 Structural Optimization

There are a number of different types of structural optimization used in this thesis. Some techniques used actually alter the model's structure and elements. Topography optimization is used on shell structures to change the topography of the piece being optimized to meet the constraints. Size optimization changes the gauge thickness of shell elements to optimize the model. Shape optimization can be applied to 2D or 3D elements, because it moves the outer boundaries of the model to make a new shape that

meets the set constraints. Finally, topology optimization changes the elements' densities to try and optimize 2D or 3D models.

2.3 Topography Optimization

Topography optimization is a special application of shape optimization that allows the design of stamped beads in shell structures [29]. Shell components are usually stamped out from pieces of sheet metal. Furthermore, these structures are always modeled with shell elements; therefore topography, optimization can be applied to shell elements only. To stiffen components, ribs or grooves can be added at different areas to yield different results. Topography optimization helps the user decide where and what the properties of these beads (the grooves or ribs) are. The approach is the same used in topology optimization, except that the design variable is the shape of the model, and not the density [30]. The program uses the stress pattern that is present from all the loads and boundary conditions along with bead parameters to meet the objective function. This optimization creates bead patterns that are within the boundaries specified by the user. The user is able to specify the minimum width of the bead pattern, the height, and the draw angle. The draw angle is the maximum angle that the slope between the top and the base of the bead can be. By defining different values for these bead parameters the user can end up with many designs that meet or exceed their expectations.

2.3.1 Topography Optimization Example

The following is a brief example that demonstrates topography optimization. The purpose of the example is to mimic the results seen in a topography optimization study from Kilian et al [31]. In the paper the optimization of the suspension of a computer hard disk drive is executed, the suspension before optimization can be seen in Figure 2.2 [31].

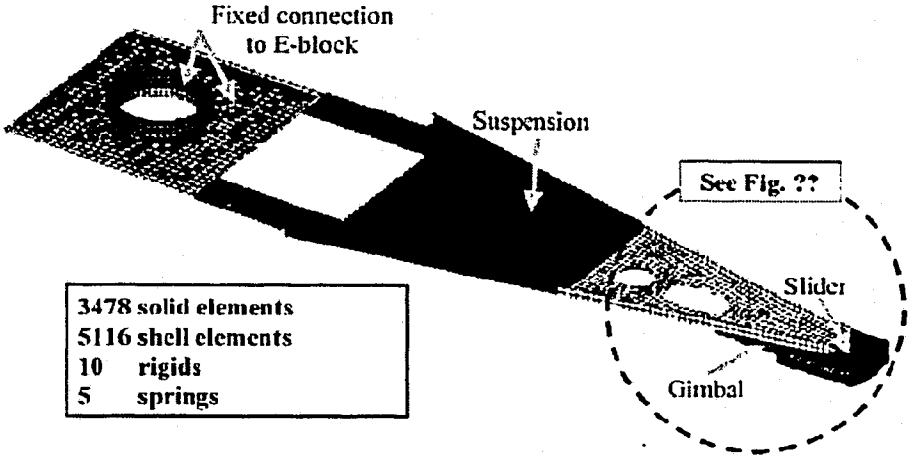

Figure 2.2 - HDD Suspension before Optimization [31]

The design area includes the dark part marked suspension, and the area inside the circle. The objective is to maximize the 2nd torsion mode. This leads to the familiar X-pattern seen in Figure 2.3.

The example tries to mimic this result by maximizing the 2nd torsion mode of a wedge-shaped shell structure that can be seen in Figure 2.4. The wedge shape was created using Altair HyperMesh and optimized using Altair Optistruct [32]. The red elements are part of the non-design component of the wedge which will not be modified during the optimization. All the blue elements are part of the design area and may be modified as needed. The exact dimensions and material properties of the HDD

suspension were not known, that is why the example aims to only mimic the resulting bead pattern, and not the exact frequency results.

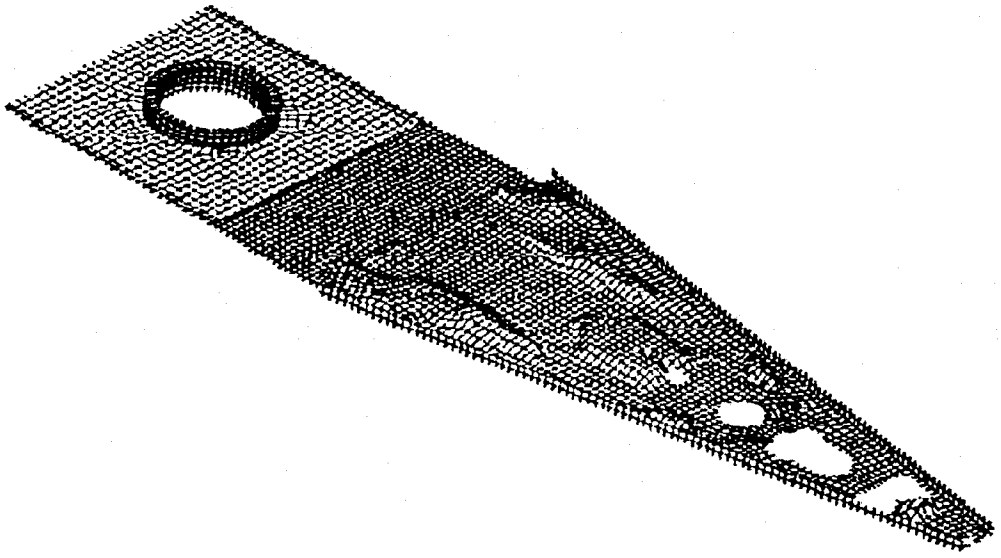

Figure 2.3 - Topography Optimization Results of HDD Suspension

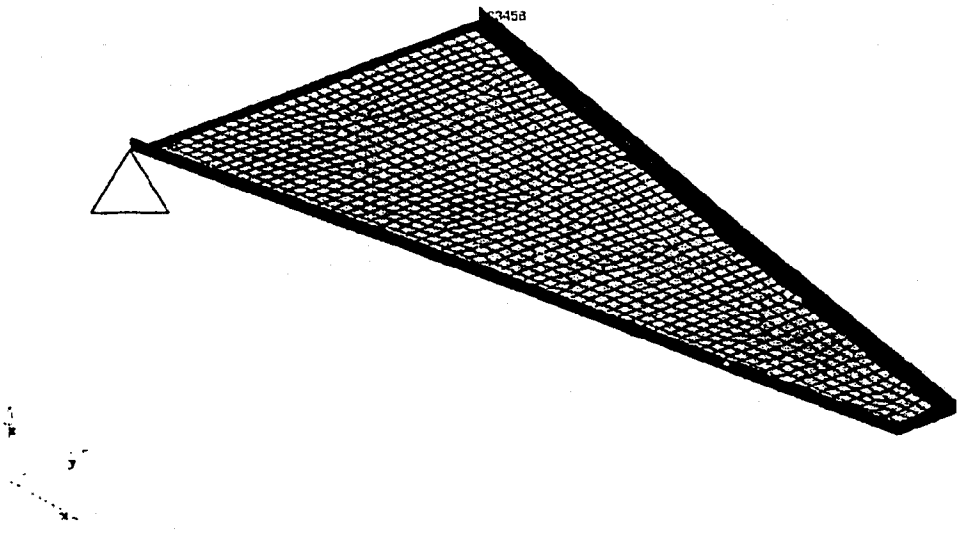

Figure 2.4 - Wedge Shaped Shell Structure before Optimization

The optimization took 15 iterations and successfully raised the 2nd torsion mode of the structure from 58 Hz to 148 Hz. Also, the familiar X pattern as can be seen in Figure 2.5 quite clearly. The X pattern occurs when a shell structure is being stiffened

[31]. The colour of the elements indicates the height that the beads have protruded up from the surface of the wedge. As has been proven, X-shaped corrugations are the most effective protrusions in case high torsion stiffness is needed.

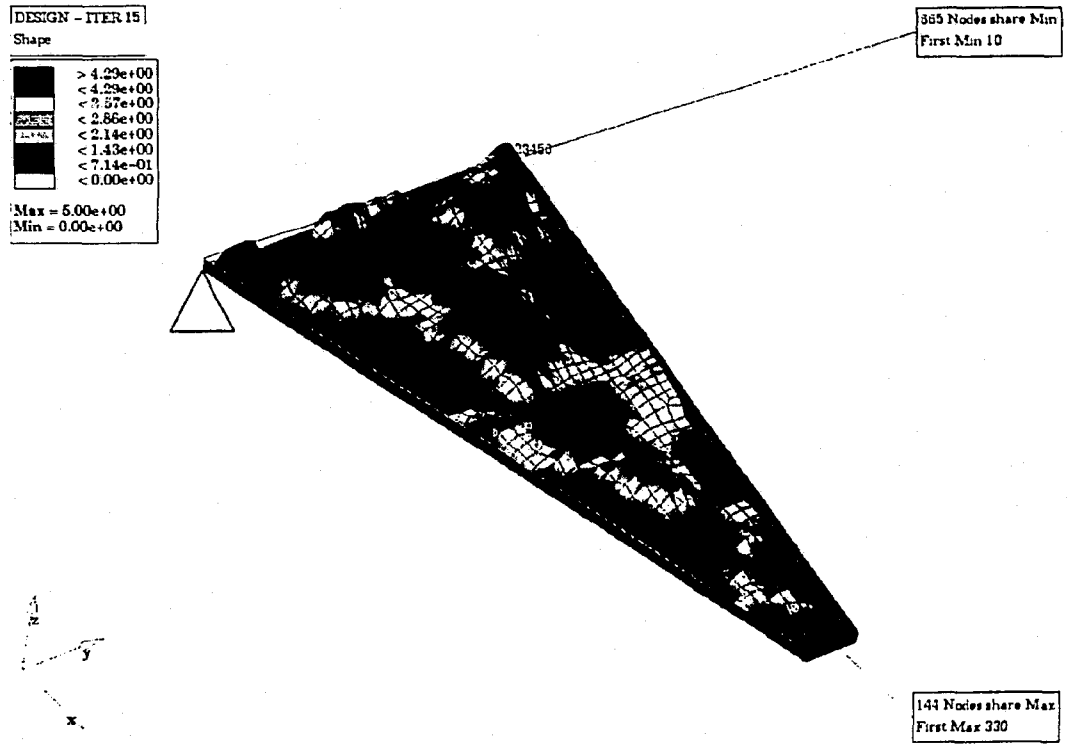

Figure 2.5 - Wedge Structure after Topography Optimization

2.4 Size and Shape Optimization

Size optimization can only be performed on shell elements because they have a thickness variable to make up for the 3rd dimension that is missing in the graphics interface. To change the thickness of a 3D element, you would have to move the nodes of the element, which is shape optimization. The design variable in size optimization is the thickness of the shell element. The gauge thickness is modified between the bounds that the user defines so that the structure can meet the objective function and boundary conditions set forth by the optimization.

Shape optimization uses the boundaries of the model as design variables. The user must first create handles; which are special nodes that indicate which points on the boundaries of the model can move. The user also has to define the move limits and the directions (x, y, and z) the handles can move in. During optimization, the boundaries of the model are manipulated, changing the shape of the model, to meet the boundary conditions, and satisfy the objective function.

2.4.1 Shape Optimization Example

The following is a shape optimization example of a torque arm. The objective function is to minimize the mass of the torque arm while meeting the stress and force conditions. Again, Altair Optistruct is used to mimic the optimization. Figure 2.6 shows the geometry and other properties of the example model from the paper by Fourie et al [33].

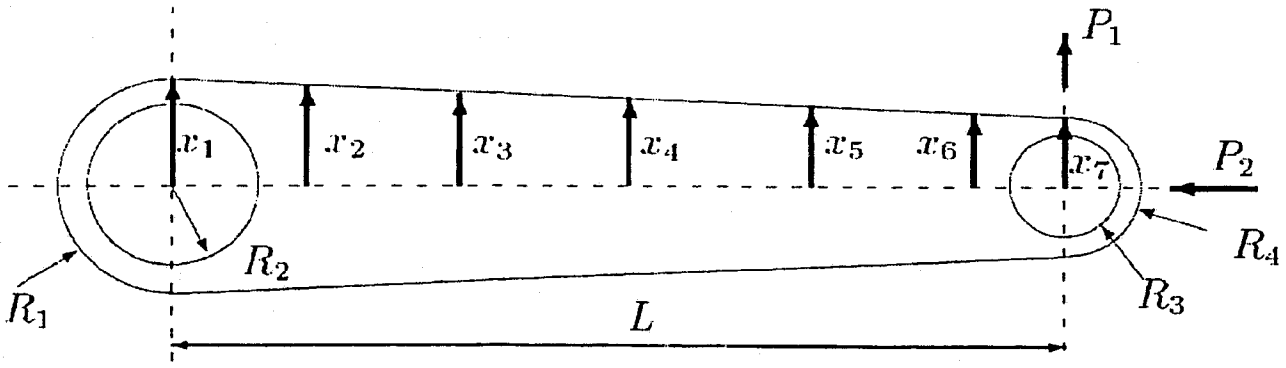

$R_1 = 5.42$ cm	$P_1 = 50.66$ kN
$R_2 = 4.0$ cm	$P_2 = 27.89$ kN
$R_3 = 2.5$ cm	$E = 207.0$ GPa
$R_4 = 4.27$ cm	$\nu = 0.3$
$L = 42$ cm	$\rho = 7850$ kg/m^3
$t = 3.0$ cm	$\sigma_y = 0.8$ GPa

Figure 2.6 - Torque Arm - Geometry, Loads, and Material Properties [33]

As can be seen, there are seven design variables (x_1, ..., x_7) and two loads P_1, and P_2. The design variables mark the position on the edge of the torque arm where changes are to be made. Table 2.1 displays the design variable limits. Of course, the bottom half of the arm will be symmetrical to the top half.

Table 2.1 – Design Variable Move Limits [33]

Design Variable	Lower Bound	Upper Bound
1	4.5	10.0
2	1.1	10.0
3	1.1	10.0
4	1.1	10.0
5	1.1	10.0
6	1.1	10.0
7	3.0	10.0

Figure 2.7 shows the Optistruct model of the torque arm. The red balls indicate the global boundaries; the handles (yellow balls) can never extend outside these boundaries. This limits the amount of memory needed to solve the problem. The handles in Figure 2.7 are located at the exact spots where the arrows in Figure 2.5 are. These points are where the geometry will change. Also, the geometry, proper loads, and material properties are modelled the same.

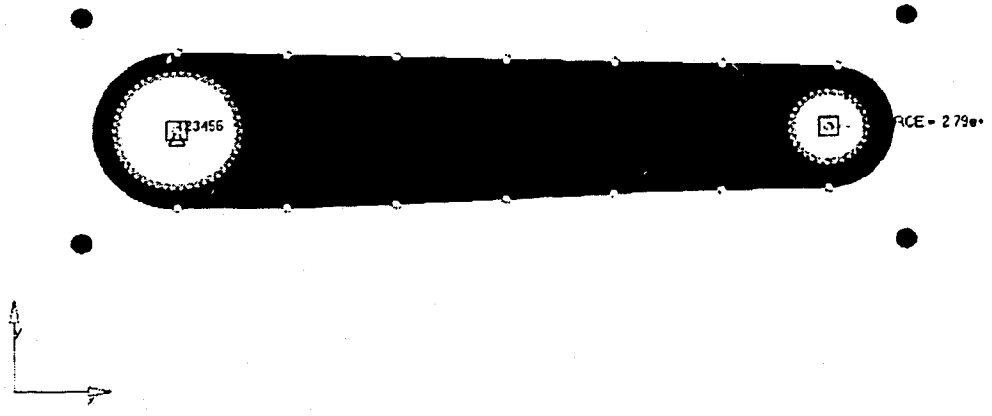

Figure 2.7 - Optistruct Torque Arm Model

The objective of the optimization is to minimize the mass according to the displacements of the handles (the torque arm edges). The optimization is subject to a maximum stress constraint of 800 MPa, no element stress is allowed to exceed this. Figure 2.8 shows the original and final designs of the torque arm from the journal paper [33], and Figure 2.9 shows the final form of the arm after Optistruct optimization.

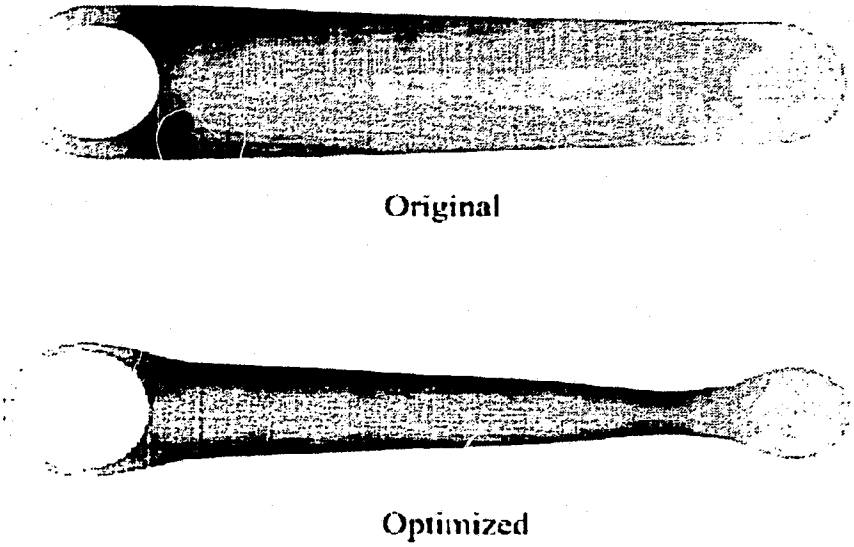

Figure 2.8 - Torque Arm - Original and Optimized Designs [33]

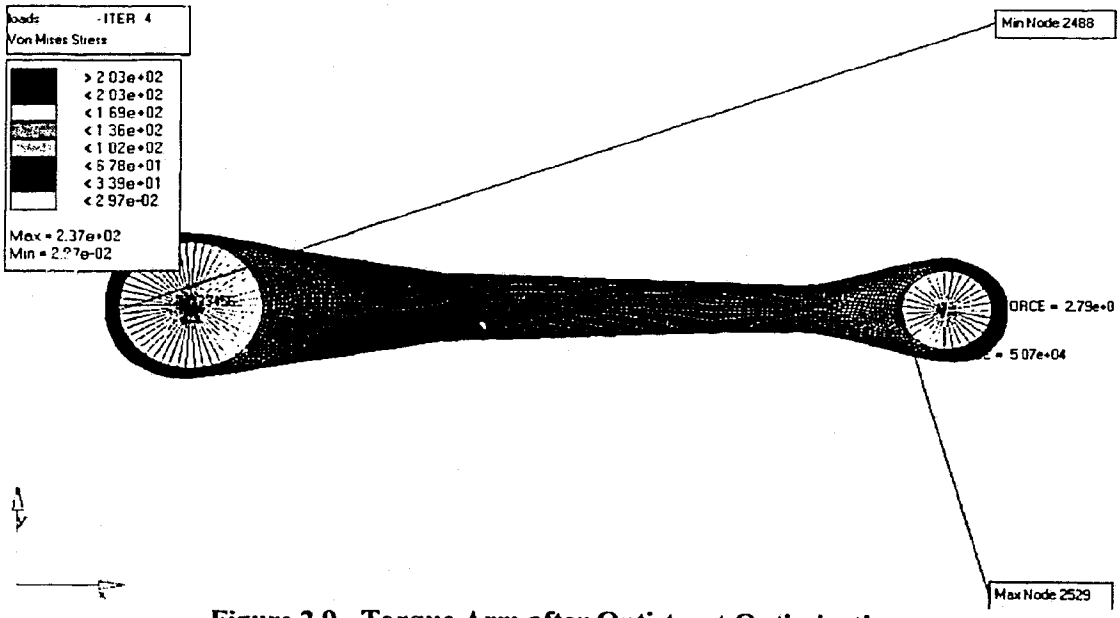

Figure 2.9 - Torque Arm after Optistruct Optimization

The two final forms of the torque arm (Figure 2.8 optimized arm, and Figure 2.9) are identical, except for the fact that in Fourie et al. [33] a smoothing function was used to give the optimized arm in Figure 2.8 a more rounded, professional look. The maximum stress in the Optistruct model is 240 MPa and is below the constraint of 800 MPa. Furthermore, the mass of the Optistruct arm was reduced to 4.387 kg from 9.7 kg, this is a 45% savings in mass, whereas in Fourie et al. the arm's mass was reduced from 9.7 kg to 4.615 kg. The Optistruct optimization took only 3 iterations and about 3 minutes to complete, whereas the paper optimization which used a Particle Swarm Optimization Algorithm (PSOA) took 12 iterations and did not report the time needed.

2.5 Topology Optimization

Topology optimization is the most used type of structural optimization, and there are many papers on research into this field. Not only can topology optimization be applied to shell structures just like the above two techniques, but it can also be applied to 3D structures. This is because both 2D and 3D elements have a density characteristic that can be altered.

Topology optimization is able to comply with the objective function and constraints of a problem by manipulating the relative density of each element through strain energy density equations [34]. Topology optimization takes a design domain, Ω, which can either contain solid, or voids. The domain is then discretized using an FEM code such as MSC-NASTRAN or Altair Optistruct. The design variable is the relative density, ρ^e, of each element and is given by:

$$\rho^e = x^e \rho_0 \tag{2.4}$$

where x^e represents the fraction of the total density and is between 0 and 1, and ρ_0 is the density of the material being used in the model. The stiffness matrix for an element is given by:

$$k^e = \left(x^e\right)^p k^0 \tag{2.5}$$

where, k^e is the element's stiffness matrix, k^0 is the global stiffness matrix, and p is the penalty factor. By choosing a penalty factor equal to 1, elements with intermediate densities are often found. Such a structure is difficult to manufacture in real life, so by choosing a penalty factor greater than or equal to 3, Kutylowski [35] indicates that a design where each element is either filled with material, or contains no material at all, will occur. Once the engineer sees what elements can have a density of zero after the optimization, he/she can go about removing those elements and retest the design to see if it conforms. Topology optimization is usually used to minimize the mass of structures as will be seen in the upcoming example.

2.5.1 Topology Optimization Example

One of the biggest problems with topology optimization is checkerboard patterns. Buhl et al. [36] reports that checkerboard patterns occur because the checkerboard has an artificially high stiffness compared to a structure with uniform material distribution. It has been shown by various people, including Shyy et al. [37], that checkerboard material distribution is not optimal and is, in fact, caused by errors in the FEM mathematical formulation. There are many ways to help control this problem, one way is to use higher order element. However, this increases computational time dramatically. For example, if a 9-node shell element is used instead of a 4-node element, the computational time

increases 16 fold. Another ways to combat this is to use filtering techniques such as perimeter control method, mesh independent filtering, and density slope control. In Shyy et al. [37], the creation of the checkerboard filter control option in Altair Optistruct is discussed.

The example being presented is one that was not in any published paper, but was created just to see how the checkerboard fixing option worked in Optistruct. Figure 2.10 shows the model with a checkerboard pattern that has occurred from optimizing the 2D plate. The objective was to minimize the mass of the plate which has a force applied in between two boundary constraints. The red elements indicate element densities of 1, and blue is 0. This means that any element that is blue can be removed. However, there is a checkerboard pattern in the center of the structure.

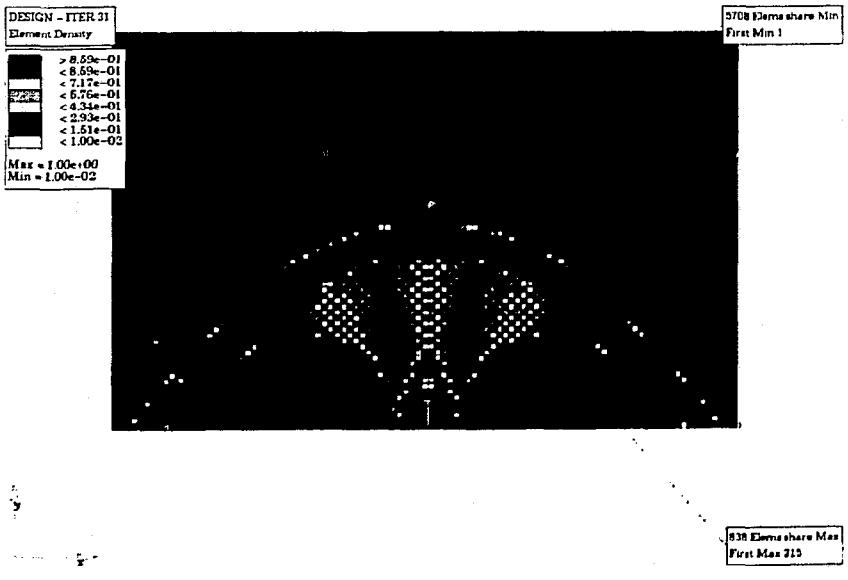

Figure 2.10 - Non-Optimal Solution for Topology Optimization

Figure 2.11 shows the same plate after the topology optimization was run again with the checkerboard parameter activated. As can be seen, there are no checkerboard patterns anywhere within the structure. Now it is clear what material can be removed to minimize

the mass. This example shows some of the problems with topology optimization, and how they can be easily fixed.

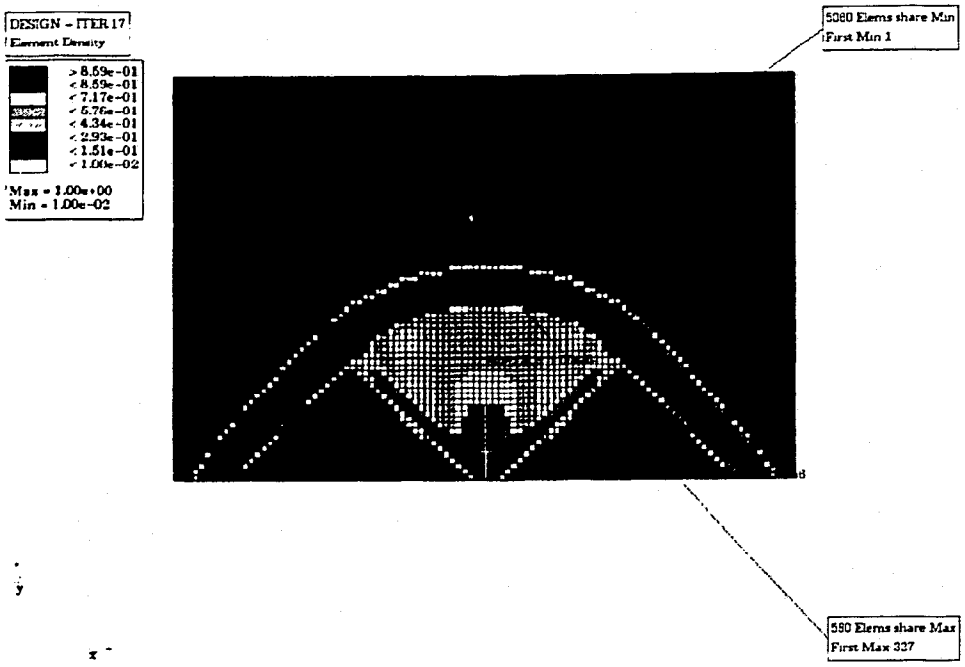

Figure 2.11 - Optimal Solution for Topology Optimization

2.6 LS-DYNA Background Information

As was mentioned in Section 1.5, LS-DYNA is used to optimize a non-linear model along with the MDO procedure that is developed.

LS-DYNA is an explicit finite element program for the analysis of the non-linear dynamic response of three dimensional structures [38]. LS-DYNA can be used to analyse vehicle crashworthiness, occupancy protection, sheet metal forming and other areas.

The general equation of motion that the solver has to solve is:

$$[M]\{\ddot{u}\} = \{f\} = \{f\}_{ext} - \{f\}_{int} \tag{2.8}$$

where M is the mass matrix, $\ddot{u}$ is the nodal acceleration vector, f_{ext} and f_{int} are the external and internal force vectors from the model. Once the unknown values in the acceleration

vector are found, element stresses and other values the user wants to know can also be found.

2.7 Optimization Software Methodology

Altair HyperStudy is a program that is used for the MDO processes in this thesis. First, the user must make a model and runs an initial simulation in HyperStudy. Then, using the result files and HyperStudy's interface, one can set up any number of constraints, design variables, and objective function. As the optimization is running, results are displayed in a graphical form, and the user can see if the optimization is going as planned.

HyperStudy controls the MDO, after the initial runs it will takes those results and passes them to HyperOpt, the programs response surface creator. HyperOpt uses advanced response surface methodology (RSM) and sensitivity analysis to come up with values for each design variables for the next iteration. The control is then passed back to the FEM solver (Optistruct, MSC-NASTRAN, LS-DYNA, or any other program) which will use the new values and create another set of results files. This procedure continues until the objective function value is within some limit of the previous iteration, or until the user specified amount of iterations is completed (see Figure 2.12).

One of the methods in RMS is the *method of steepest ascent*, or in terms of minimizing, *descent* [39]. This method uses linear regression to evaluate if the slope of the line created by the data is positive or negative, and then marches that way. Once it is determined that the slope has changed direction, a maximum, or minimum has been reached. However, it may only be a local maximum or minimum. That is why

HyperStudy's code is licensed, as it is able to find the global maximum, or minimum using advanced RSM techniques.

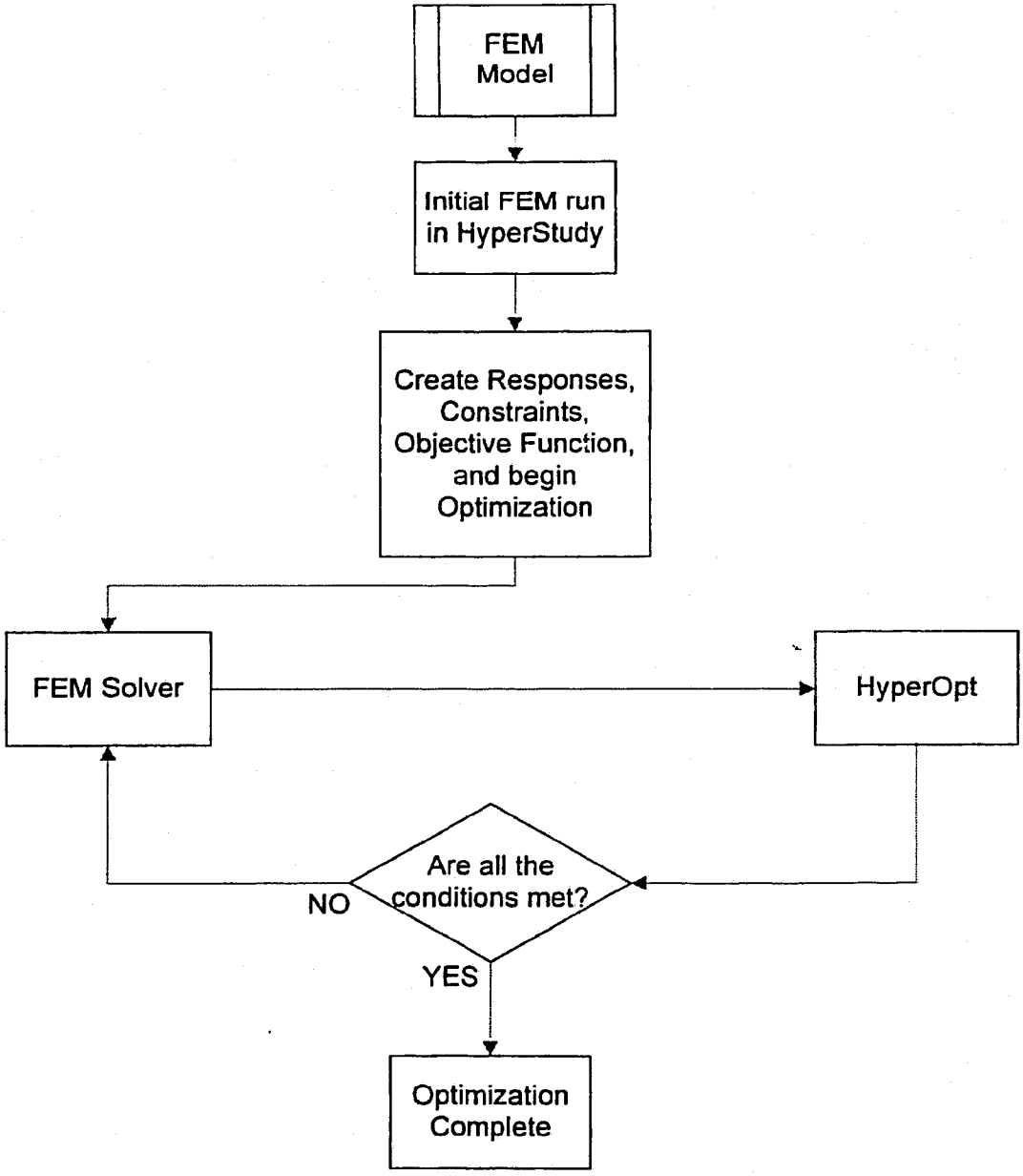

Figure 2.12 – A HyperStudy Simulation Example

2.8 Optimization Methodology for this Thesis

This thesis uses a collaborative optimization (CO) approach. That means that the MDO is done in more than one step. The first step would be to complete topography, topology, and shape optimizations on the model. Since these disciplines are very specific, they cannot be combined with the other types of optimization for use in HyperStudy and therefore must be completed first. The design variables for shape, topography, and topology optimization are not the same as the design variables used for size and other optimization techniques used in Chapter 3. Therefore these optimizations had to be separated.

Once the results from these techniques are collected and applied to the model being used, the new model is then used by HyperStudy to perform an MDF optimization using size optimization and some techniques that are described in Sections 3.3.2 and 3.3.3. The degree of coupling between these disciplines is very high, since all the techniques in the MDF have the component gauge thickness as their design variable. Therefore an MDF optimization is the perfect candidate.

Chapter 3

MDO Procedure Development

3.1 Introduction

This chapter is dedicated to introducing the initial design steps of the MDO procedure. Flow charts indicate the decisions that were made in each iteration; and also the problems within each iteration are discussed.

3.2 Design Procedure - Iteration 1

Figure 3.1 shows a flow chart that outlines the first iteration in the design process for the MDO procedure. The optimization process begins with topology and topography optimization. These optimizations are fast because they do not have a lot of constraints. Also, the computational time is less as will be seen later in Chapters 3 and 4. Topology and topography optimizations can be performed by separately or simultaneously to save computational time.

In Figure 3.1 the flow chart starts with a predefined FEM model. The objective is to maximize the 1^{st} natural frequency of this model by means of topology optimization, topography optimization, or simultaneous topology and topography optimizations. The flow in Figure 3.1 loops so that all the optimization techniques can be applied and then the results are obtained. Next, a decision on whether more optimization techniques are needed is made.

Evolution of Multidisciplinary Design Optimization (including Cost) – Iteration 1

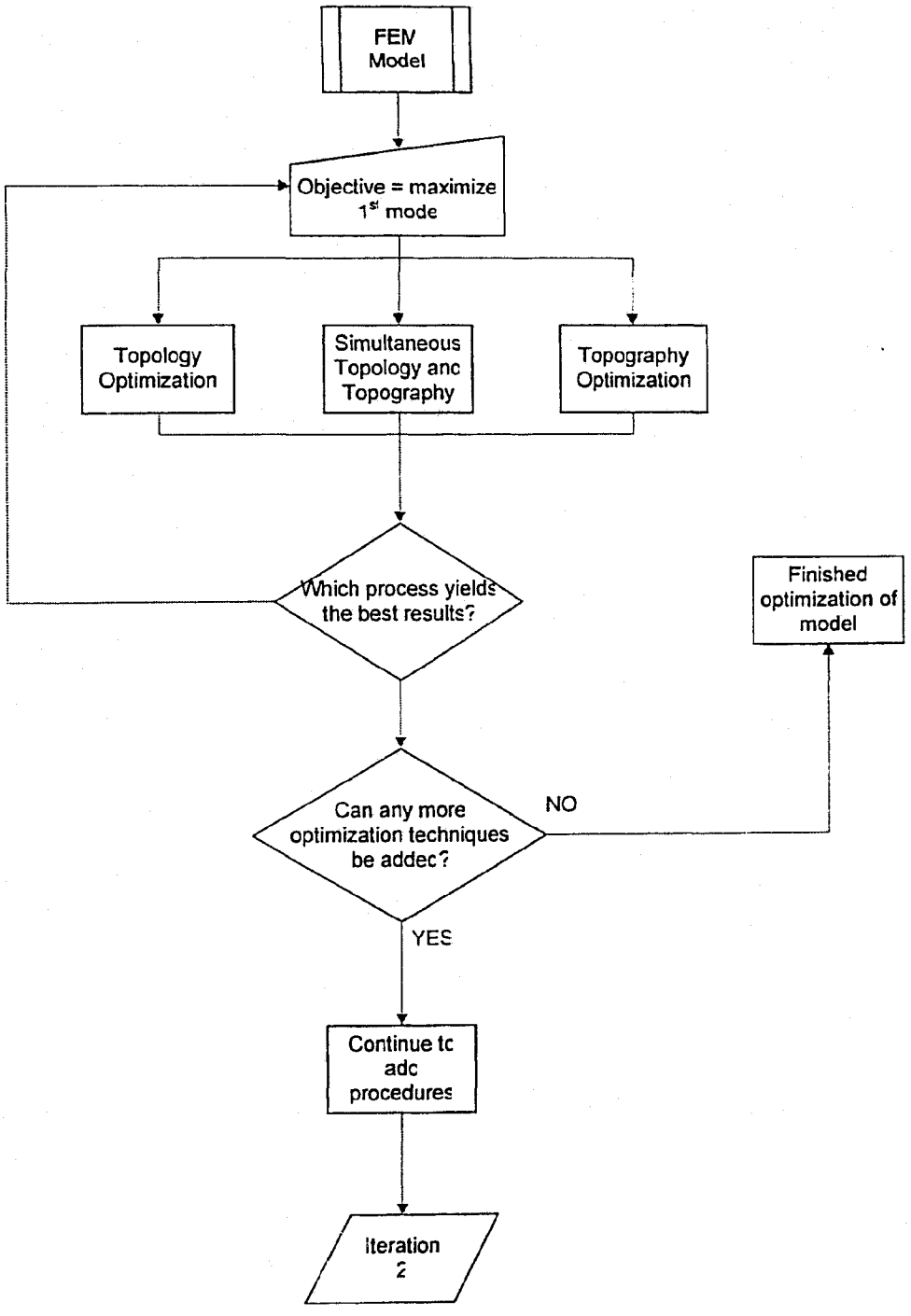

Figure 3.1 - Evolution of Multidisciplinary Design Optimization Procedure - Iteration 1

3.2.1 FEM Model for Iteration 1

An FEM model of a bracket is used for the first iteration. Since this is the first step of the design procedure process, a simple model with a small number of elements is used. This yields fast results and allows the design procedure to go to the next iteration. Figure 3.2 shows a discretized model of the bracket. It has two 75 N forces applied to the holes near the top, and all 6 DOF are constrained at the two holes near the bottom. The purple areas around these holes are non-design areas. This means that these areas are ignored during the optimization process. If they were not it would disrupt the force and constraint boundary conditions. The blue area indicates the design space that will be modified to meet the requirements and constraints. The material of this bracket is steel with a Young's modulus of E = 210 GPa, Poisson's Ratio, $\upsilon = 0.3$, and a density, $\rho = 7850\ kg/m^3$.

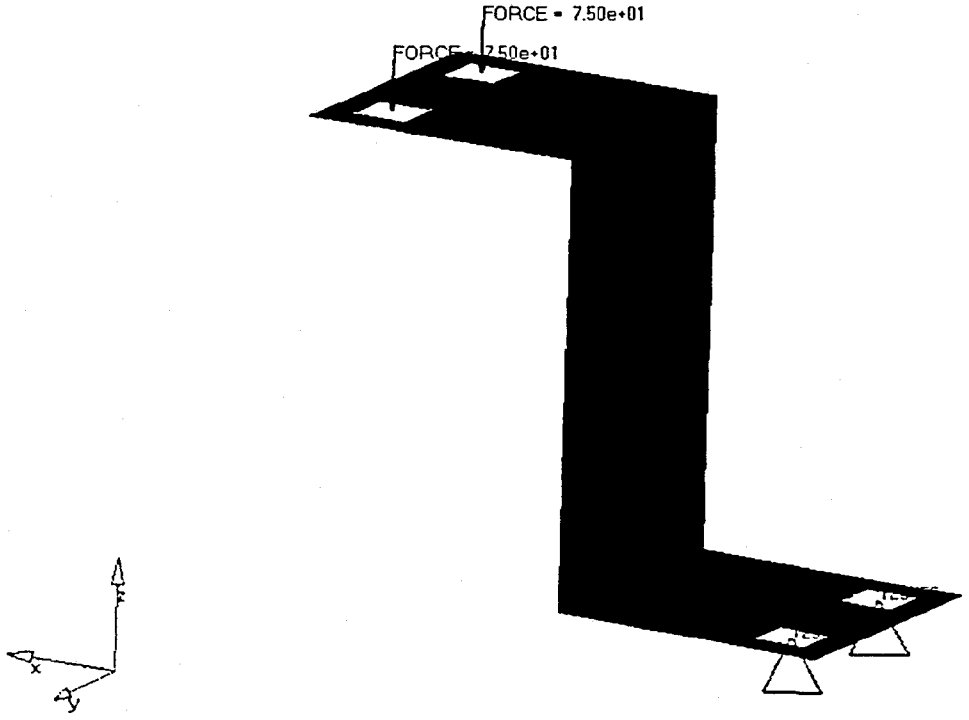

Figure 3.2 - Bracket FEM Model for Iteration 1

3.2.2 Optimization Problem Description

The optimization problem for the bracket is described below. It is subject to a few constraints. The tip displacement refers to the center node along the top front edge of the bracket (the front edge is the edge nearest to the two forces).

Objective = maximize 1st natural frequency

Subject to:

- Two 75 N forces in the –z direction
- Nodal DOF boundary conditions (the two bottom holes, all six degrees of freedom constrained – see Figure 3.2)
- tip maximum x displacement = ±5 mm
- tip maximum z displacement = ±5 mm

3.2.3 Results and Discussion

The results of the various types of optimization can be seen in Table 3.1. The program used for the optimizations was Altair Optistruct. Each optimization took about the same amount of time - 5 minutes using the HP platform with 2 processors that was mentioned in Section 1.4.

Table 3.1 – Results for first Iteration

Type of Optimization	1st Natural Freq. Before Optimization (Hz)	1st Natural Freq. After Optimization (Hz)	Number of Iterations	All constraints met?
Topology	292	528	9	YES
Topography	292	426	7	YES
Topology and Topography	292	568	8	YES

As can be seen, all the techniques took about the same amount of iterations to complete, and all the constraints were met in all cases. The difference can be seen in the 1st natural frequency. The simultaneous optimization technique yielded the best result raising the frequency from 292 Hz to 568 Hz. Figure 3.3 shows the bracket after the results of the simultaneous technique have been applied. The natural frequency is raised by making the elements thicker through the center column with a rib shape, thereby stiffening the bracket.

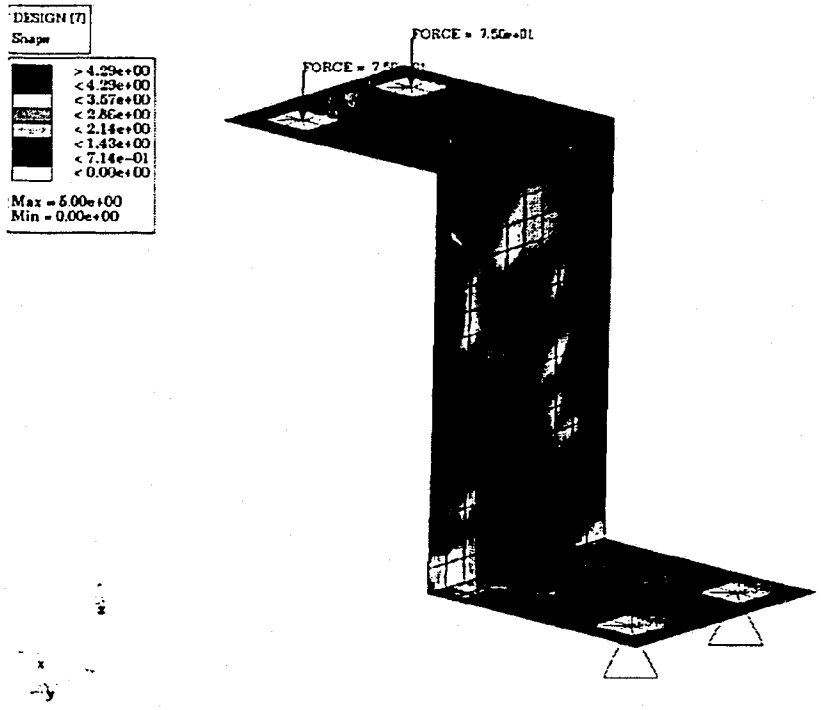

Figure 3.3 - Bracket After Results are Applied

Colours other than blue indicate spots where the bracket material would be thicker and bulging out. The rib shape (marked by red) is well defined through the center of the bracket.

Therefore, if we were to continue with this model, this simultaneous topology and topography optimization would always be the first step in the design optimization

process. This iteration must be completed for every model, so that the optimization procedure can include as many optimization techniques as possible.

Since this iteration was successful, the flow in Figure 3.1 can continue passed the decision block "Can more techniques be added?" Decisions that were followed are marked in red for all flow charts. In this case, more techniques can be added if needed to make the MDO procedure complete. Therefore, the flow continues on to iteration 2.

3.3 Design Procedure - Iteration 2

The flow chart for iteration 2 can be seen in Figure 3.4. Here, the design procedure becomes a bit more involved. First, a new model is used, one that has three components. The first objective is to minimize the mass using the techniques learned in Iteration 1. It is assumed that this has been performed beforehand and will not be discussed further. Now a new objective arises: minimize the mass via changing the thicknesses of the components and choose the proper material for each component. Also, a new weld constraint optimization technique is included. All the techniques must work together and if they do not then the problems must be fixed before continuing.

3.3.1 FEM Model for Iteration 2

The new FEM model that is used for iteration 2 can be seen in Figure 3.5. It is a plate structure that is comprised of three components named patch 1, patch 2 and shell.

Evolution of Multidisciplinary Design Optimization (including Cost) – Iteration 2

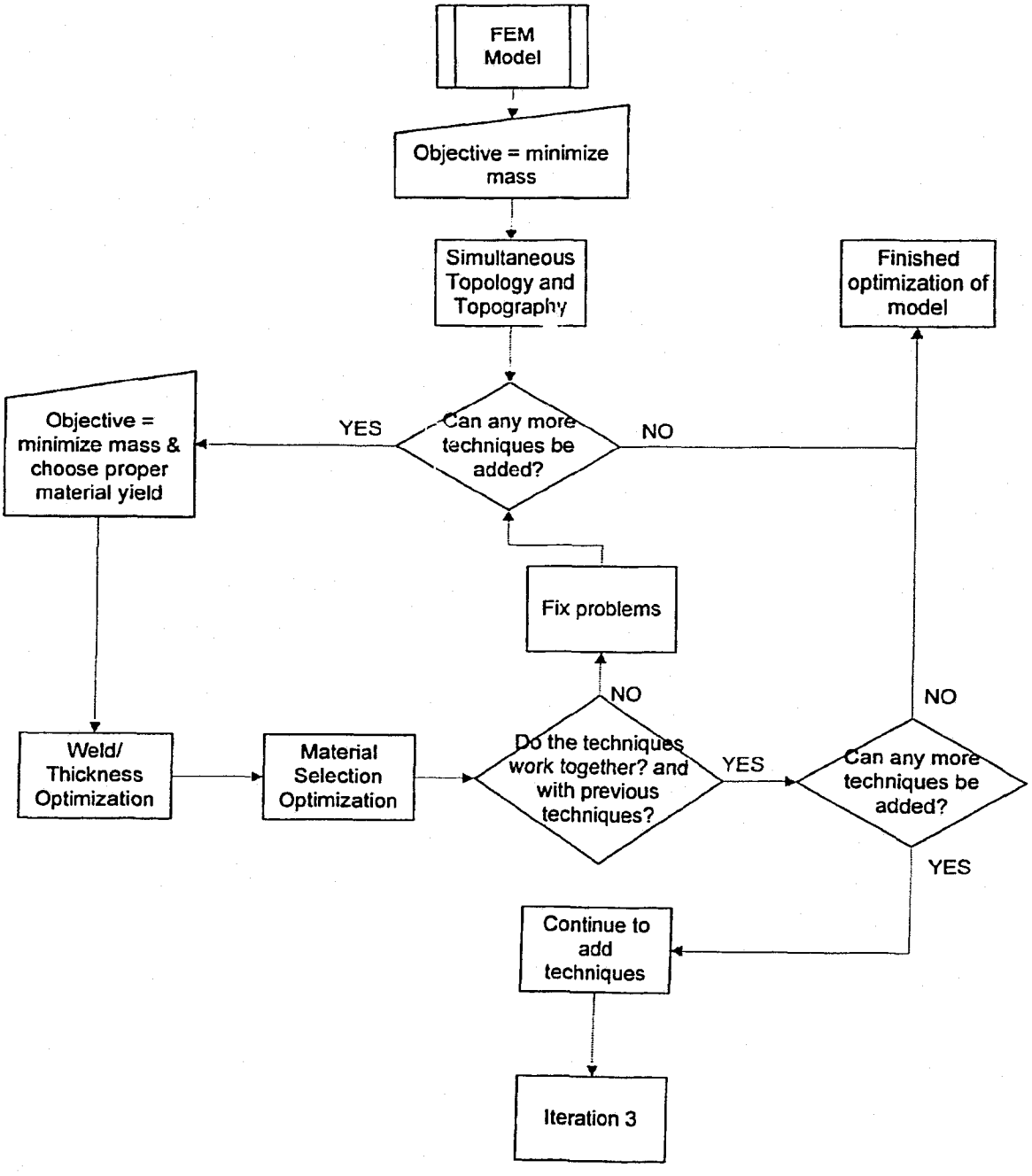

Figure 3.4 - Evolution of Design Optimization Procedure - Iteration 2

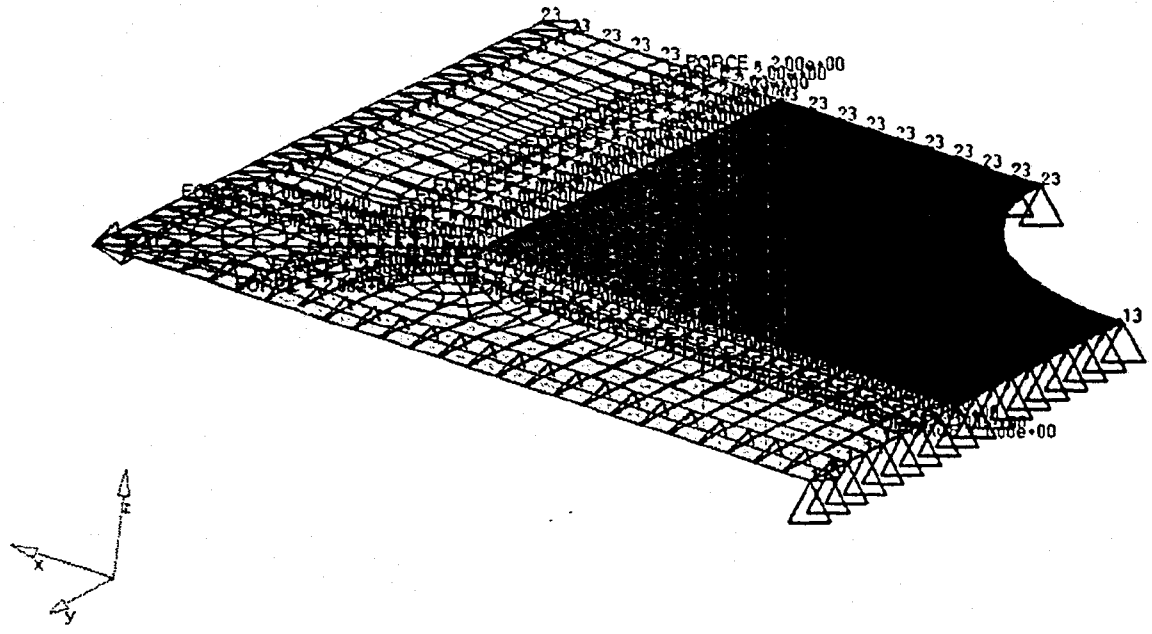

Figure 3.5 - FEM Model of Plate Structure for Iteration 2

The components patch 1 and 2 are the outer pieces of the model which are yellow and green in colour. The shell component is the center piece that is orange. The boundary conditions (blue triangles) and forces (red arrows) can also be seen in the Figure 3.5. The material for each component is steel with the same properties as in the first iteration.

3.3.2 Weld Constraint Optimization

As was noted earlier, the plate structure is made up of three components. If these components are to be welded together, then the difference between the thicknesses must not be greater than 50% either way. If the difference is too large then there will be problems in welding the two together. It occurs mainly because the extra heat needed to weld a thicker piece will burn right through a thinner piece of metal. Therefore, by

providing an upper and lower constraint on a ratio of the two component thicknesses, they will be within 50% of each other.

$$\frac{th_1}{th_2} < 2.0$$
$$\frac{th_1}{th_2} > 0.5 \qquad (3.1)$$

Equation (3.1) can be applied to any two materials that are welded together. As is shown here, the thicknesses must be within 50% of each other.

3.3.3 Material Selection Optimization

The material selection for each component is done based on the maximum stress of that component. The material of each component is set up as a design variable, so that it can be modified during the optimization process. The value of the yield stress for each component can be chosen from a discrete list or it can be continuous. The following constraint is set up for each component:

$$\frac{\sigma_{yield}}{\sigma_{max}} > 1.0 \qquad (3.2)$$

Therefore, as the maximum stress, σ_{max}, of the component approaches the yield strength, σ_{yield}, the ratio gets closer to 1.0. If the ratio becomes less than 1.0 then the yield strength is forced up to the next entry in the list (for discrete situations) to keep the constraint from being violated. The maximum stress for each component must be less than the maximum yield strength of the material currently being used for that component. The material yield for each component can be changed every iteration, however, the other properties such as density, Poisson's Ratio, and Young's Modulus remain the same.

3.3.4 Optimization Problem Description

Objective = minimize the mass

Subject to:

- All 2 N forces applied along the outer edges
- All DOF boundary conditions (degrees 1 & 3 for bottom left edge, degrees 2 & 3 for top right edge – refer to Figure 3.5)
- 1^{st} natural frequency > 31.4 Hz
- Max stress of any element < 50 MPa
- Weld constraint optimization (equation 3.1)
- Material selection optimization (equation 3.2)

In the MDO process HyperStudy was used with MSC-NASTRAN, as the FEM solver and HyperOpt as the response surface creator. HyperStudy regulates the optimization process. It first gets the results from an initia run in MSC-NASTRAN then gives these results to HyperOpt which modifies the design variables for the next iteration and checks the response. HyperOpt uses all these results to come up with quantities for each design variable and, eventually, a feasible solution.

3.3.5 Results and Discussion

The results are presented as a series of graphs. The first graph, Figure 3.6, shows that the natural frequency constraint was met. This can be seen by checking the last iteration (iteration 16) and noting that the value of the 1^{st} natural frequency is about 32 Hz which is above 31.4 Hz.

The next graph (Figure 3.7) displays the maximum stresses of each component. One element from each component was chosen as the maximum stress element. This was done before the optimization by viewing the results of the initial run and seeing which element had the maximum stress. Then a response was set up for this element so that it could be monitored throughout the optimization. Figure 3.7 details the stress variations throughout the optimization for these three elements. Note that all the stresses end up below 50 MPa at iteration 16, which was the given constraint.

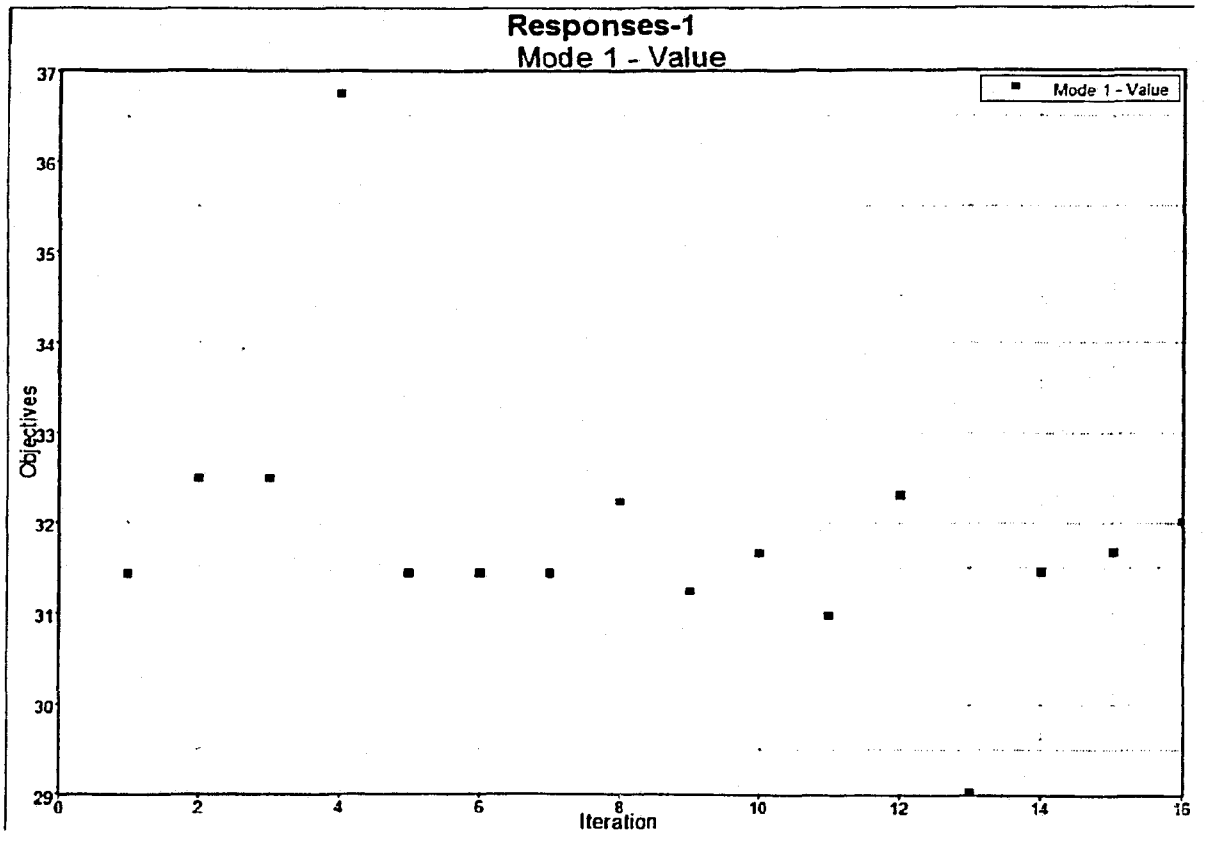

Figure 3.6 - 1st Natural Frequency of Plate Structure (Hz vs. Iteration #)

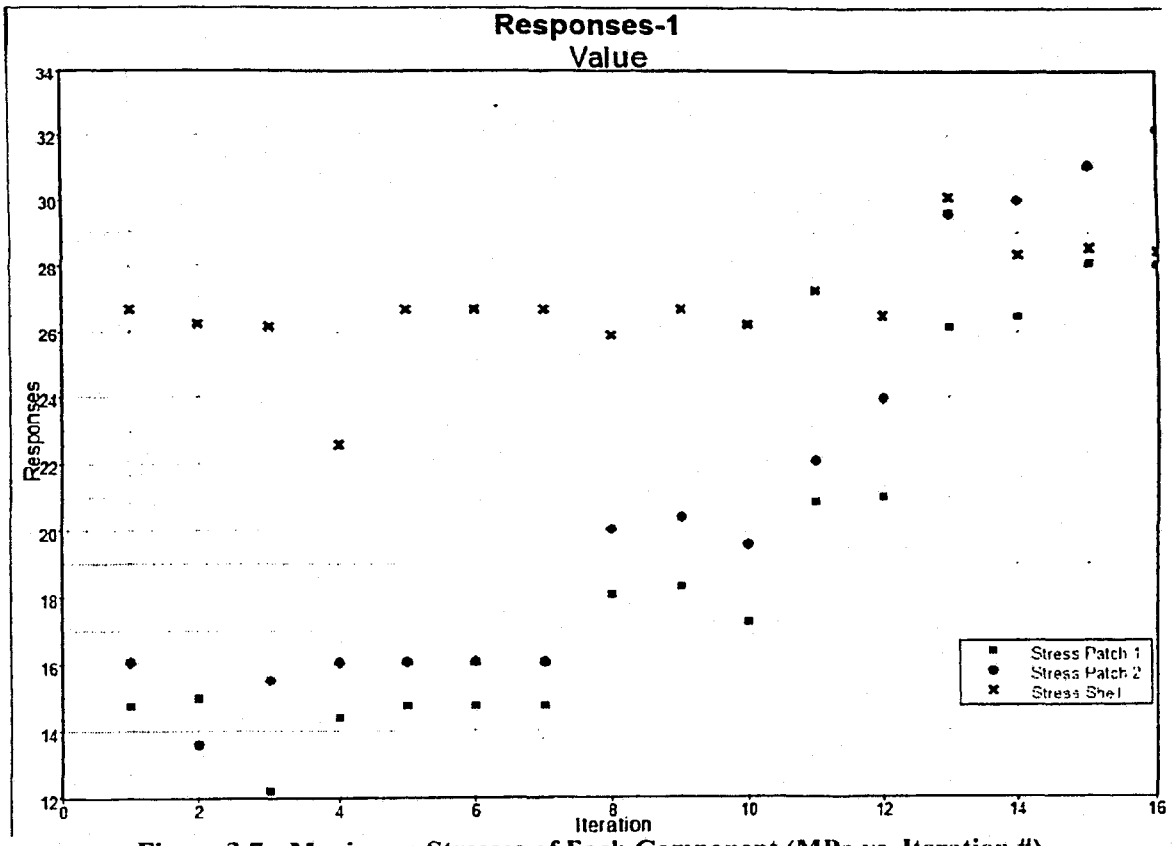

Figure 3.7 - Maximum Stresses of Each Component (MPa vs. Iteration #)

Figure 3.8 shows the results for the mass objective function. The mass was minimized from $1.825e^{-6}$ kg, to $1.3e^{-6}$ kg, which is a 29% reduction in mass. Figure 3.9 shows how the thicknesses of patch 1 and patch 2 were decreased to achieve the reduction in mass. Notice how the shell thickness was increased to offset the stress that the other two components cannot carry with a thinner gauge. Also notice that the thicknesses are not within the given constraints from equation (3.1).

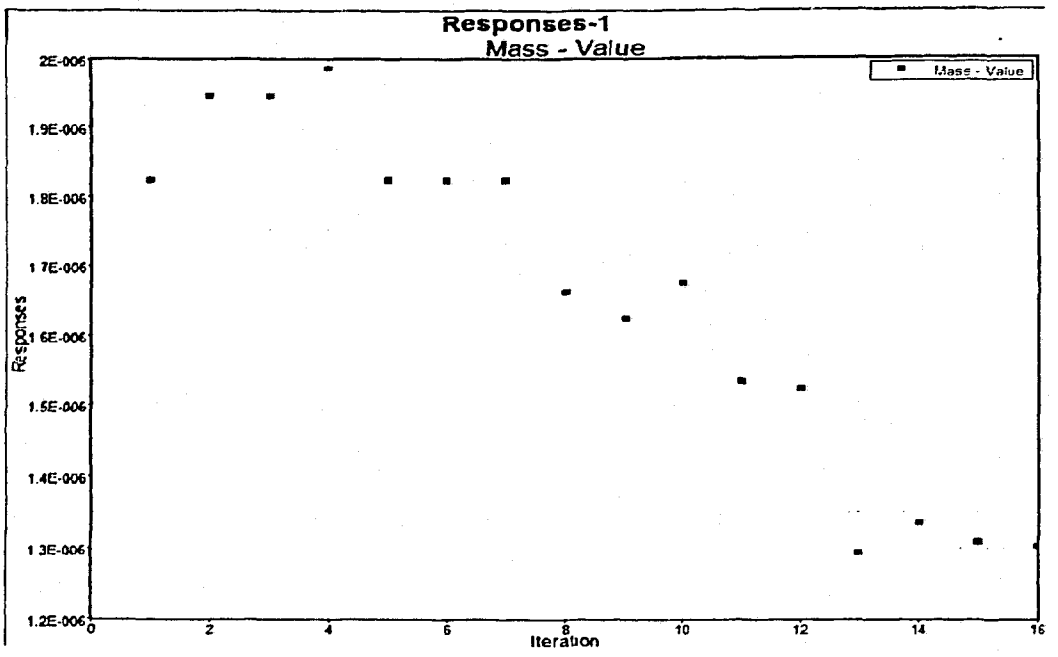

Figure 3.8 - Objective Function: Mass (kg vs. Iteration #)

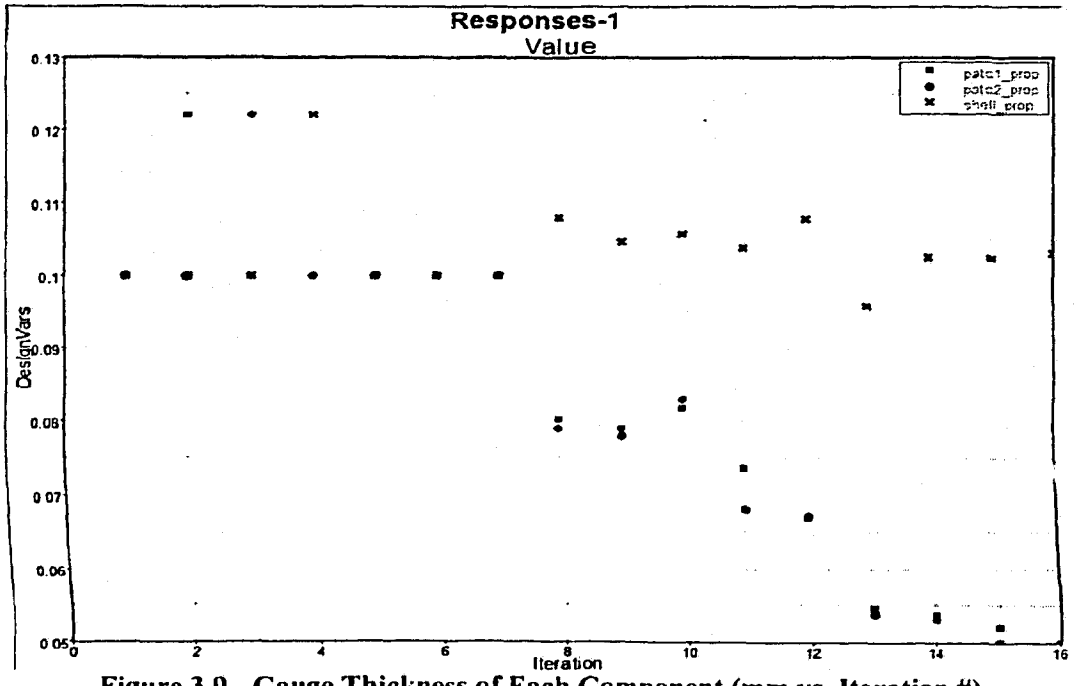

Figure 3.9 - Gauge Thickness of Each Component (mm vs. Iteration #)

The thicknesses are only slightly violating the constraints from equation (3.1). HyperStudy has a constraint violation tolerance to help with optimizing complicated problems. The violation tolerance is set at 5% for this optimization. The violation seen in the results is only 3%, so this does not affect the optimization.

The next three Figures 3.10, 3.11, and 3.12, show the design variable material yield strength for each component (patch 1, patch 2, and shell respectively) along with the maximum stress for that component in the same graph. Notice how the yield strength is generally always above the maximum stress throughout the iterations. The yield strength for all three is above the maximum stress at the last iteration. The yield stress was chosen from a discrete list of yield strenghts that are: {6, 20, 30, 35, 40, 45, 50} MPa. In the above Figures, the material yield strength is always one of these values. If it needs to rise because of the above constraint (equation (3.2)), it just jumps to the next value, whereas the stress is continuous. In each of the three figures the red symbols (●) are the component maximum stress values, and the blue symbols (■) are the material yield values. This proves that the material selection optimization works properly.

Therefore, referring back to Figure 3.5, since all the optimization techniques work together and with the previous techniques, the decision to move onto iteration 3 and add more optimization techniques was made.

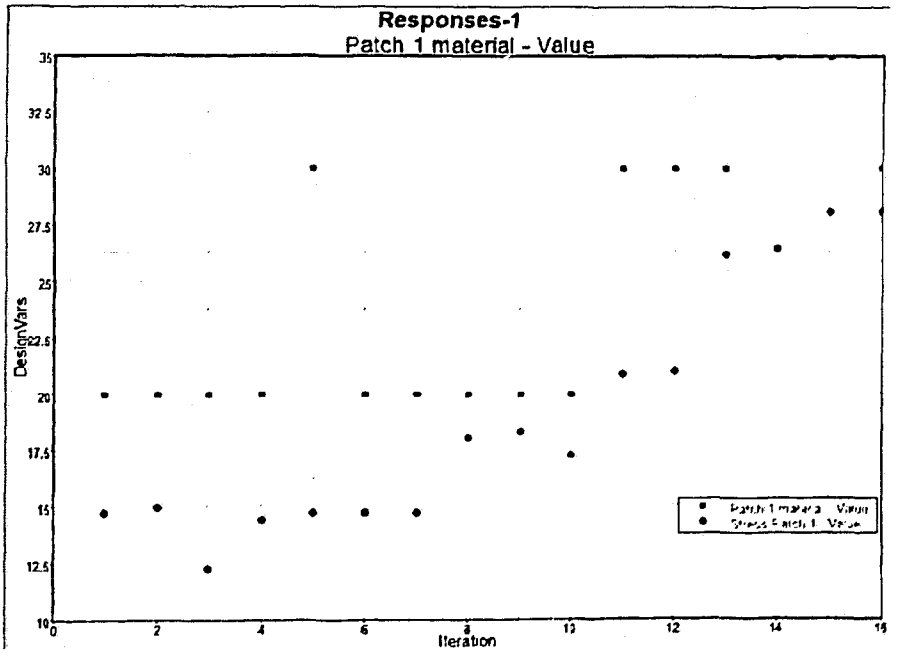

Figure 3.10 - Patch 1 Max Stress and Yield Strength (MPa vs. Iteration #)

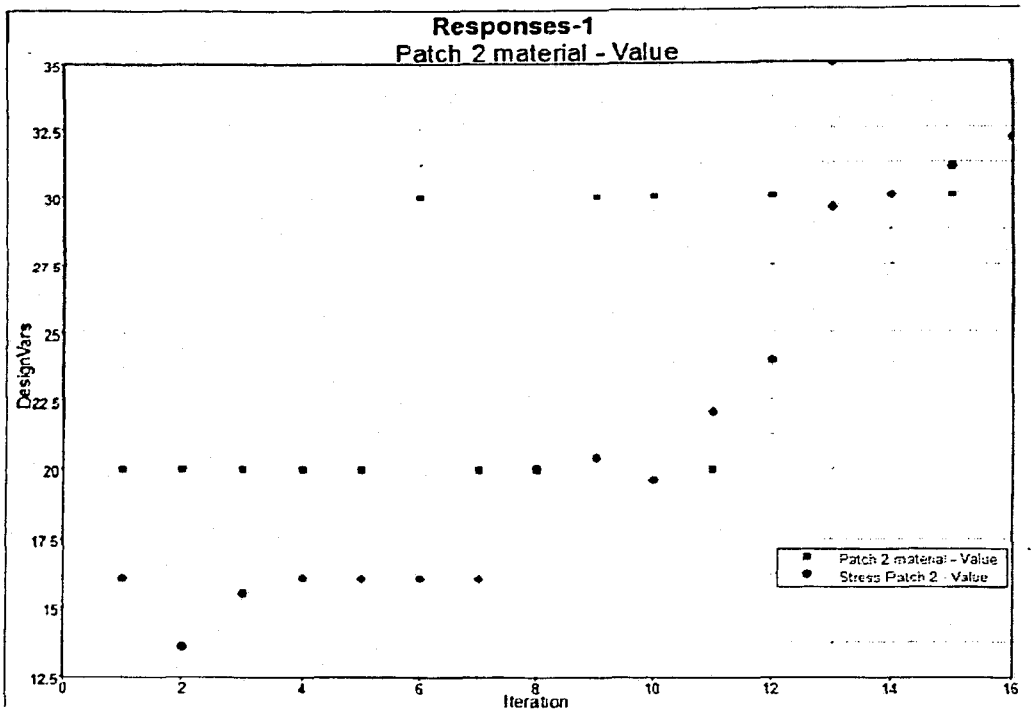

Figure 3.11 - Patch 2 Max Stress and Yield Strength (MPa vs. Iteration #)

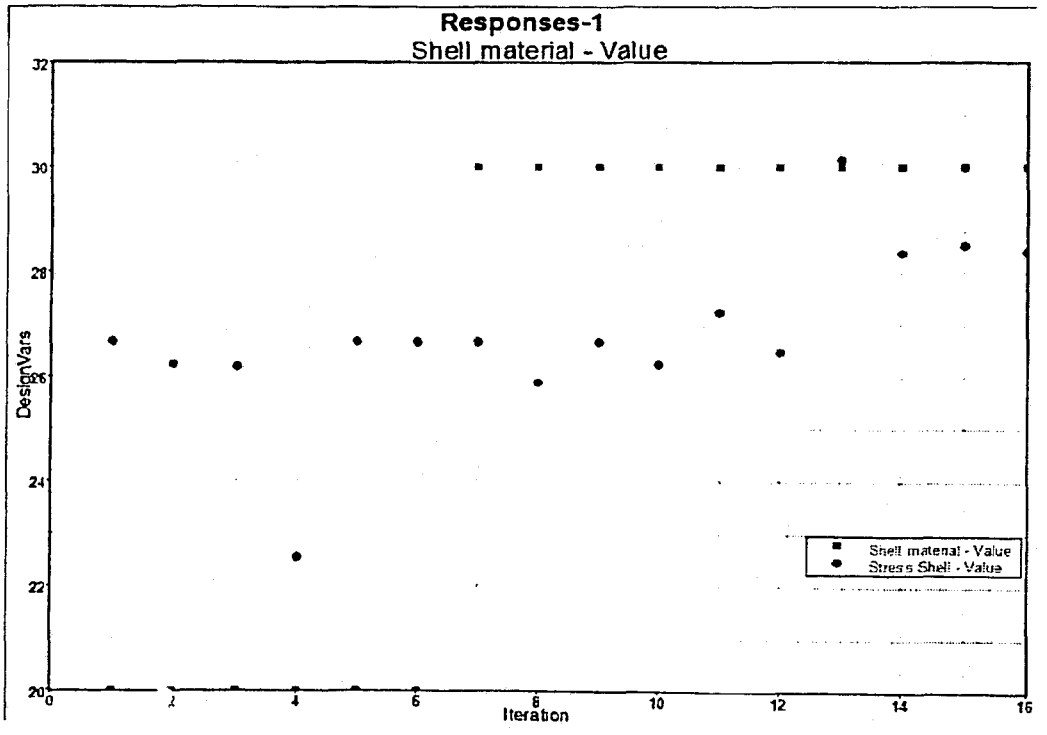

Figure 3.12 - Shell Max Stress and Yield Strength (MPa vs. Iteration #)

3.4 Design Procedure - Iteration 3

Figure 3.13 is the flow chart for iteration 3. It is basically the same as iteration 2 when it comes to minimizing the mass and choosing the correct material for each component. However, it takes the optimization one step further. Now, there is a cost optimization technique and the objective function is to minimize the total cost of the same plate model. The cost optimization technique is derived from a cost model which is itself derived from information about material pricing. The material pricing matrix is supplied by Van-Rob Stampings Inc. The first use of the cost model only involves cold rolled steel and later on a hot rolled steel model is added. But to understand the basics of the technique, only one type of steel is used in this iteration. This technique can be extended to any structure and use any material matrix, as long as the material yields and prices can be related to each other via a single function as will be described below.

3.4.1 Cold Rolled Steel Cost Model

The material price model is derived from the Van-Rob pricing matrix. Table 3.2 shows where the average base price originates from. It also shows the price for each specific gauge in dollars per 100 kilograms. To get the average base price, these prices are added up and divided by 4. The base price is then added to the cost for each specific yield strength from Table 3.3. This price is then divided by 100 to get the final cost of a specific yield in dollars per kilogram. Table 3.4 shows the final cost matrix that can be used to create a graph. From this graph a polynomial best fit function can be created and used in the MDO process.

Evolution of Multidisciplinary Design Optimization (including Cost) – Iteration 3

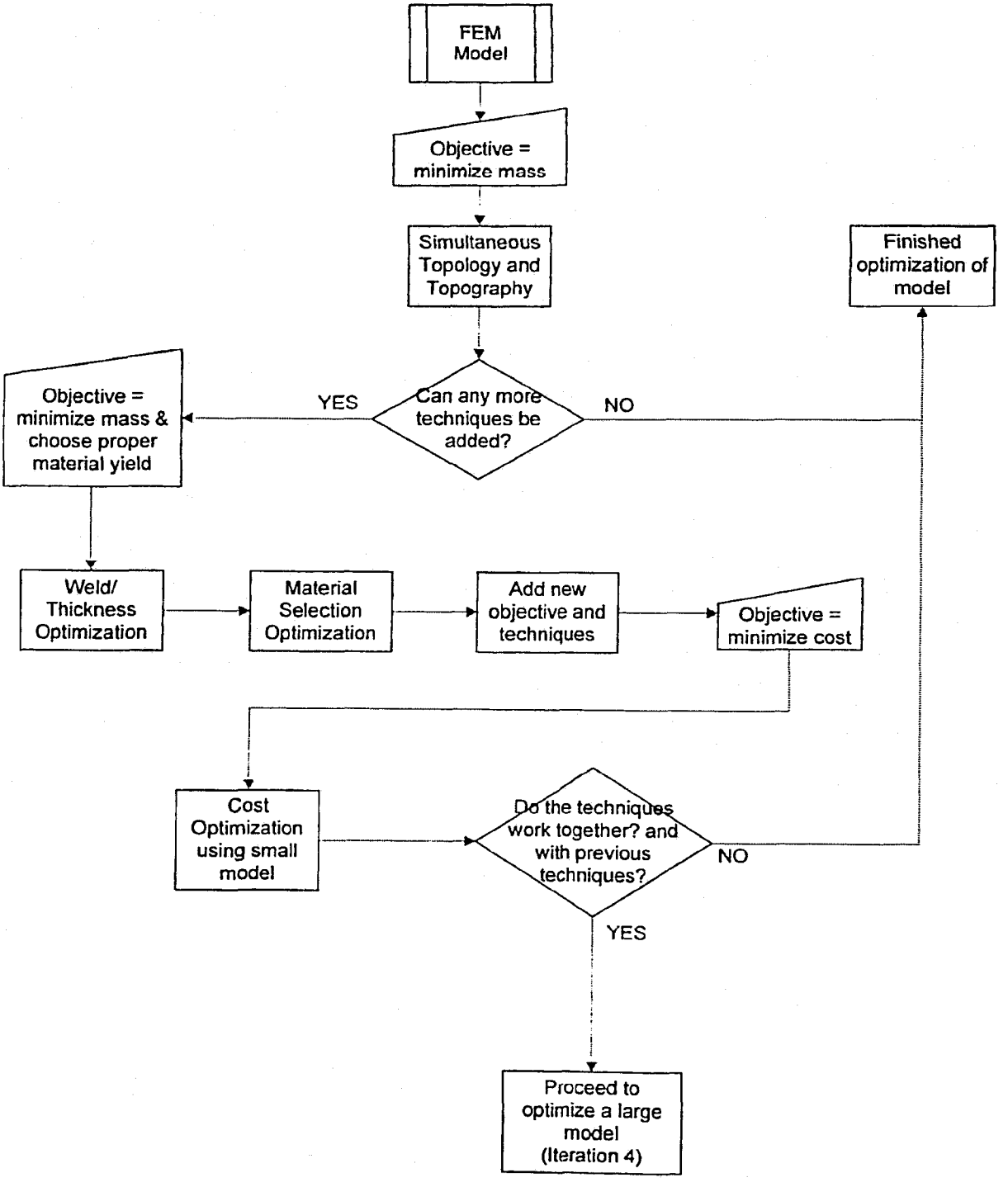

Figure 3.13 - Evolution of Design Optimization Procedure - Iteration 3

Table 3.2 – Base Price for Specific Gauge

COLD ROLLED	(SPEC -1008, SAE-J2329)	
	Metric (mm)	
Sheet Width	600 to 800	Dollars per Ckg
Gauge	0.49 and UNDER	92.77
	0.5 to 0.69	85.47
	0.7 to 1.49	81.20
	1.50 and OVER	80.76

Table 3.3 – Cost for Each Specific Yield Strength

COLD ROLLED	High Strength Low Alloy
Yield Strength (MPa)	Dollars per Ckg
270	11.85
300	13.12
340	14.03
380	16.45
420	18.52
500	21.50
550	22.38

Table 3.4 – Final Cost Matrix

Material: CQ [CR-1] Cold Rolled - 600 x 800 mm sheet - High Strength Low Alloy					
Yield Strength (MPa)	Altered Yield (MPa)	Price for Specific Yield ($/Ckg)	Average Base Price ($/Ckg)	Final Cost ($/Ckg)	Final Cost ($/kg)
270	520	11.85	82.41	94.26	0.94
300	550	13.12	82.41	95.53	0.96
340	590	14.03	82.41	96.44	0.96
380	630	16.45	82.41	98.86	0.99
420	670	18.52	82.41	100.93	1.01
500	750	21.50	82.41	103.91	1.04
550	800	22.38	82.41	104.79	1.05

The altered material matrix is based on the fact that for a complex structure, car design companies are looking at the instantaneous stress of the entire structure. Say, for instance, if the car went over a speed bump or into a pot hole. So, the material with a yield strength of 550 MPa can withstand only 550 MPa of stress in a static loading situation, but in an instantaneous situation, and with the rest of the structure around to aid in bearing the load, the 550 MPa yield strength steel can withstand stresses up to 800 MPa. This is the stress situation that is tested in MSC-NASTRAN. Therefore, it is important that the function can handle stresses up to 800 MPa. Therefore, the yield strengths are 'altered' by adding 250 MPa to each to create a proper graph. This graph can be seen in Figure 3.14.

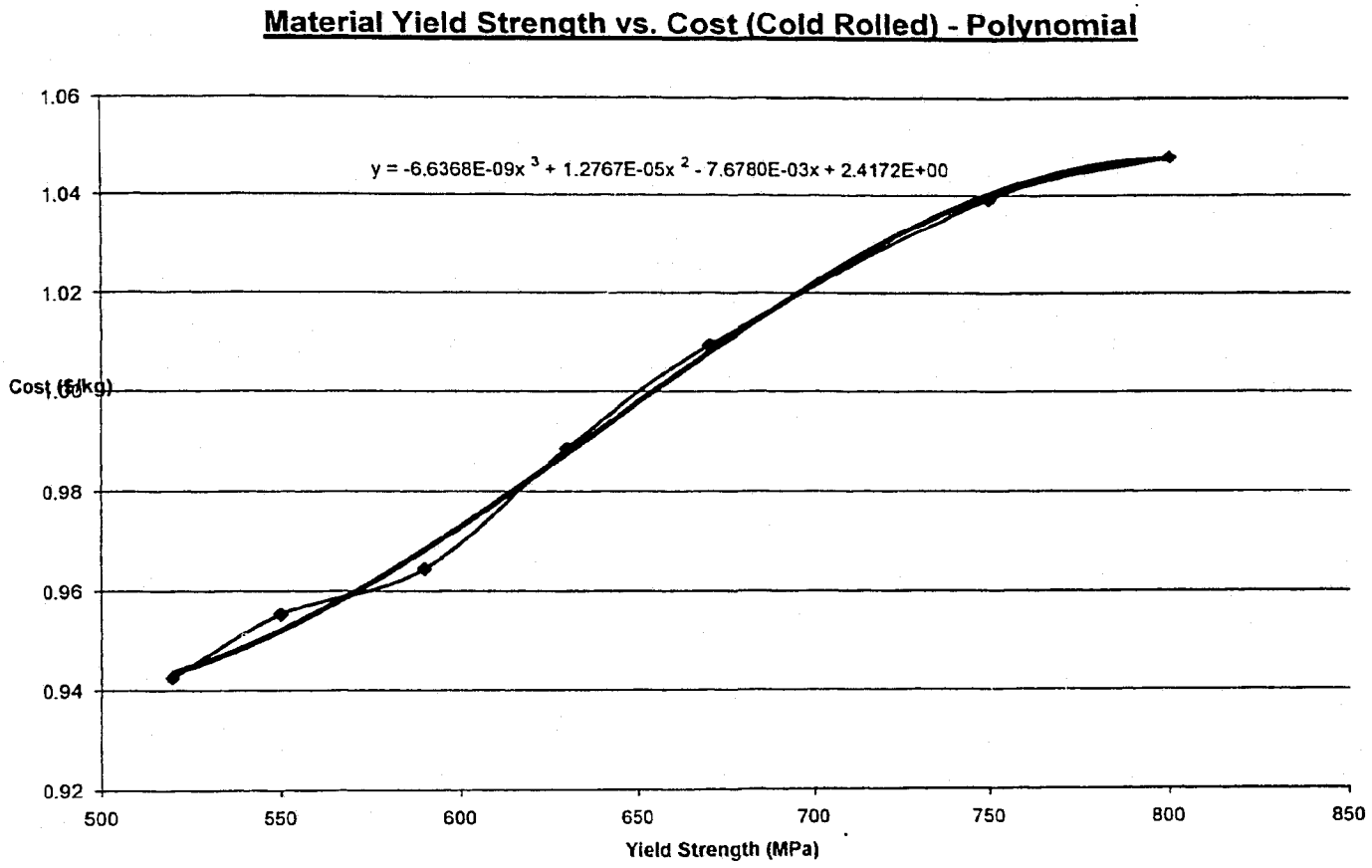

Figure 3.14 – Best Fit Function for Cold Rolled Steel Model

3.4.2 Implementing the Cost Function into the MDO

Now that a best fit function has been created, it can be implemented into HyperStudy. Each component gets a cost response, and there is a total cost response which is just the addition of all the component cost responses. The total cost response is the objective function which will be minimized. An example of the cost response for one component is as follows:

$$\left(\rho_{steel} \times th_{comp} \times area_{comp}\right) \times f_{cost}(dv) =$$
$$\left(7.85e^{-6} \times m\_i\_patch1\_th \times 694.445\right) \times \ldots \quad (3.3)$$
$$\left(-6.6368e^{-9} \times dv^3 + 1.27e^{-5} \times dv^2 - 7.6780e^{-3} \times dv + 2.4172\right)$$

The first part of the function is the density of the material (ρ_{steel}, which is constant) multiplied by the area of the component ($area_{comp}$, which is constant) and thickness of the component (th_{comp}, which is a design variable). The second half of the equation is the function derived from the graph in Figure 3.14. The variable *dv*, is the material design variable (or yield strength) for that component in MPa.

Therefore, the minimization process is outlined as follows:

- The program will try to minimize the mass/cost by reducing the gauge thickness of the component.
- As the thickness drops, the maximum stress of that component goes up and so does the material yield strength via equation (3.2).
- As the yield strength goes up, so does the cost via the best fit function from equation (3.3).
- The program must find a balance between the two conflicting variables as well as meet all the other constraints.

3.4.3 Cost Optimization Problem Description

Objective = minimize total cost

Subject to:

- forces and boundary conditions (same as iteration 2)
- 1st natural frequency > 31.4 Hz

- Max stress of any component < 50 MPa
- Weld constraint optimization (equation 3.1)
- Material selection optimization (equation 3.2)

3.4.4 Results and Discussion

The results for the total cost of the plate can be seen in Figure 3.15. The mass, thicknesses, stresses, and yield strengths behaved almost exactly the same as in the optimization of the plate in iteration 2. This means they followed the same trends in the graphs.

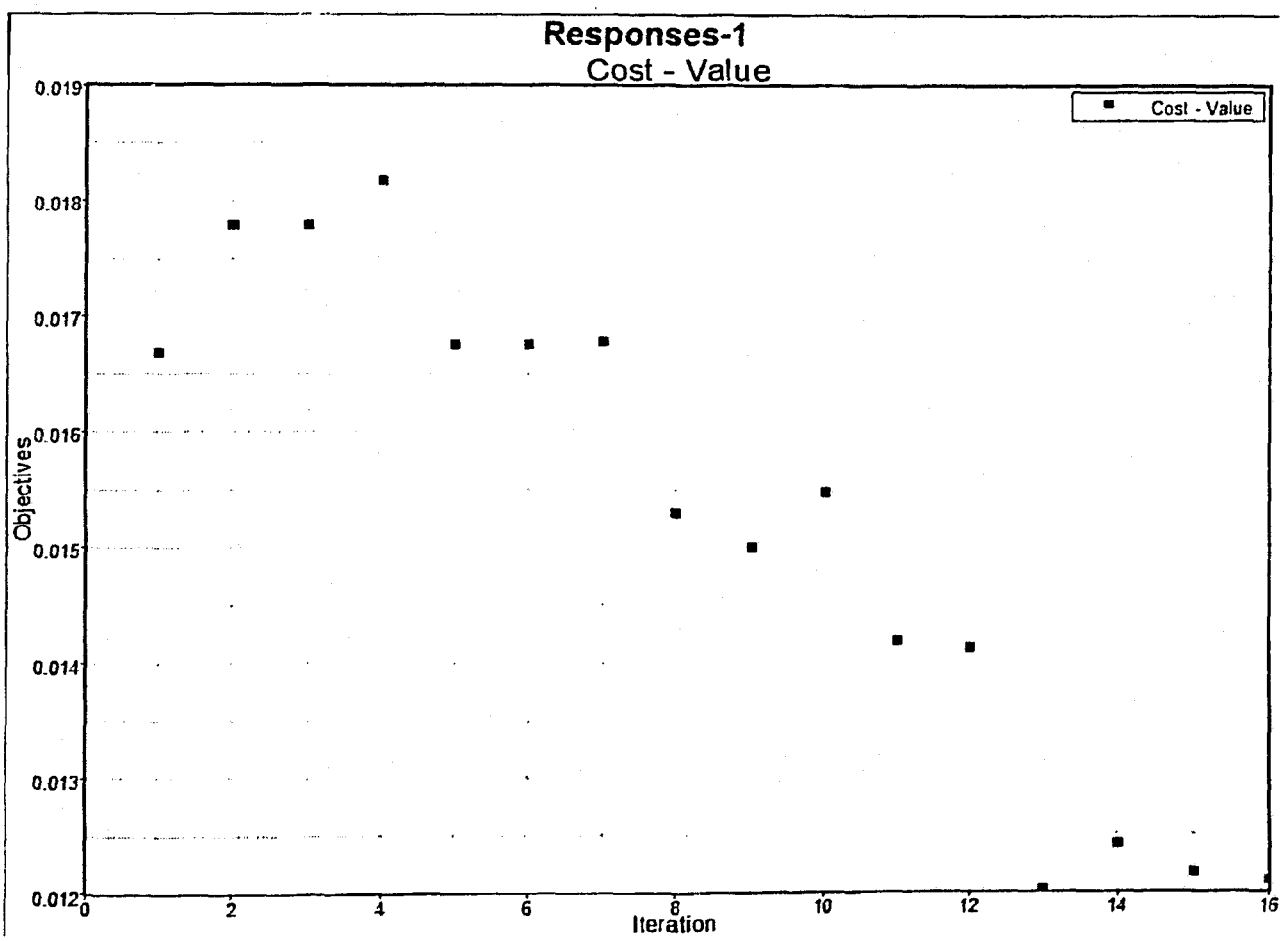

Figure 3.15 - Total Cost of the Plate (Dollars vs. Iteration #)

The cost of the plate was minimized from $\$1.675e^{-2}$ to $\$1.225e^{-2}$, a 27% reduction. Although the cost of the plate is less than 1 cent, this optimization was done as a step to prove that the cost optimization technique works properly. All these techniques, weld, material, and cost optimizations can now be applied to a large model.

So, following the flow in Figure 3.13, all the techniques again worked together. Now it is time to proceed to iteration 4 and use these new techniques on a large model.

Chapter 4

MDO of a Radiator Support Structure

4.1 Introduction

Chapter 4 finalizes the MDO procedure using a model of a radiator support structure from the automotive industry. The previous techniques from Chapter 3 will be applied, and a few new additions to the procedure are also discussed.

4.2 Design Procedure – Iteration 4

The flow chart for iteration 4 can be seen in Figure 4.1. Following the flow from the model of the radiator support, first, a topology optimization was done followed by all the other optimizations that were introduced in Chapter 3. But before the discussion, the new model must be introduced.

4.2.1 Radiator Support Structure Model Description

The model of a radiator support and the front end of a pickup truck can be seen in Figure 4.2. However, the radiator support structure that will be optimized is only one part of this model. The radiator support in Figure 4.3 is located at the front of the vehicle and underneath the hood. It is connected to the other structures via various spring, welds, and bolts. During optimization, the entire model must be used and not just the radiator support structure by itself. Doing so would put the radiator support outside its proper environment, and the results could not be used.

Evolution of Multidisciplinary Design Optimization (including Cost) – Iteration 4

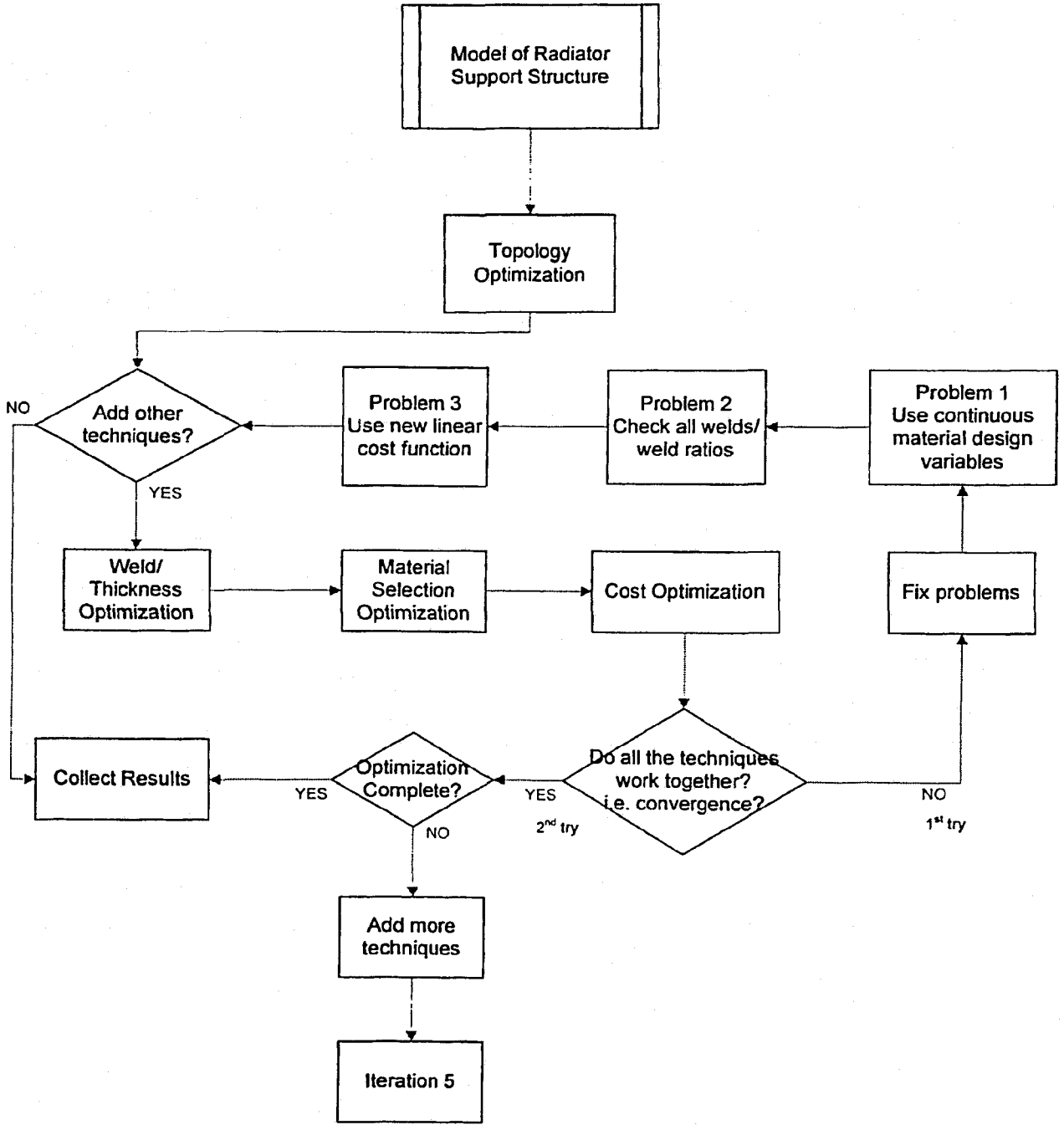

Figure 4.1 - Evolution of Design Procedure - Iteration 4

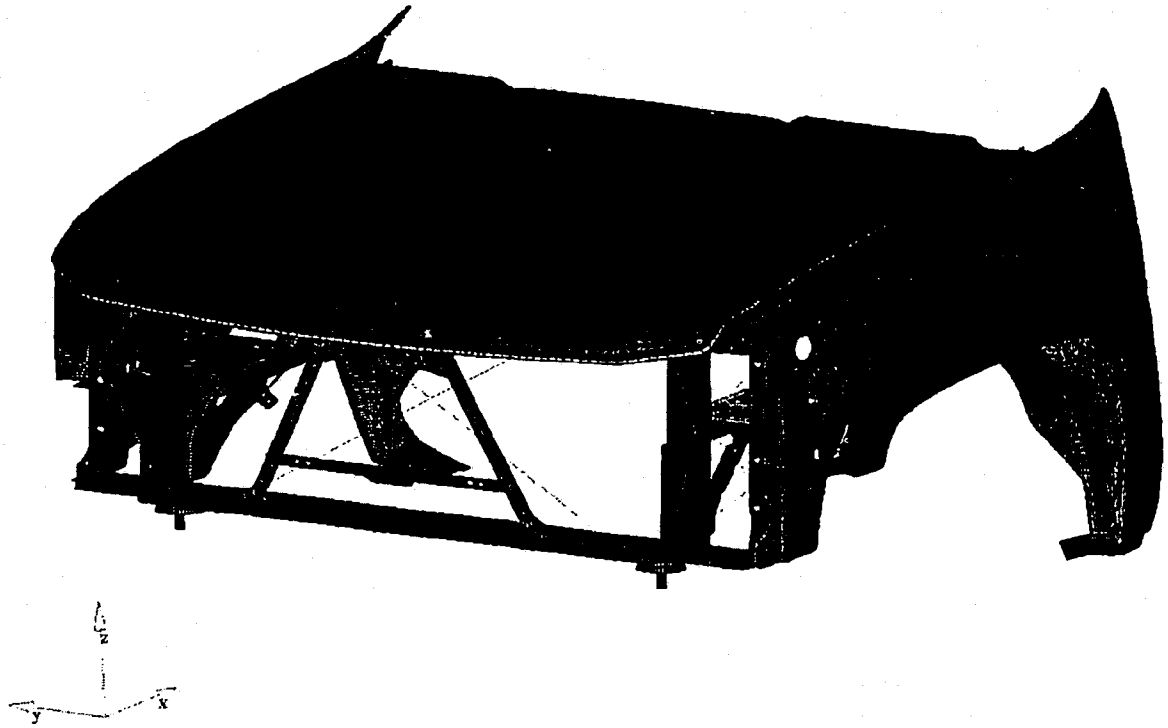

Figure 4.2 - Large Model Including Radiator Support Structure [40]

This model consists of 185024 nodes, and 183227 elements. It also uses 8 different materials for all of the 78 components.

4.2.2 Topology Optimization Problem Description

Figure 4.3 shows the radiator support before optimization. Non-design areas were created around the holes and where different parts are welded together, so that the optimization algorithm would leave these connection areas alone; the same as was done in Section 3.2.1 with the bracket model. The radiator support by itself contains 61910 nodes with 59624 shell elements. It also has 16 components and uses 1 material model for steel, which has the following properties: $E = 210$ GPA, $\upsilon = 0.3$, and $\rho = 7850$ kg/m^3.

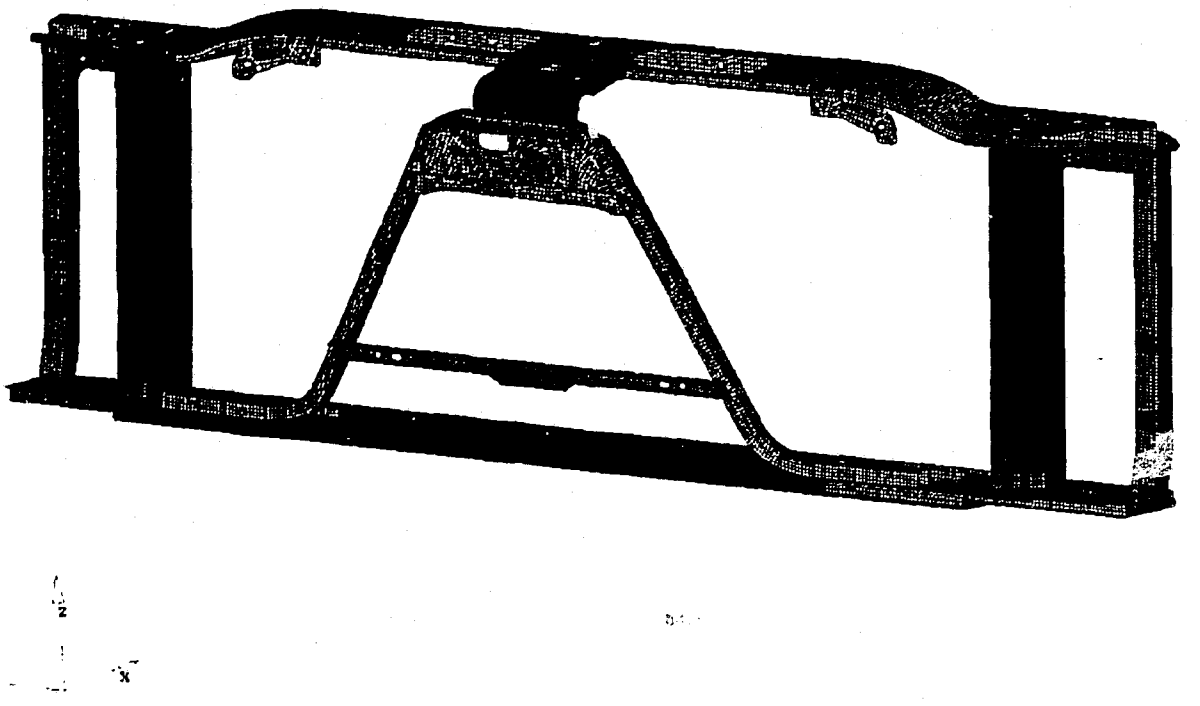

Figure 4.3 - Radiator Support Structure before Topology Optimization

The topology optimization problem description is below:

Objective = minimize mass

Subject to:

- All force and boundary conditions
- 1st natural frequency > 11.8 Hz
- 2nd natural frequency > 16.1 Hz

4.2.3 Topology Optimization Results

The resulting element densities are shown in Figure 4.4. Blue areas are areas of low element density and can be removed if needed without violating the constraints. Areas of red and other colours must be kept to satisfy the constraints.

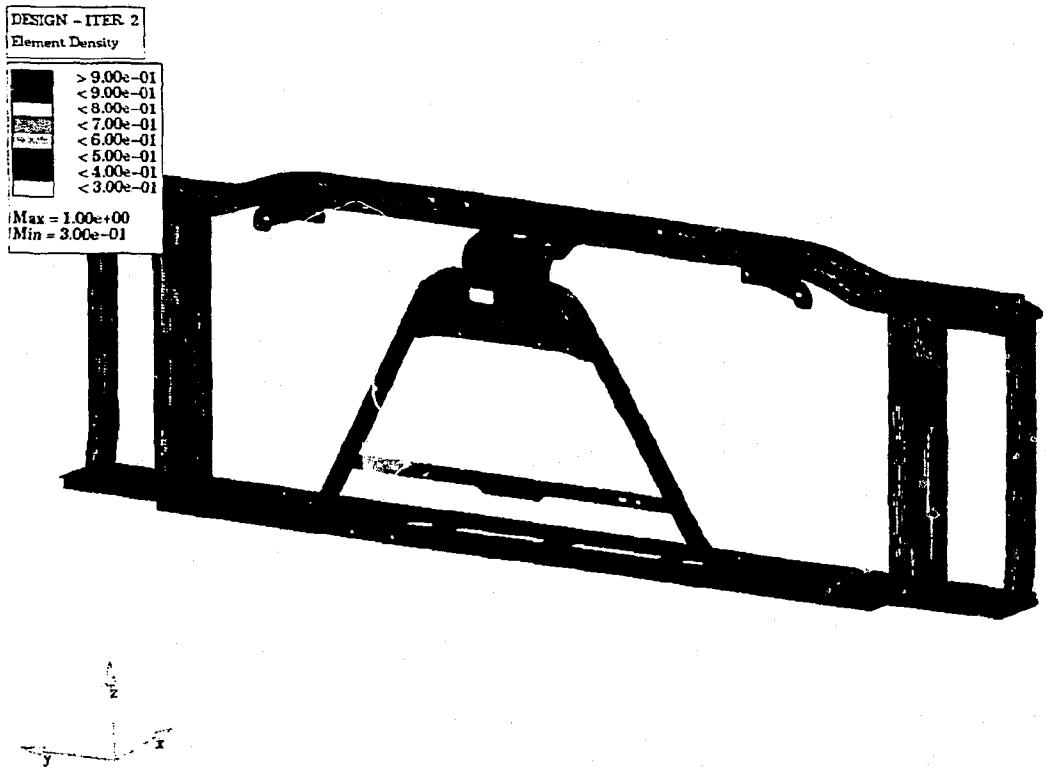

Figure 4.4 - Element Density Results

Figure 4.5 and 4.6 show (circled in red) where material was removed from the upper tie bar and inner post, respectively, in an effort to minimize the mass of the structure. There are no specific guidelines for removal of material, except for that the density of the elements being removed must be the lowest, and symmetry should be kept.

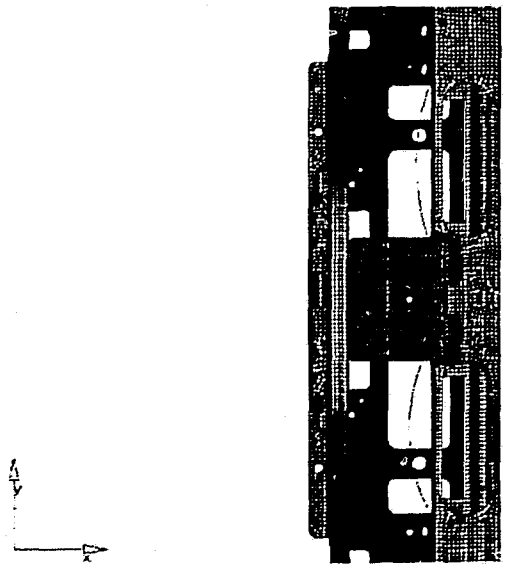

Figure 4.5 - Upper Tie Bar Cut-outs

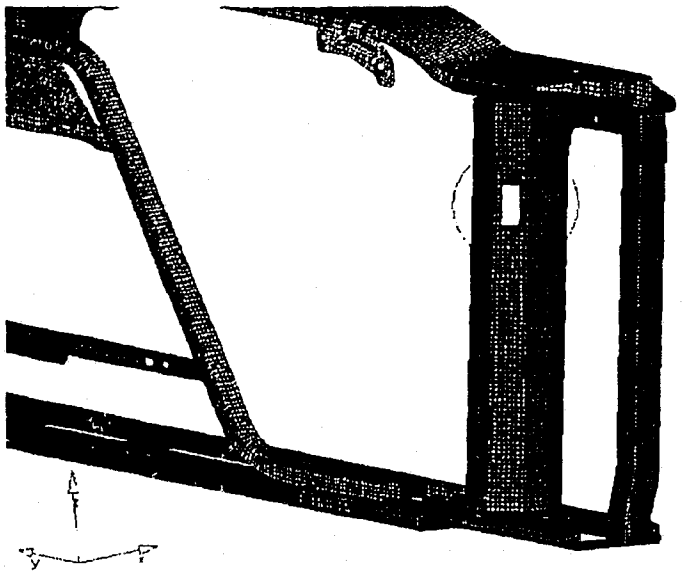

Figure 4.6 - Inner Post Cut-outs

After the cut-outs were complete, the model is run again to see that the constraints were not violated. As it turns out, they were not.

The mass of the structure was reduced from 11.957 kg to 11.630 kg, this is a 3% savings in mass. After the topology optimization, all the previously discussed techniques are added to the model and an optimization was run to minimize the total cost of the radiator support. However, moving along the flow chart in Figure 4.1 to the decision block, as a first try, the model did not converge with all the optimization techniques that were included. There were a few problems that had to be fixed first.

4.2.4 Problem 1 – Continuous Material Design Variables

As was mentioned in the plate case above, the material design variables were chosen from a discrete list of yield strengths. This is not possible with the larger model. As was seen above, the radiator support consists of 16 components. Each component

gets the same list of yield strengths from Table 3.4 column 2 – Altered Yield Strengths. As it turns out, there are too many discrete variables and, therefore, too many combinations of variables for HyperStudy to handle. Therefore, the design variables all must be converted to continuous. By doing this, the combination of material design variables is greatly reduced, and the program can proceed.

4.2.5 Problem 2 – Weld Responses

Each set of components that are welded together have a weld ratio response that will have an upper and lower constraint set on it. In this case, there were repeat responses. Say material A is welded to B, then there is a response of thickness A over thickness B. However, in some cases there was a repeat of a thickness B over thickness A response that is not needed. All of these repeat responses were found and eliminated.

4.2.6 Problem 3 – Polynomial Cost Function

The polynomial cost function used for each component caused minor problems, and was therefore replaced with a more streamlined linear cost function. As can be seen in Table 4.1, the results that the linear function produces are only slightly off from the actual cost. However, the benefit lies within the expression itself.

Table 4.1 – Comparison of the Two Cost Functions

Line of Best Fit	Results (CR Steel)		
Yield Strength	Cubic Polynomial	Linear	Actual Cost
(MPa)	($/kg)	($/kg)	($/kg)
520	0.94	0.94	0.94
550	0.95	0.95	0.95
590	0.97	0.97	0.96
630	0.99	0.99	0.99
670	1.01	1.00	1.01
750	1.04	1.03	1.04

Figure 4.7 shows a graph of the linear function as cost vs. yield strength, which was created from Table 4.1. The linear function is: $y = 3.9759e^{-4}x + 7.3630e^{-1}$, where the linear function only needs to execute two mathematical operations, the cubic polynomial $y = 6.63e^{-9}x^3 + 1.27e^{-5}x^2 - 7.68e^{-3}x + 2.42$, has to execute 12. The linear function is an obvious time saver, and easier to input from the user's standpoint. Furthermore, it does not compromise the end result to a great degree.

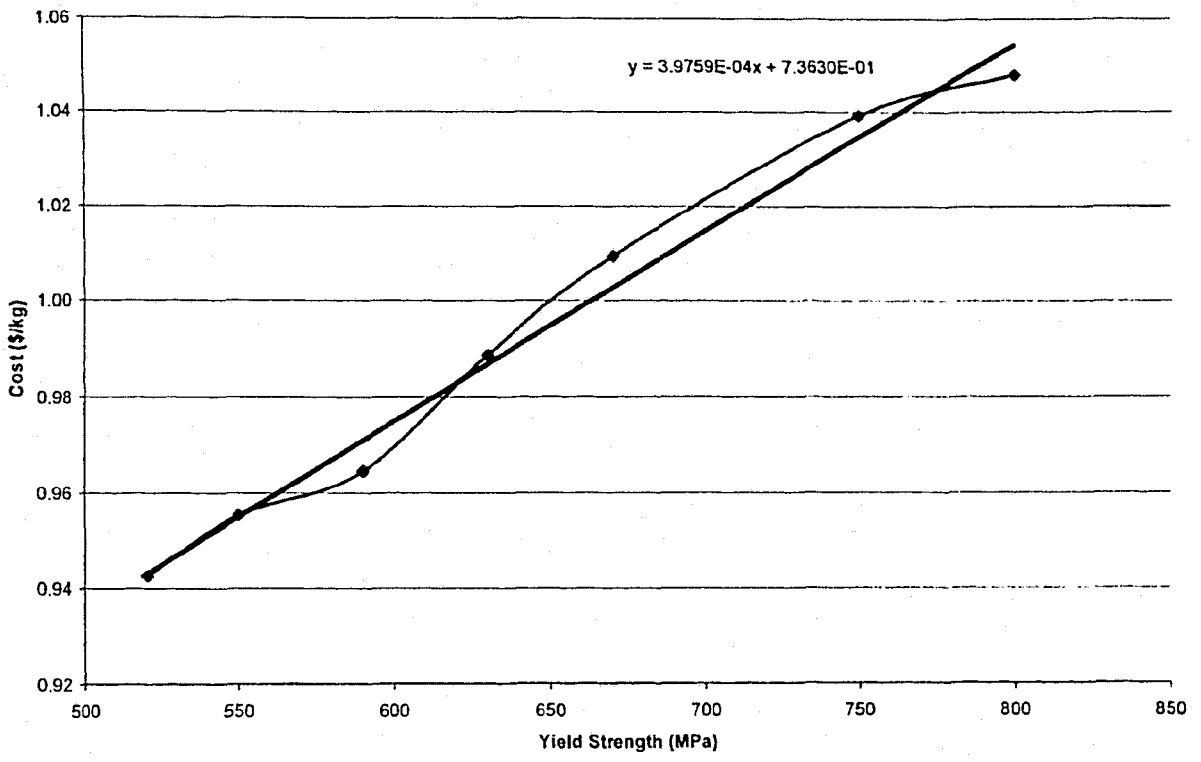

Figure 4.7 - Linear Cost Function

4.2.7 Cost Problem Optimization Description (1st Trial)

Once the model has been modified using the results of the topology optimization, and all the above problems are fixed, the multidisciplinary optimization can take place. This is done using Altair HyperStudy with MSC-NASTRAN due to the fact that there is stress, natural frequency, and other constraints present at the same time. The problem description is as follows:

Objective = minimize total cost

Subject to:

- All force and boundary conditions
- 1st natural frequency > 11.8 Hz
- 2nd natural frequency > 16.1 Hz

- Weld constraint optimization (equation 3.1)
- Material selection optimization (equation 3.2)
- Maximum stress of any element < 800 Mpa

4.2.7.1 Parameter Matrix of Constraints

All of the above constraints can be found in the so called Parameter Matrix of Constraints. This matrix lists the natural frequency, and stress constraints and can be seen in Appendix A. Notice, that there are two subcases for the stress constraints.

Subcase 103 and 106 are two different static stress models. One subcase models the left front wheel falling into a pot hole, and the other models the right side. This is a worst case scenario for the front end of the vehicle, and more specifically the radiator support. Both must be used at the same time along with a natural frequency model to determine the proper solution.

The matrix of constraints also lists and labels the upper and lower weld constraints and indicates which parts are welded to each other.

4.2.7.2 Design Parameter Matrix

Another important set of matrices are the Design Parameter Matrices. These matrices can be seen in Appendix B. These matrices contain all the relevant information that belongs to the model*. Each component is listed along with its material yield strength and gauge for that iteration. Furthermore, the component's area, volume, mass, maximum stress, and maximum stress element number for both subcases are included.

* The three models' (stress 103, stress 106, and NVH) thicknesses are linked together in HyperStudy

This information is needed to setup the various responses such as cost, and stress. The Design Parameter Matrix for the initial model is used to set up all the problems in this Chapter. A parameter matrix can be created for each design iteration, and by looking at various iterations the matrices can be quickly compared to show how the design is improving or not. The matrices for each iteration can be found in Appendix B.

4.2.8 Results and Discussion (Trial 1)

The optimization took approximately 24 hours and 53 iterations to complete. The most important result of this optimization is the cost. The total cost of the radiator support was minimized from $9.86 to $8.99. After the gauges are rounded up to proper gauge sizes, the model is run again to check that the constraints are not violated. Now, the cost increased only slightly to $9.00, this is still savings of $0.86 or 9%. The results of this iteration can be seen in Appendix A, HyperStudy MDO Results (Trial 1). The gauges must be rounded off to the nearest five-hundredth, (0.05) this is called the user gauge in results matrices in Appendix B. This is done since the gauges that HyperStudy provides are to four decimal places and are not practical. It would cost too much money to make these gauges so precise. Figure 4.8 is the graph of the Total Cost of the radiator support structure per iteration, and it shows that the cost was indeed minimized.

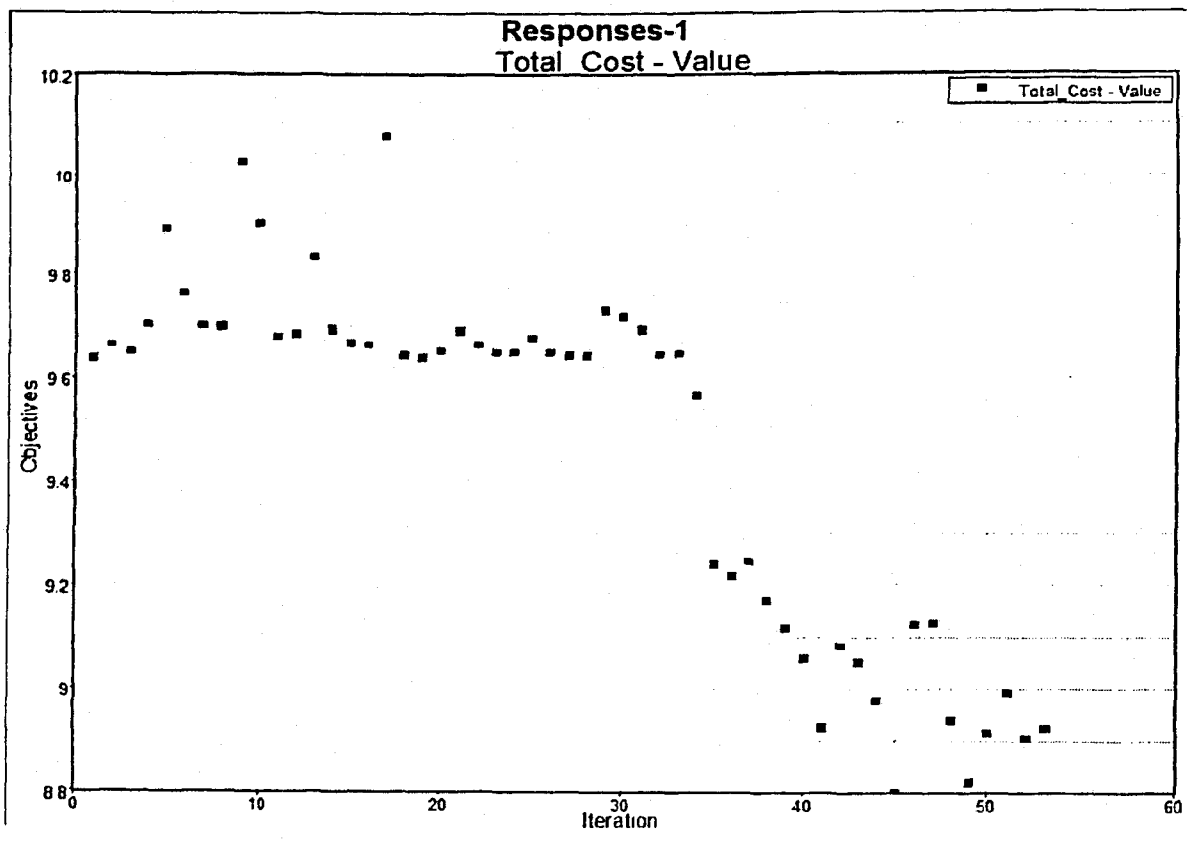

Figure 4.8 - Total Cost of the Radiator Support (Dollars vs. Iteration #)

Furthermore, the above mentioned matrix (HyperStudy MDO Results (Trial 1)) also shows the HyperOpt, and User yield strengths. The yield strengths during the optimization were continuous and did not fall into the list of discrete yields like in the plate example. Therefore, the User must make the decision and chose the next highest yield above the HyperOpt yield from the discrete list. This must be done before the final cost is calculated since the cost function depends heavily on the yield strengths.

Figure 4.9 shows how the total mass of the radiator support decreases throughout the optimization. Most of the component gauges decreased, but some component gauges increased. An increase in gauge thickness occurs because of the fact that several other component gauges around it are decreasing then it has to increase to keep that part of the

structure strong and within the constraints. This may seem odd, but the end result is a cheaper and lighter structure that is just as strong as the original.

Therefore, since all the techniques worked together on the second try after all the problems had been fixed, and the results are acceptable; the flow in Figure 4.1 now proceeds to the 5th and final iteration.

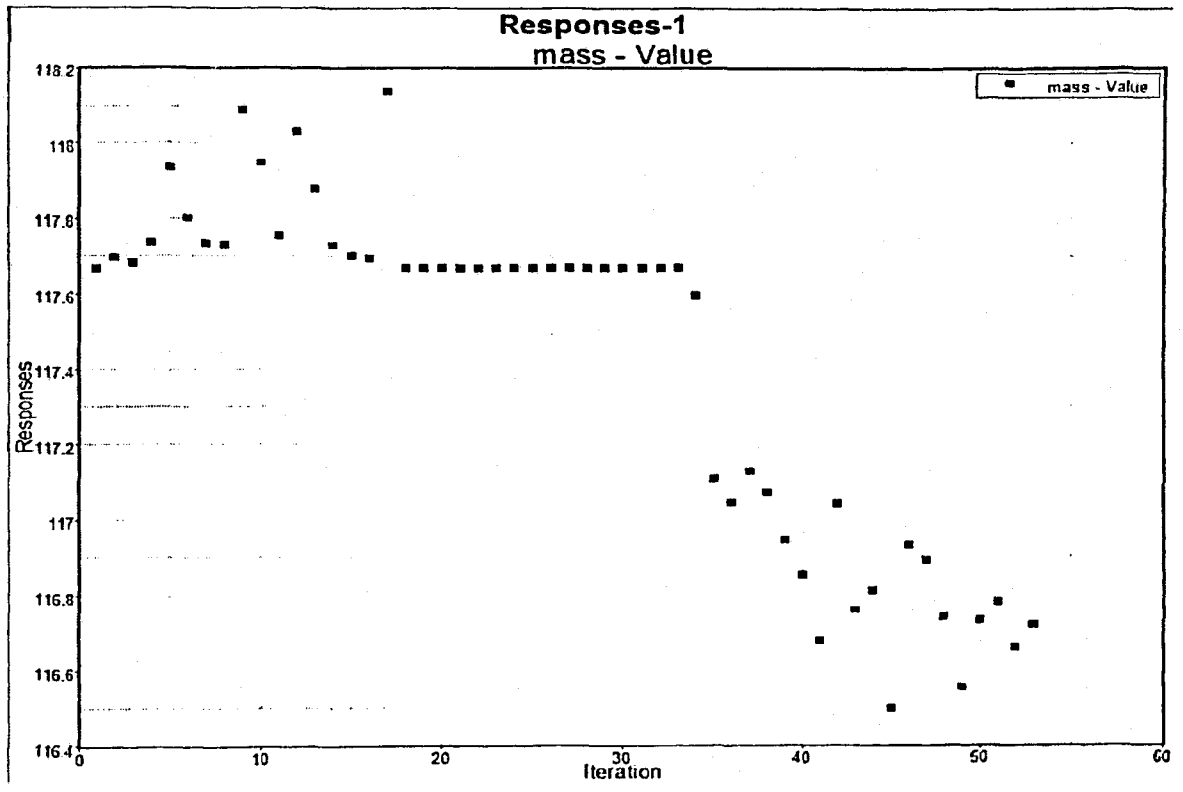

Figure 4.9 - Total Mass of the Radiator Support (kg vs. Iteration #)

4.3 Design Procedure - Iteration 5

The flow chart for iteration 5 can be seen in Figure 4.10. It is an extension of iteration 4 with the addition of two new trials of the optimization techniques, a new hot rolled steel model, and now the results are collected and verified by a MATLAB program, not by the user.

Evolution of Multidisciplinary Design Optimization (including Cost) – Iteration 5

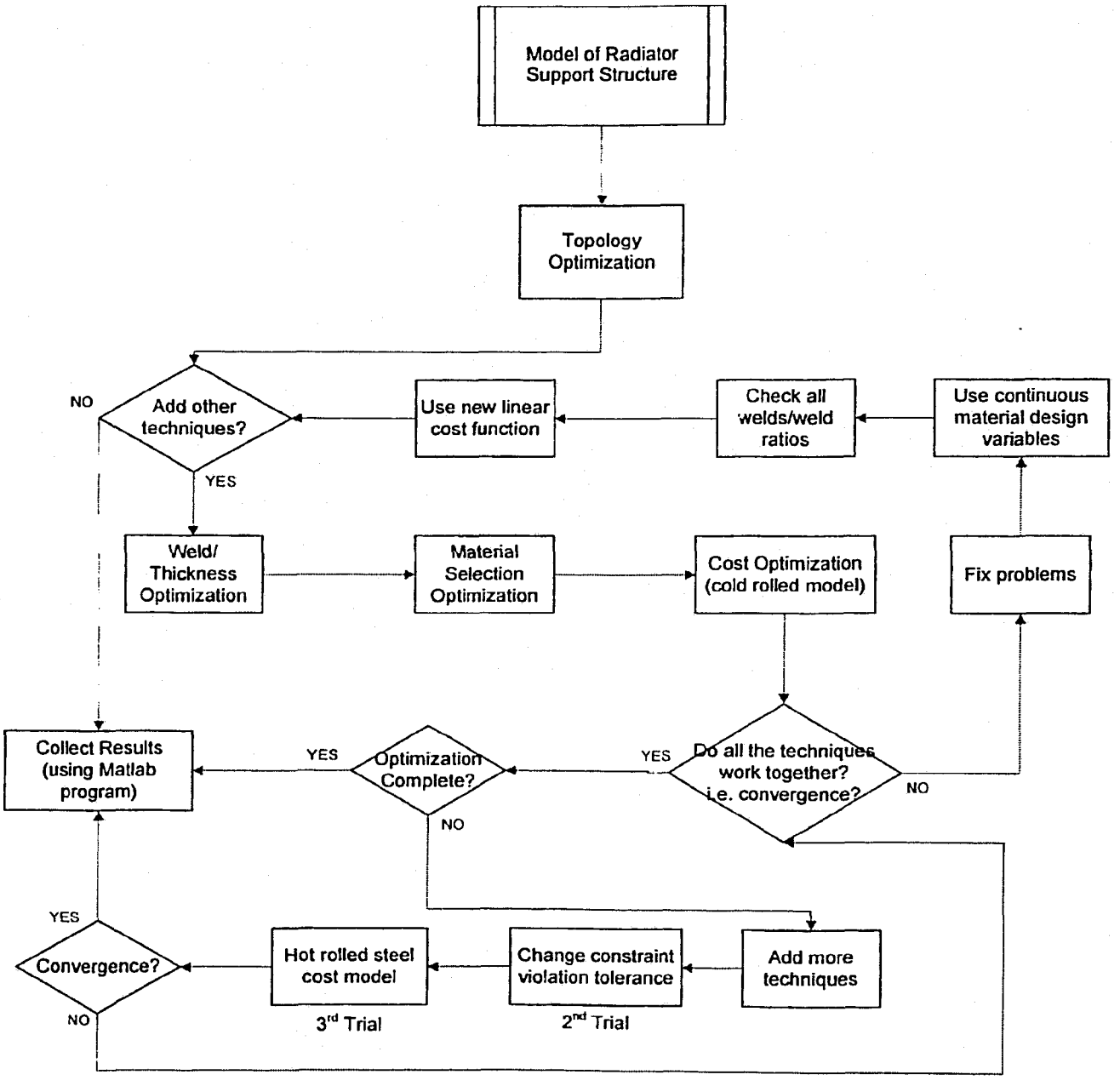

Figure 4.10 - Evolution of Design Procedure - Iteration 5

4.3.1 Cost Problem Optimization Description (Trial 2)

Trial 2 has almost the exact same problem description as the previous example except for one minor change. One of the optimization parameters, called the constraint violation tolerance, is modified from 0.5% to 0.25%. This means that any constraint is allowed to be violated by 0.25%. So, if the maximum stress allowed is 800 MPa, then it is allowed to reach 802 MPa, for the sake of the program. This helps HyperOpt find a solution and keeps the problem from being extremely rigid. The bigger the violation tolerance, the easier to find a solution, and therefore will take less iterations to complete. By lowering the tolerance, the program is forced to find a more rigid solution, which takes more iterations. Furthermore, a solution with a lower tolerance may not even exist. The problem description is as follows:

Objective = minimize total cost

Subject to:

- All force and boundary conditions
- 1^{st} natural frequency > 11.8 Hz
- 2^{nd} natural frequency > 16.1 Hz
- Weld constraints (see Appendix A, equation 3.1)
- Material selection (see equation 3.2)
- Maximum stress of any element < 800 Mpa
- Constraint Violation Tolerance = 0.25%

4.3.2 Results and Discussion (Trial 2)

This trial of the radiator support model optimization took approximately the same amount of time (24 hours) as Trial 1 but more iterations (58), as was expected when the constraint violation tolerance was lowered. The total cost and mass per iteration of the structure are shown in Figures 4.11 and 4.12.

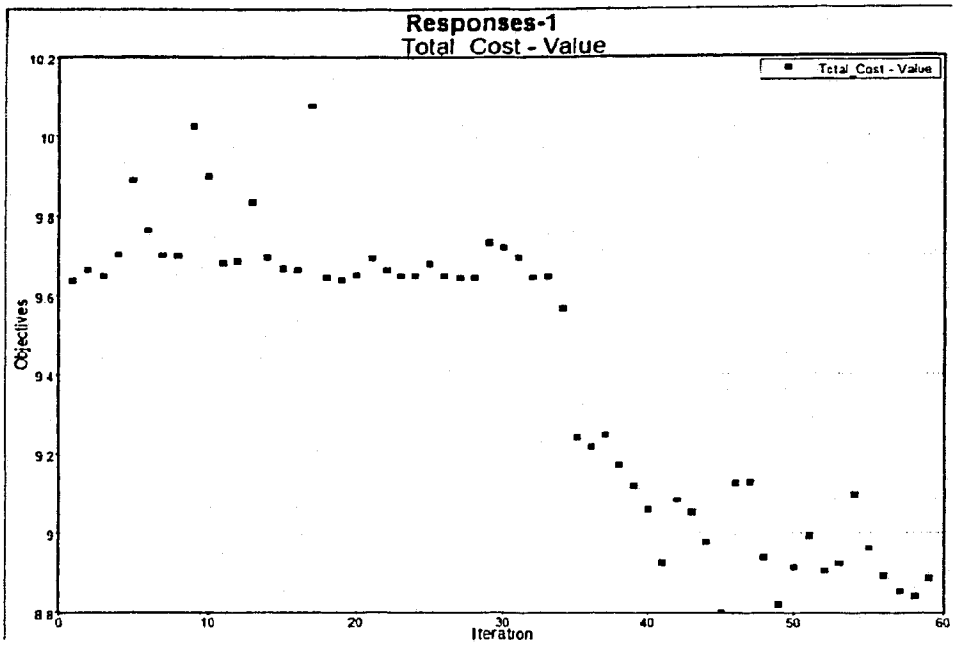

Figure 4.11 - Total Cost of the Radiator Support (Dollars vs. Iteration #)

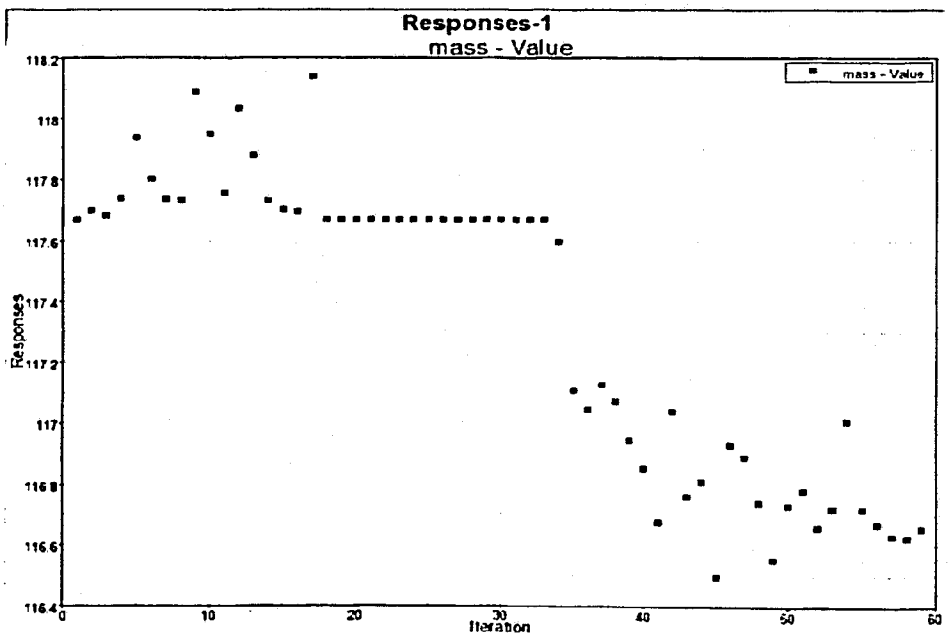

Figure 4.12 - Total Mass of the Radiator Support (kg vs. Iteration #)

The total mass of the radiator support was reduced from 11.630 kg to 10.889 kg. After the user rounds the gauges off to the proper dimensions and reruns the model to check the constraints, the mass increases to 11.284 kg, which is a 5.63% positive change. All the constraints were met with the new gauge sizes.

Furthermore, the total cost was reduced from $9.86 to $8.89 by HyperOpt. However, after the model's gauges were fixed, the cost increased to $9.25, only a 6.3% positive change. This price is $0.25 more expensive than the previous trial that has a constraint violation of 0.5%. The reason is that this model, with the more strict violation tolerance, ends up using more expensive and higher yield strength materials. So, even changing the gauge size slightly, as was done by the user to eliminate the HyperOpt values, will increase the price by a lot. This can be seen in the Appendix B – HyperStudy MDO Results (Trial 1 & Trial 2). The mass of the user model in Trial 1 is 11.362 kg, and the user mass in Trial 2 is 11.284 kg. The mass of the Trial 2 model is less but the total cost is more. This proves that the Trial 2 model uses more expensive materials.

4.3.3 Hot Rolled Steel Cost Model

The hot rolled (HR) steel model directly follows the footsteps of the cold rolled model discussed above. The only differences are the cost for specific gauges and yields, and the range of gauges available.

Table 4.2 displays the base price for different gauge sizes, and Table 4.3 displays the costs for each specific yield. These tables were derived from the GM Material Database [41] which can be found in Appendix C.

Table 4.2 – Base Price for Specific Gauges

HOT ROLLED – Pickled and Oiled	(SPEC. - 1008, GM6409M, SAE-J2329, AND GMW2M-ST-S HR)	
	Metric (mm)	Dollars per Ckg
Sheet Width	600 x 800	
Gauge	1.49 and under	74.36
	1.50 to 1.79	71.94
	1.80 to 2.29	70.42

Table 4.3 – Price for Specific Yield

HOT ROLLED	High Strength Low Alloy
Yield Strength (MPa)	Dollars per Ckg
270	6.95
300	7.94
340	8.11
380	8.70
420	9.59
500	14.83
550	15.45

The final cost matrix can be seen in Table 4.4. Figure 4.13 is the graph that is created using the yield strength and final cost per kilogram columns. The line of best fit for this model can also be seen in Figure 4.13; it is a 4^{th} order polynomial. The results of using a 4^{th} order polynomial and a linear line of best fit are compared in Table 4.5. As can be seen, the 4^{th} order polynomial is exact to two decimal places whereas the linear function is slightly off, therefore the polynomial was used in the implementation of the hot rolled model into HyperStudy. A graph of the line of best fit for HR can be seen in Appendix C.

Table 4.4 – Final Cost Matrix for Hot Rolled Steel

Material: CQ [HR-1] Hot Rolled - 600 x 800 mm sheet - High Strength Low Alloy					
Yield Strength (MPa)	Altered Yield (MPa)	Price for Specific Yield ($/Ckg)	Average Base Price ($/Ckg)	Final Cost ($/Ckg)	Final Cost ($/kg)
270	520	6.95	72.24	79.19	0.792
300	550	7.94	72.24	80.18	0.802
340	590	8.11	72.24	80.35	0.804
380	630	8.70	72.24	80.94	0.809
420	670	9.59	72.24	81.83	0.818
500	750	14.83	72.24	87.07	0.871
550	800	15.45	72.24	87.69	0.877

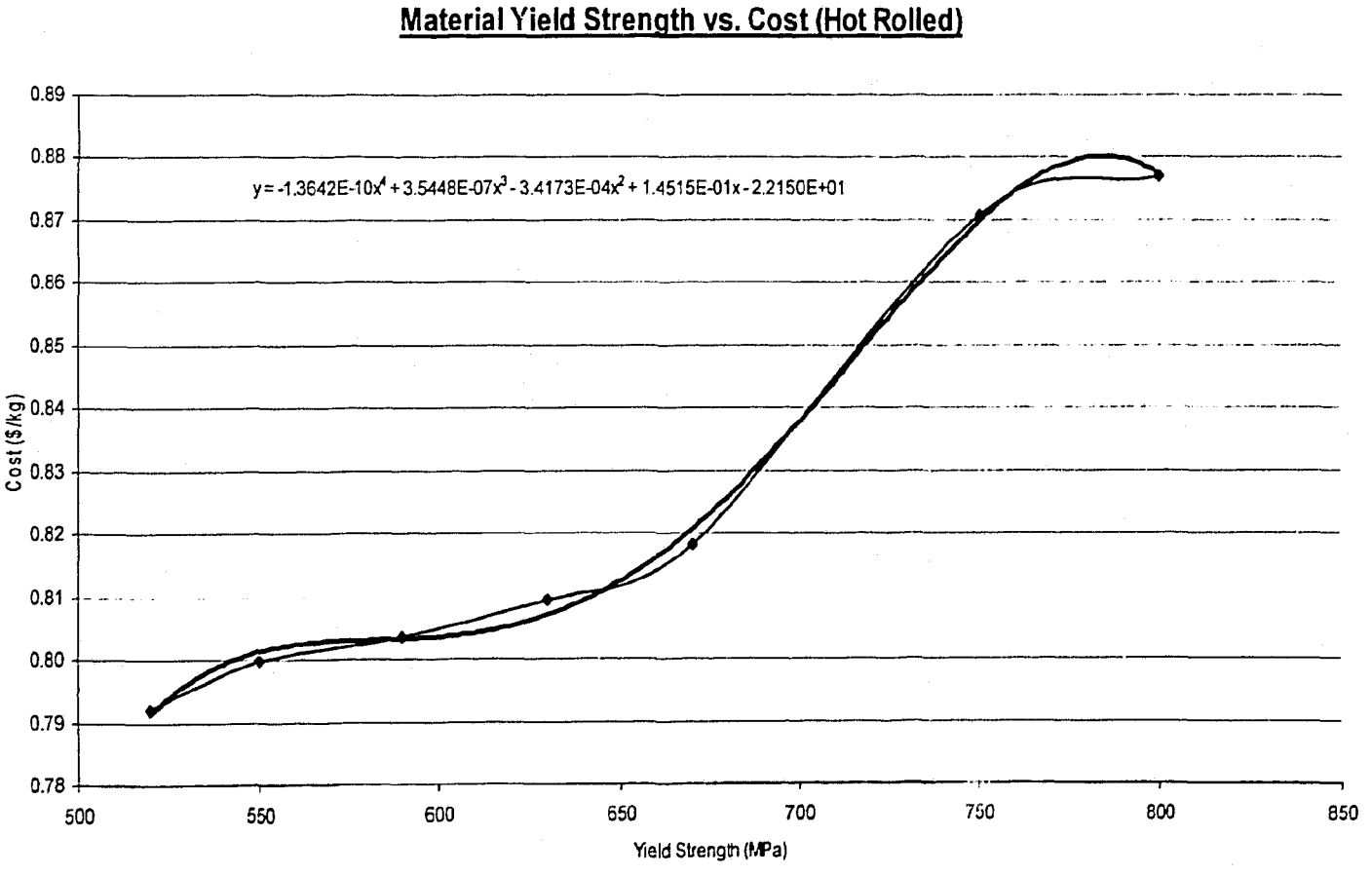

Figure 4.13 - Best Fit Function for Hot Rolled Model

Table 4.5 – Comparison of Line of Best Fit Functions

Yield Strength (MPa)	4th Order Poly Cost ($/kg)	Linear Cost ($/kg)	Actual Cost ($/kg)
520	0.79	0.78	0.79
550	0.80	0.79	0.80
590	0.80	0.81	0.80
630	0.81	0.82	0.81
670	0.82	0.83	0.82
750	0.87	0.86	0.87
800	0.88	0.87	0.88

4.3.4 Implementation of Hot Rolled Cost Model

The hot rolled model was implemented slightly different than the cold rolled model. It was not used alone, but in conjunction with the cold rolled model. Furthermore, it was only used on 4 components; it is easy to see why by looking at Table 4.2. The thinnest gauge available from the hot rolled steel equals to 1.5 mm, and only 4 components (the reinforcement strap, lower tie bar 1.9, end cap, and the reinforcement lower tie bar) had a gauge thickness over or close to 1.5 mm. All the other components must use the cold rolled model to be accurate.

Therefore, the cost response for the 4 components listed above has to be changed. What is done is that each component now has a hot and cold rolled cost response, each using their respective functions. There is also a response for that same component that chooses the minimum cost of the two. This minimum cost is used to help calculate the total cost of the structure.

4.3.5 Cost Problem Optimization Description (Trial 3)

The problem is formulated exactly as Trial 2, except for the inclusion of the hot rolled steel model for the 4 components listed above, and the constraint violation tolerance is back up to 0.5%. The problem description is as follows:

Objective = minimize total cost

Subject to:

- All force and boundary conditions
- 1^{st} natural frequency > 11.8 Hz
- 2^{nd} natural frequency > 16.1 Hz
- Weld constraints (see Appendix A, equation 3.1)
- Material selection optimization (equation 3.2)
- Maximum stress of any element < 800 Mpa
- Constraint Violation Tolerance = 0.5%

4.3.6 Results and Discussion (Trial 3)

Again, the solution took 24 hours, but only 53 iterations. Graphs of the total cost and total mass vs. iteration number can be seen in Figures 4.14, and 4.15. The total mass increased from 11.630 kg to 11.713 kg, but the total cost decreased from $9.86 to $8.92. After running the result files through the MATLAB program (which is explained in the next section) that does the rounding, and checks the boundary conditions, the mass increased again to 11.903 kg. This means only a slight savings in mass from the original model before topography optimization. This increase in mass is due to the slight rounding up of every component's gauge. Also, as was mentioned earlier, to use hot

rolled steel the gauge must be larger than 1.5 mm. The program will more than likely chose the hot rolled cost because it is cheaper, and, therefore, this ensures that the component will have more mass than if cold rolled steel was used. However, the cost was reduced even more to $7.94, which is approximately a 20% savings in cost.

The cost was reduced even more because of the MATLAB program. As will be explained below, sometimes HyperOpt will choose a yield strength that is too high for a component making the cost artificially high when in fact, a material that is cheaper and has weaker yield strength can be used. The MATLAB program ensures that each component has the cheapest material allowed by the stress constraints.

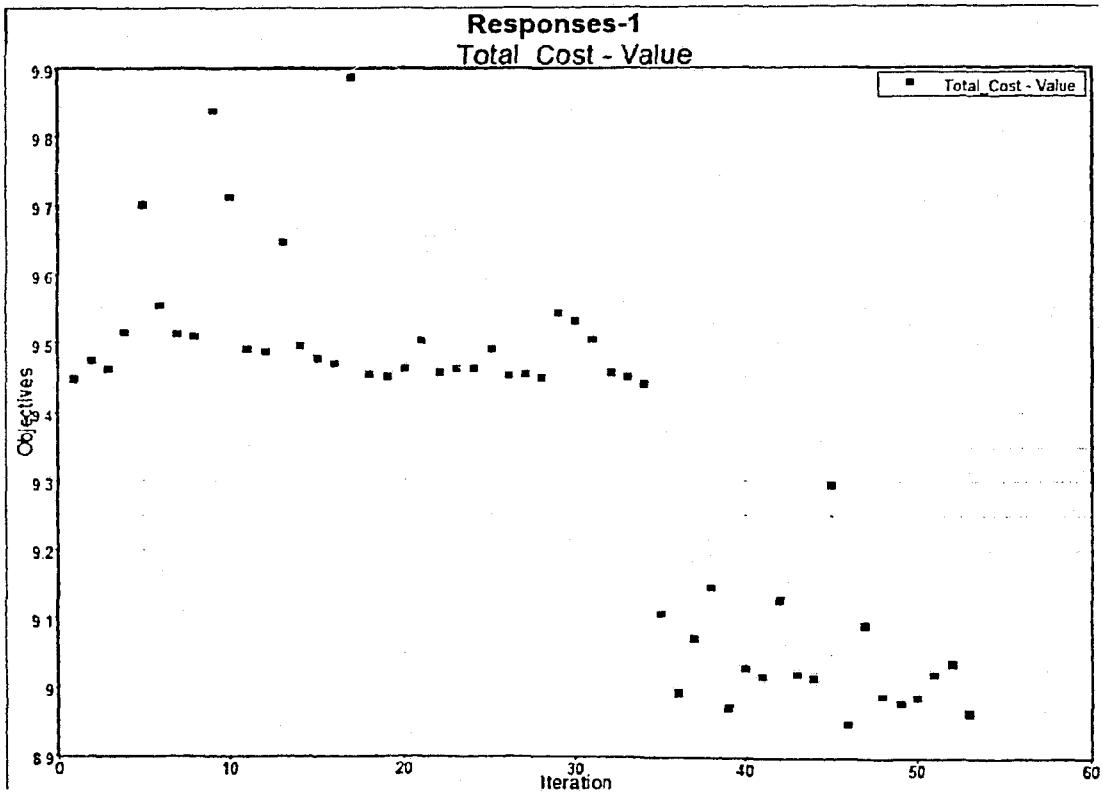

Figure 4.14 - Total Cost of the Radiator Support (Dollars vs. Iteration #)

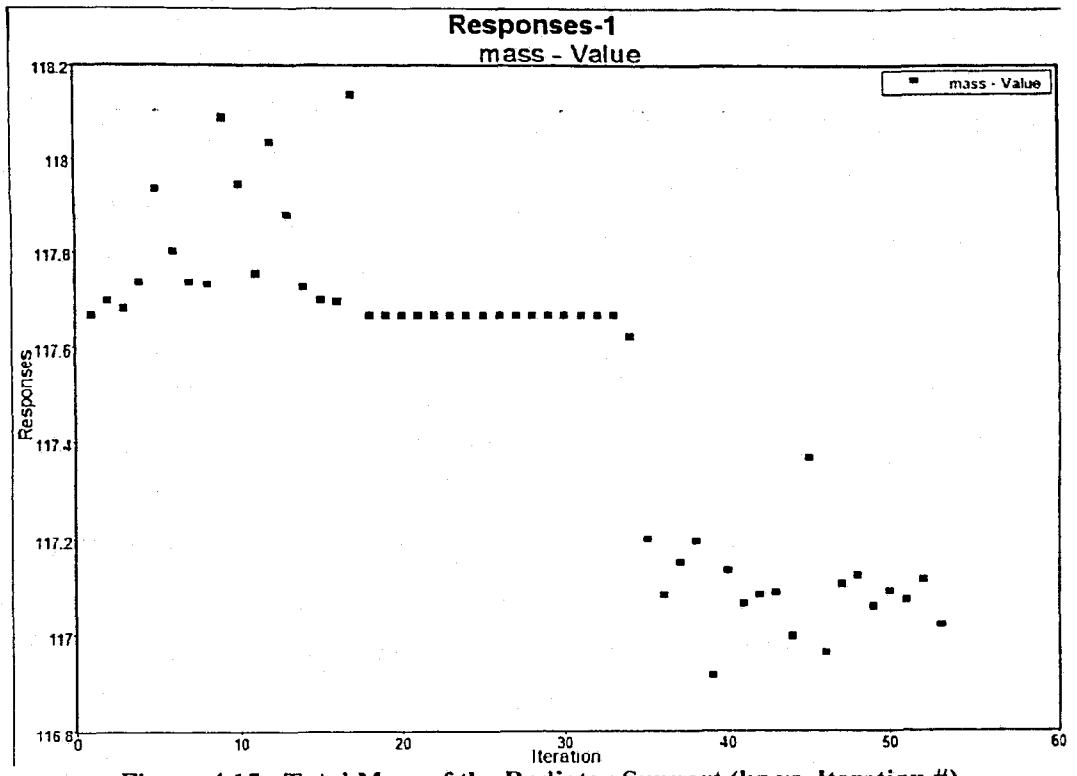

Figure 4.15 - Total Mass of the Radiator Support (kg vs. Iteration #)

As was noted before the cost and mass follow almost the exact same pattern throughout the optimization.

4.4 MATLAB Program

The MATLAB program was developed to assist the user in gathering results after the MDO is complete. It was used in the third optimization (Trial 3) of iteration 5. The program has three main functions: read_thickness(), read_stress(), and read_yields(). The program code and results examples can all be found in Appendix D.

4.4.1 Function read_thickness()

This function does exactly what its name says, it reads the thickness of the each component. First, it opens the correct file (*.dat – MSC-NASTRAN file in this case) and

searches every line for the string 'PSHELL'. This is where the PSHELL component cards are located. Then the program knows the format of the PSHELL card, and reads in every value even though it only needs the thickness. Once the thickness value is read, it is rounded off to the nearest five-hundredth (0.05). Why this is done was mentioned earlier, sheet metal gauges of two decimal places are easier and cheaper to manufacture than ones that are to 4 decimal places. Once the thickness has been rounded off correctly, it is reprinted into the correct spot in the PSHELL card, and is saved to a matrix A, which will eventually house all the results information. The matrix A is arranged with the components as the rows, and all the information needed for each component as the columns. This process is repeated for each PSHELL card, then the altered file is closed. Next, the program runs the data file with the new rounded off thicknesses to get an updated stress results file. Then the next function read_stress() is called. Appendix D contains an example of a PSHELL card that is read and the thickness for each card is marked in bold.

4.4.2 Function read_stress()

The only argument passed to read_stress() is the matrix A. Read_stress() opens the MSC-NASTRAN results file (*.f06) which contains all the displacement and stress values for every node and element. A list of maximum stress elements for each component is read into the program, so it knows which elements to search for. Again, the program has the correct format for reading the stress results, and therefore it only takes the Von Mises stress of each of these elements. The problem is that there are two rows of results for each element and therefore two Von Mises stress results, one for the top side

of the shell element and one for the bottom side (see the example below). The program takes these two stresses and chooses the maximum, and then stores it in the matrix A. This procedure is repeated for each maximum stress element, for each component, and then the file is closed and the final function read_yields() is called. Appendix D contains an example of a few lines that would be read from an MSC-NASTRAN output file. This is for the shell element with ID 4994.

4.4.3 Function read_yields()

This is the final function in the program. It also gets the matrix A passed to it after the read_stress() function is complete. The function first opens the HyperStudy results file (*.hyperopt) which contains the values of all the design variables, and then reads in a list of yield strengths that is created by the user. It is the same yield strengths from the material tables above. Next, a list of design variables that need to found are read in. Then, the function searches for the last run of the optimization (53 in this case) and begins to read in the correct design variables and stores them in matrix A. Next, it checks if the yield value is artificially high or not (this was mentioned in Section 4.3.6) and chooses the correct yield strength that is needed from the list of yields that was read in at the beginning of the function. For each component, the function checks that value of that components design variable (its yield strength) against the maximum stress for that component and chooses the correct yield. These stress values come from the newly updated file and are read from matrix A. For example, if the maximum stress is 384 MPa, then the program would give that component a yield of 520 MPa. However, if the maximum stress was 600 MPa, then the program would input 630 MPa as that component's material yield strength. These new yield strength values are stored in the

final column of matrix A, which is then output onto the screen for the user to note the results. These results can then be input into the parameter matrices using Excel and the actual total cost can be found. The program ends by closing the HyperStudy results file. Appendix D also has an example of a HyperStudy output file that could be read by this function.

The general flow of this program can be used to gather the results from any programs as long as the card formats are read correct, and the list of things to find (elements, cards, design variables) are correct as well.

This concludes the design iterations for the MDO procedure. In the next chapter this procedure is applied to a different type of model.

Chapter 5

MDO of a Wheel Chair Ramp

The next welded structure that is to be optimized is a wheel chair ramp. This particular ramp is designed to fit a Ford Freestar van. The addition of this ramp makes the van wheel chair accessible. For the ramp to be attached, the rear end of the van, plus the inside floor and many other component have to be modified. The ramp is already welded together, and is then welded to the van. After the van is modified, it must be tested to evaluate that it still complies with the government safety standards for front, rear, and side crash situations. This chapter only deals with a rear crash situation which means a moving wall crashes into the van to simulate an SUV hitting the van from behind.

This particular ramp is in use today, however, the manufacturers are looking for help in optimizing the design; mainly minimizing the mass while still meeting the safety standards.

5.1 Model Description

The model shown in Figure 5.1 was created in HyperMesh using the geometry files from the manufacturer [42]. It contains ten components that all have the same thickness of 4.75 mm. The components are welded together, and this is simulated by shell elements, so that topology optimization on the shell elements can be performed. There is one material, steel, that is used for all the components. This steel has a Young's

modulus of 210 GPa, a Poisson's Ratio of 0.3, and a yield strength of 200 MPa. The model contains 20855 nodes and 19985 2D shell elements.

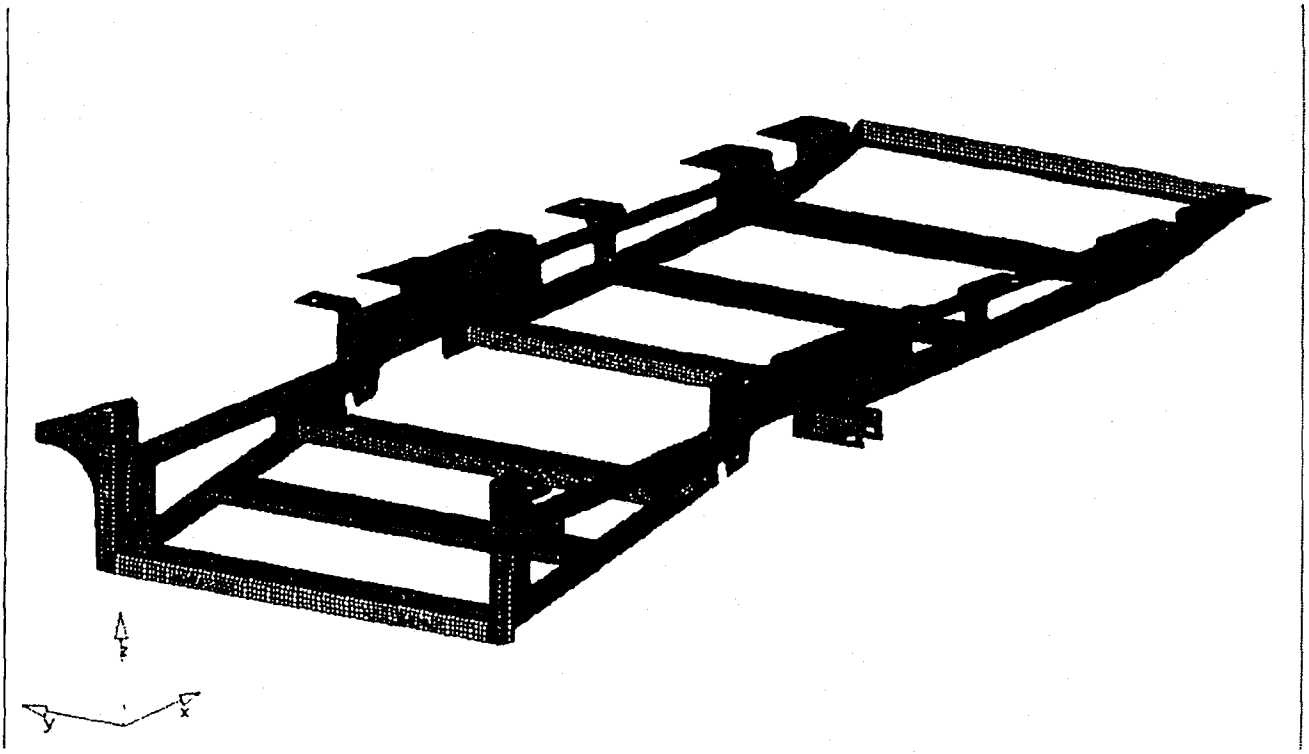

Figure 5.1 - Wheel Chair Ramp HyperMesh Model [42]

5.2 Topology Optimization Problem Description

The MDO procedure for this structure is outlined in Figure 5.2. Again, it starts with a topology optimization. For this topology optimization, the proper boundary conditions had to be in place. First, the structure is welded and bolted to the van at a few different places, and the nodes in these areas have all six degrees of freedom constrained to simulate this. Furthermore, the wall crashing into the rear off the structure had to be simulated. Since Optistruct is being used for the topology optimization, the non-linear situation of the moving wall had to be transformed into a linear static case through a series of approximations and calculations. An example of these constraints and forces can be seen in Figure 5.3.

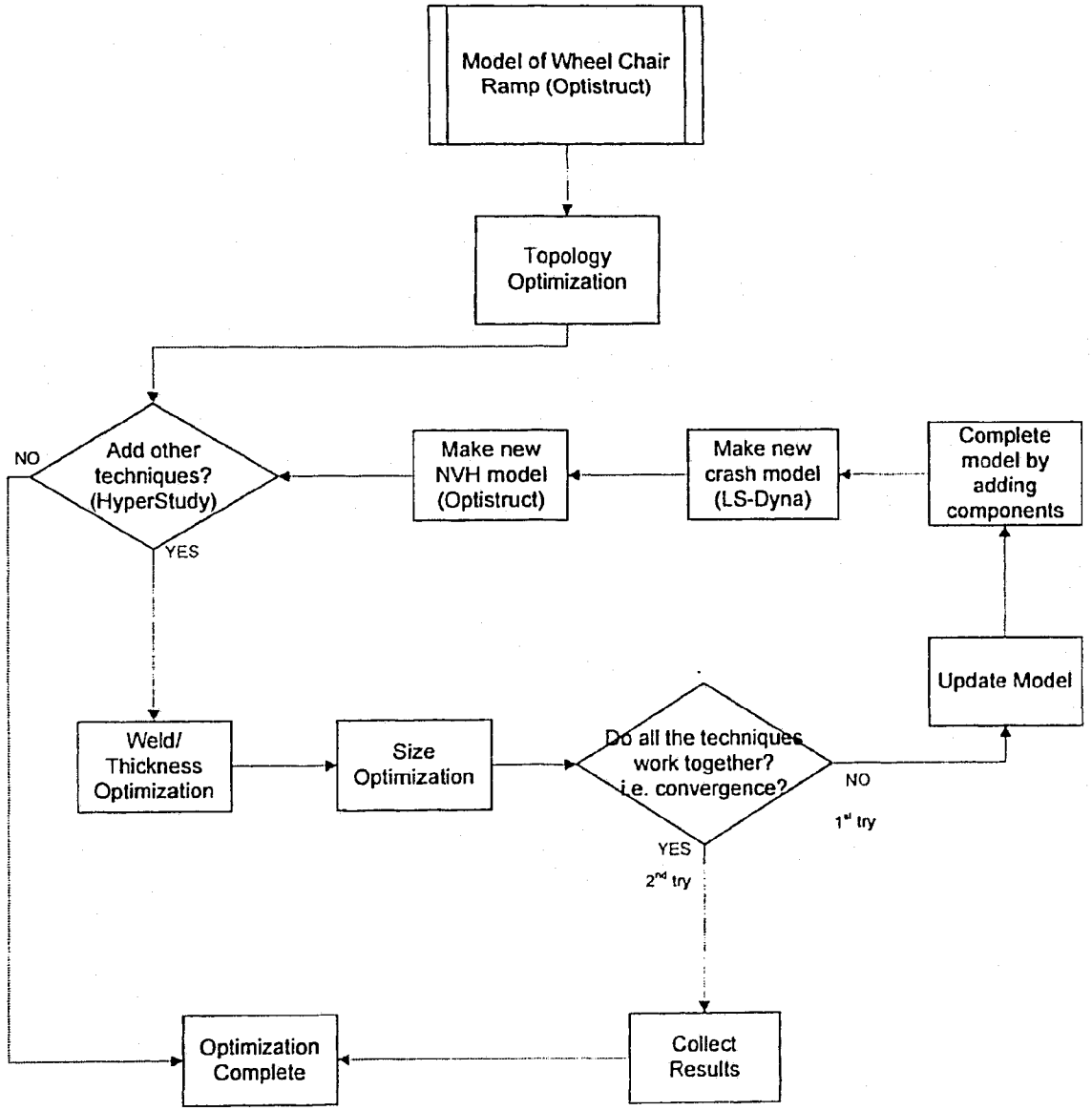

Figure 5.2 - MDO Optimization Procedure for Wheel Chair Ramp Model

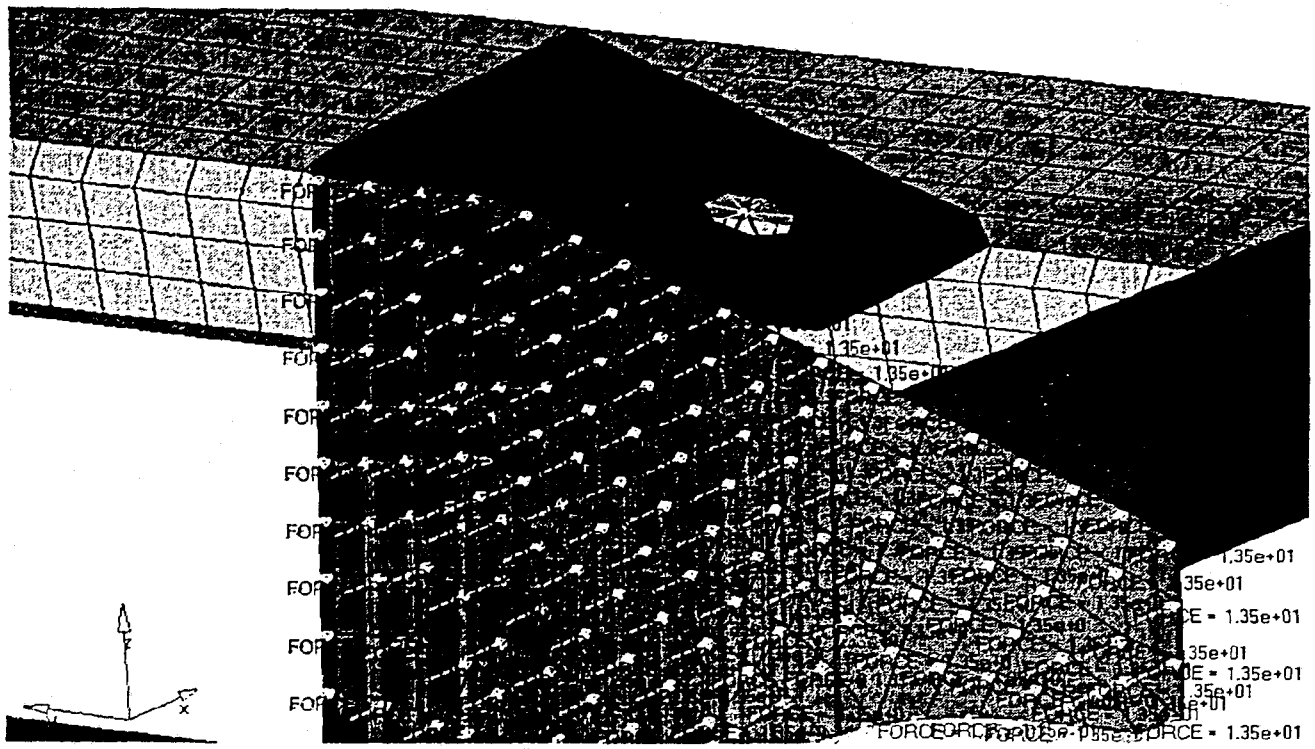

Figure 5.3 - Boundary Conditions on Wheel Chair Ramp

The procedure to determine the forces on the rear of the structure was done by using impulse theory. Impulse theory can be used in assumption that the force exerted on the van by the moving wall is large in comparison with other forces applied to the van [43]. It is also assumed that an elastic collision occurs between the wall and the car, so that all the momentum from the wall is transferred to the van. The mass of the moving wall is 2624.3 kg, and is determined from the government testing standards. The velocity of the wall before it hits the van is 48.8 km/h, or 13.56 m/s. Now, impulse theory is applied to determine the force that the wall exerts on the van.

$$P_i = mv_i = (2624.3)(13.556) = 35573.8\ {}^{kg \cdot m}/_{s}$$

$$P_f = mv_f = (2624.3)(0) = 0\ {}^{kg \cdot m}/_{s} \qquad (5.1)$$

$$F_w = \frac{\Delta P}{\Delta t} = \frac{P_f - P_i}{\Delta t} = \frac{-35573.8}{0.15} = -237kN$$

The variables P_i and P_f are the initial and final momentum of the wall, Δt is the time it takes for the collision to occur, and F_w is the force exerted on the wall by the van. Therefore, by Newton's third law, the force exerted on the van by the wall has to be: +237 kN. However, this is not the force that is applied to the rear of the wheel chair ramp. Remember that the structure is attached to the van, and so the van takes most of the impact. The force that the rear of the ramp experiences can also be determined by some approximations and calculations:

$$A_{rear,ramp} = 0.072m^2$$
$$A_{rear,van} = 3.161m^2$$
$$\frac{A_{rear,ramp}}{A_{rear,van}} = \frac{0.072}{3.161} = 0.0227$$

By dividing the rear areas of the ramp and the van, it is seen that the ramp is only about 5% (rounding up) of the total rear area that is hit by the wall. Therefore, it only takes 5% of the forces exerted on the rear of the van, this is (237 kN)·(0.05) = 11858 N. Since the rear flanges of the structure are comprised of 896 nodes, it means that a force of (11858 N)/(896 nodes) = 13.5 N/node is applied to every node on the rear of the structure. Now the topology optimization problem description can be shown:

Objective = minimize mass

Subject to:

- All forces from the above calculations
- All DOF constraint boundary conditions
- Stress on rear flanges < 200 MPa

5.2.1 Topology Optimization Results

The stress results of the optimization can be seen in Figure 5.4. It can be seen that the stress on the rear flanges does not exceed 200 MPa, in fact the maximum stress is only 192 MPa.

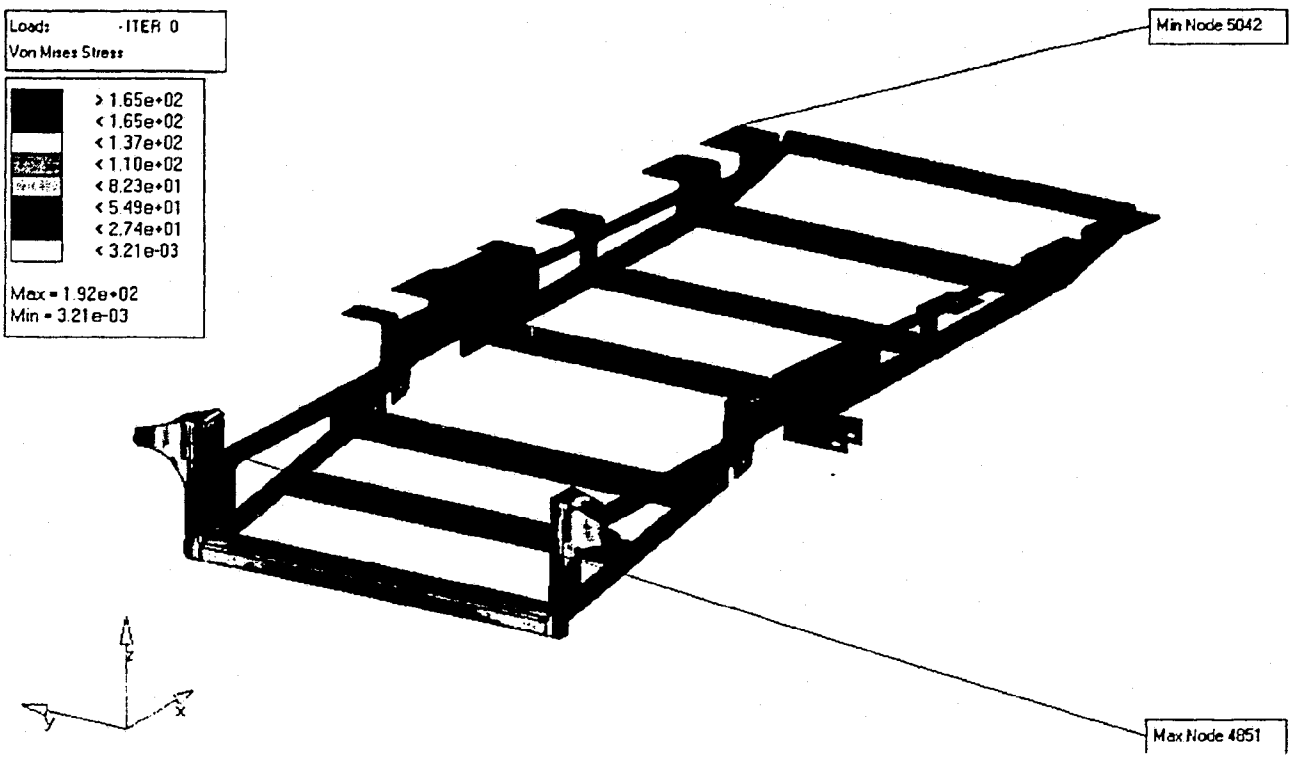

Figure 5.4 - Stress Results for Topology Optimization

The topology optimization revealed that a lot of material could be removed to save mass. Figures 5.5 and 5.6 show where some material was removed. Again, symmetry was a main factor in the decision of where to delete elements. In Figure 5.5 one can see where material was removed from the side rails (circled in red), and in Figure 5.6, it can be seen that material was also removed from the cross member bars.

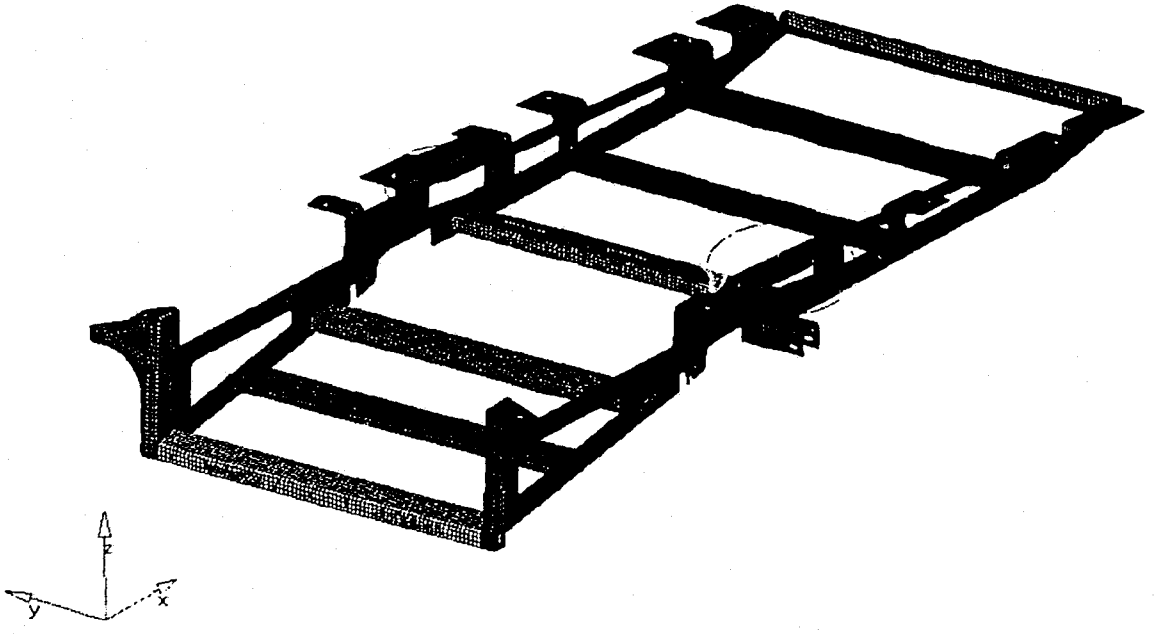

Figure 5.5 - Minimizing the Mass of the Wheel Chair Ramp

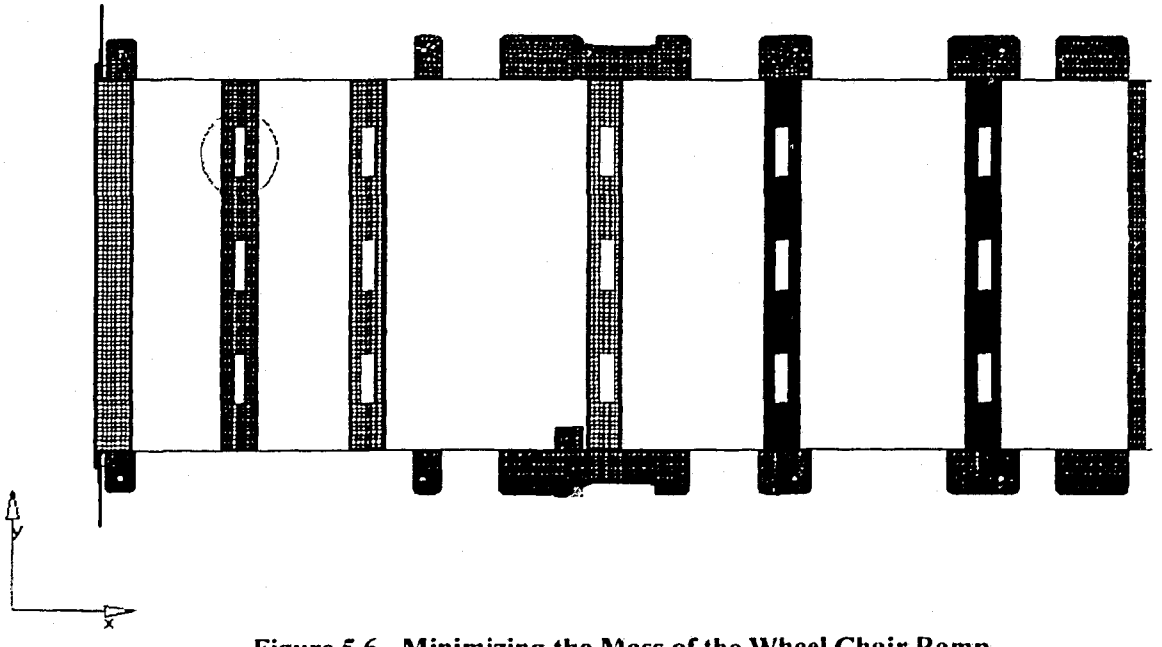

Figure 5.6 - Minimizing the Mass of the Wheel Chair Ramp

The original mass of the structure was 67.86 kg, and after the material was removed via the topology optimization, the mass was reduced to 63.33 kg. This is a 7% reduction in mass. Now, the rest of the MDO can be completed using this model. However, some problems did arise with this model, and will be discussed in the next section.

5.3 Updated Model

The rest of the MDO could only be completed after it was determined by discussing with the manufacturer that the model had to be updated. Specifically, the front and rear floor pieces had to be added to the model. These additional components can be seen in Figure 5.7. With the addition of the rear and front floor, the topology optimization that was previously completed is now unusable. This is due to the fact that the front and rear floors have to be welded to the cross member beams where material was removed. Therefore, although the topology optimization reduced the mass, the manufacturer was not really concern d with reducing the mass by only 4 kg. The trade off was that saving 4 kg was less important than saving the money and time it would take to perform the cut outs.

Another aspect that needed to be added for the most realistic results was non-linearity (the addition of time). So, the LS-DYNA user mode in HyperMesh was used to create a new LS-DYNA compatible file out of the old wheel chair ramp model. The addition of a moving rigid wall can be seen in Figure 5.8. The highlighted red nodes indicate which nodes the wall interacts directly with. The rigid wall interacts with the rear floor, side rails, and the rear three cross member bars underneath (cross member bars can't be seen in Figure 5.8).

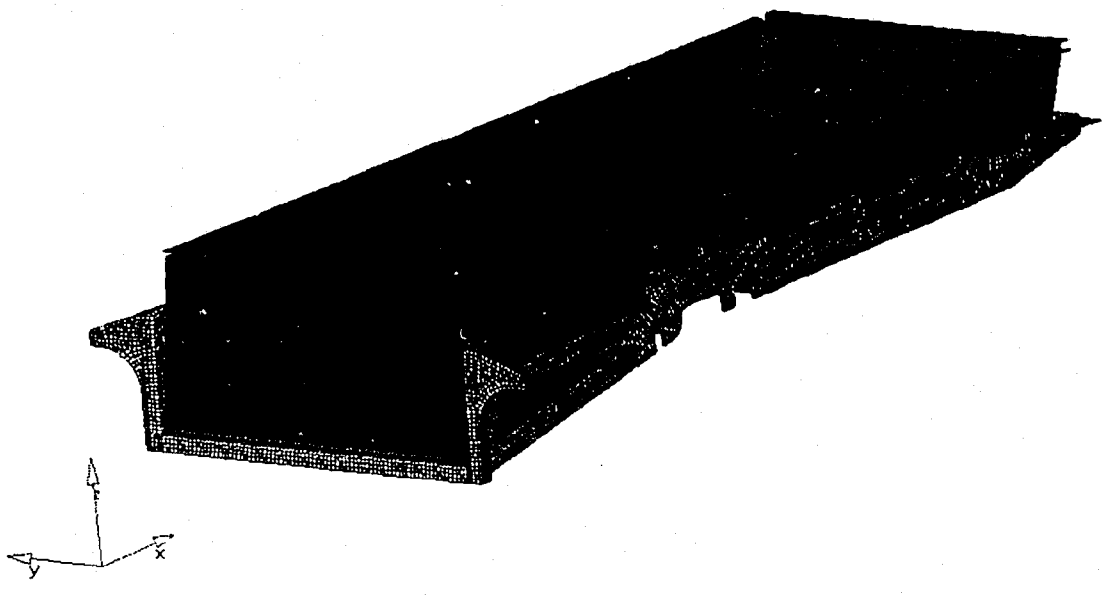

Figure 5.7 - New LS-DYNA Wheel Chair Ramp Model

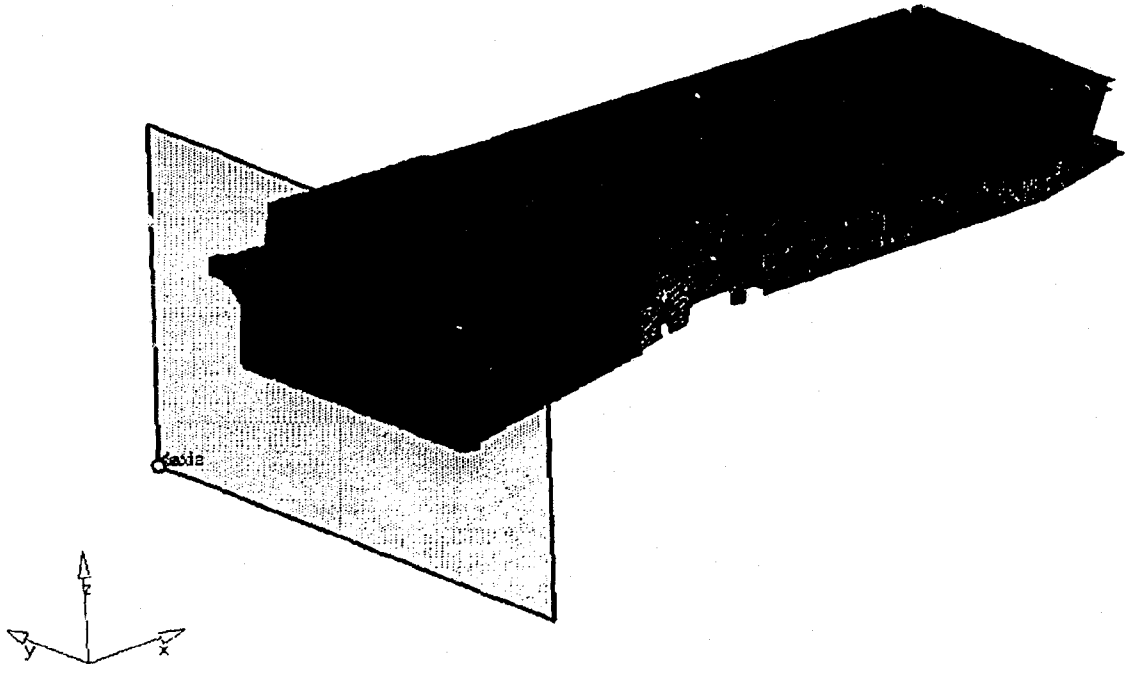

Figure 5.8 – LS-DYNA Wheel Chair Ramp Model with Rigid Wall

A similar problem to the original model arose with this model. The problem was how to get the correct results without having the entire van present within the model. Obviously, if the wall was kept at its original weight and speed, then results of just the ramp model

would be incorrect. One way to fix this is to make a complete model of the rear of the van. This requires getting all the drawings from Ford, which is not possible. Another way is to come up with some kind of equivalent boundary conditions that will mimic the van body and dynamics; however this technique is beyond the scope of this thesis. A final more simpler way is to reduced the mass of the wall to 1000 kg and run the model with many different wall velocities (100, 200, 235, 310, 500, 550, 600, 650, 700, 1000, 1500, and 2000 mm/s). Then a graph can be constructed, and the speed that makes the maximum stress just under 450 MPa can be found and used. The reason that the maximum stress must be under 450 MPa is because of two reasons. First the steel used has a yield strength of 200 MPa, and when the manufacturer did real life crash tests with the structure they stated that no components failed. And secondly, since the impact is only 0.06 s, the same approach that was taken with the model in Chapter 3 can be applied. Therefore, the maximum stress in the computer model is the real life maximum stress plus 250, so 450 MPa. The results from the runs can be seen in Table 5.1

Now, a graph of the maximum stresses of each run can be created and the right wall speed can be found. Figure 5.9 represents a graph of the maximum Von Mises stresses for each run.

Table 5.1 – Wheel Chair Ramp Model Runs

	Wall Speed	Max Von Mises Stress
	(mm/s)	(MPa)
	100.0	83.9
	200.0	102.9
	235.0	123.2
	310.0	139.8
	500.0	153.6
	550.0	209.6
	600.0	303.7
	650.0	400.0
	700.0	506.0
	1000.0	714.5
	1500.0	919.7
	2000.0	1192.0
Wall Speed for Optimization Model	675.0	448.1

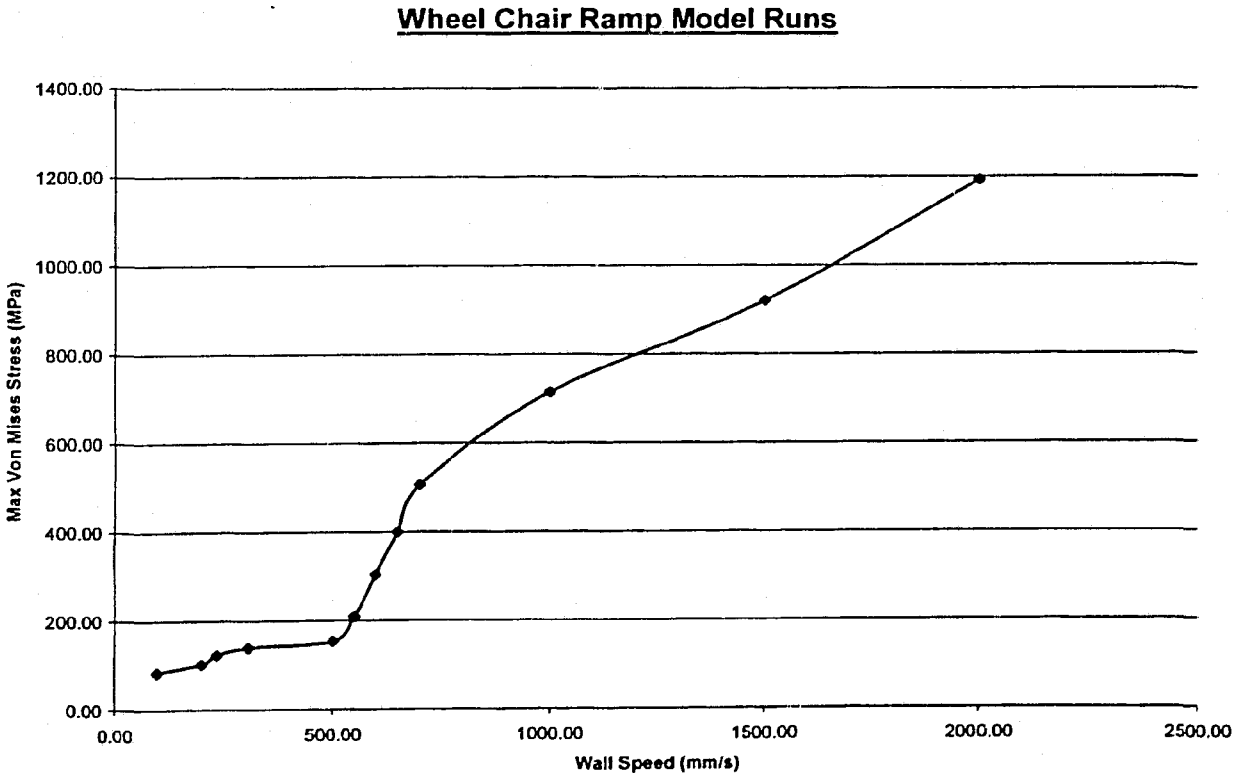

Figure 5.9 - Wall Speed vs. Maximum Von Mises Stress

Looking at Figure 5.9, the run results do not seem to follow a smooth pattern. One area of interest is between 550 mm/s and 700 mm/s. The graph is almost linear at this section, so these few results were used and the results below 550 mm/s and above 700 mm/s were ignored. Using these 4 runs and their maximum stresses, it is easy to see that the wall speed for the optimization model should be 675 mm/s. This wall speed was tested and the maximum Von Mises stress came out to be 448.1 MPa, almost exactly the stress value that was needed.

5.4 MDO Problem Description

Using the newly updated model, a series of constraints can be applied. These constraints can be found in Appendix C – Wheel Chair Ramp Crash Model – Parameter Matrix of Constraints. The natural frequencies of the structures must remain the same or be greater than the original values, also the same type of weld constraints exist just like in the radiator support MDO model. So, the problem description for the MDO of the wheel chair ramp is as follows:

Objective = minimize mass

Subject to:

- All force and DOF constraint boundary conditions
- Maximum Von Mises stress of any element < 450 MPa
- Moving rigid wall boundary conditions
- 1^{st} Natural frequency > 7.16 Hz
- 2^{nd} Natural frequency > 10.53 Hz
- All weld constraints

5.5 Results and Discussion

The results for this MDO can be seen in Appendix E. The first table is a list of all the gauges for each component. The table shows the initial, HyperOpt, User and User Preferred gauges. The HyperOpt gauge is chosen by the MDO program HyperOpt. The user gauge is the HyperOpt gauge rounded up to match one of the thicknesses from the Sheet Metal Gauges table also located in Appendix E. This gauge is rounded up by the user. The user preferred gauges are also chosen by rounding up the HyperOpt gauge but to the values that are in bold in the Sheet Metal Gauges table. These values are preferred over the others by the manufacturer because they are more readily available.

The MDO simulation ran for approximately 24 days, it took 14 iterations to complete and all the constraints were met (this can be seen in Appendix E). It was run in the Ryerson Advanced Computational Lab on the Sun Microsystems PC mentioned in Section 1.4.

The total mass of the wheel chair ramp was reduced from 181.59 kg to 139.04 kg using HyperOpt, a 23% reduction in mass. The user total mass after rounding up the gauges is 147.88 kg, and the user preferred total mass is 168.09 kg, a 19% and 7% reduction in mass respectively. Figure 5.10 shows how the HyperOpt total mass changed throughout the optimization.

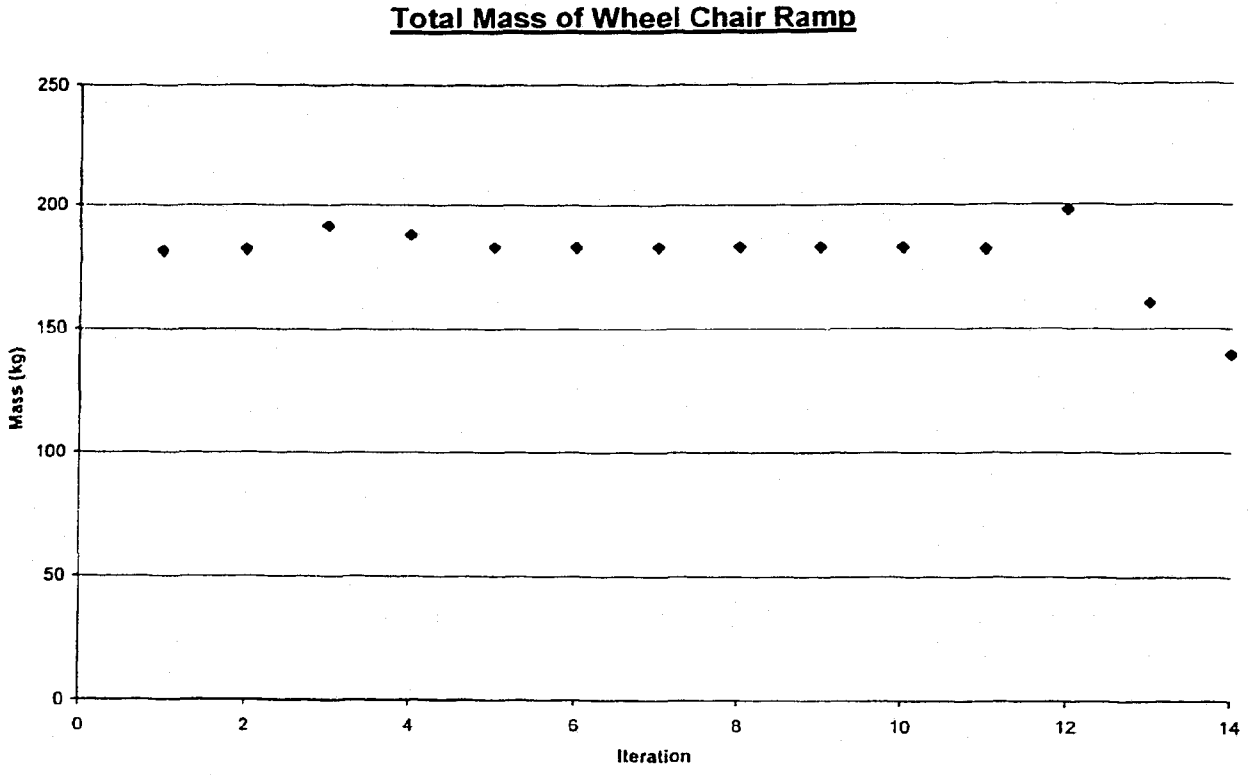

Figure 5.10 - Total Mass of Wheel Chair Ramp (kg vs. iteration #)

Almost all of the component gauges were reduced except for the flanges, and cross member 1 which were raised. The rise in gauge thickness is due to the fact that the flanges are located at the rear of the structure welded to the side rails. This is right where the structure is being hit and this area needed more support. Also, what is interesting is that cross member 1 which is located at the opposite end from the impact had an increase in gauge thickness. This was not expected but it makes the structure stronger by stiffening the far end. The increased thickness in these components allowed for the others to be lowered. Furthermore, the initial thickness for most of the components was over engineered. Every component was given the same thickness for ease of manufacturing even though some of the components can make due with a thinner gauge.

5.6 Future Work with the Wheel Chair Ramp Optimization

As was noted earlier, the current Chapter only deals with a rear crash situation. However, government safety standards include more than this situation for the structure to be certified. If the correct modelling could be derived and proper government standards applied, then a side impact and maybe even a rollover situation could be added to the MDO. Combining all of these situations into one MDO would make the optimization of the wheel chair ramp complete.

Chapter 6

Future Work

This chapter is dedicated to some ideas that should be looked at in the future to improve this MDO procedure.

6.1 Genetic Algorithm as Response Surface Creator

There is a lot of literature that uses genetic algorithms (GA) to solve many problems from simple equations to optimizations with a large number of design variables, constraints, and even more than one objective function. Using a GA in place of Altair HyperOpt would be the next logical step for this MDO procedure. A GA would have to be created that can work with HyperStudy, or even one that would not need HyperStudy at all. This could in theory, improve the time performance and even the results that are achieved. These new results would be tested against the results in this thesis to see which program optimizes better. Furthermore, by writing a new program without the need of HyperStudy, the topology and topography optimizations could be included with all the other optimizations, eliminating the need for separate runs and all the results gathering in between, this would also save time. Furthermore, optimization techniques that HyperStudy can not handle could be implemented into the GA fitness function. These are described below (keep in mind the objective is to minimize the total cost).

6.2. Material Selection Optimization

Due to the fact that different materials are made up of different chemicals and have different properties, this means that not all materials can be welded together. For instance, steel cannot be welded to aluminum since consumable inserts (weld wire to fuse the two pieces) cannot be used with aluminum, and aluminum in the molten state is harder to control since it has a high thermal conductivity. There may be a case where the user has both materials in one model and has tried to attach them. If the user inputs a list of what components are welded together then the program would go into the material card of each component and read what material is being used. The user would also need to create a list of what materials can be welded to each other, their prices, and yield strengths. Then, based on this list the optimizer would be able to choose the right material based on compatibility, cost, and mechanical properties.

6.3 Weld Wire Optimization

Weld wire optimization is related to the above Section 6.2. Once the proper materials are chosen to be welded, the proper weld wire must be selected. In the case of aluminum, a weld wire is not needed; such is the case with other types of welding. However, it is assumed a weld wire is needed. Depending on what type of welding is being used, different gases and types of weld wires are needed; as are different sizes depending on the thickness of the components. So, first the optimizer would check if the components are within the correct gauge size of one another, then it would determine the

size of the weld wire. Next, based on a database of weld wires and their properties the optimizer would search for the cheapest wire that is compatible with the material(s) being welded. Finally it would determine the cost of the weld by multiplying the length of the weld by the cost per meter of wire. This length could be input by the user for each weld, or a program could be written that would figure out the lengths of each weld before the optimization starts. These lengths would be given a number and stored for retrieval during the optimization.

Each of these two above techniques would take some programming skill and time to complete. The GA approach would definitely make this MDO procedure more compact, save time, and possibly achieve better results.

6.4 Thesis Conclusion

In this thesis the history of MDO and different ways, new and old, to implement it were discussed. The optimization techniques used were also discussed. These techniques include: weld constraint optimization, material selection optimization, topology optimization, and cost optimization. All of these techniques were employed in the MDO procedure that was developed through five design iterations. The MDO procedure was designed specifically to handle stamped and welded structures.

The developed MDO procedure was applied to a real life FEM model of a radiator support structure in a static loading situation. The MDO procedure plus the use of hot and cold rolled steel cost models helped to minimize the cost of the radiator and lower the price by 20% from $9.86 to $7.94. As an example, if a company made 10,000 radiator

supports per year, using the materials and gauges from the results in Section 4.3.6 and Appendix B, they would stand to save $19,200.

The MDO procedure was also applied to another stamped and welded structure that is involved in a crash situation. This structure is a wheel chair ramp which is attached to a modified van to make the van wheel chair accessible. The MDO procedure was able to successfully minimize the mass of the structure by 20%, reducing it from 181.59 kg to 147.88 kg using the User selected gauges.

This MDO procedure can be applied to any stamped and welded structure from the aerospace or automotive industries.

References

[1] Multidisciplinary Design Optimization – History. http://en.wikipedia.org/wiki/Multidisciplinary_design_optimization. *Accessed Dec 28th, 2005*

[2] Barthelemy, J.; Giesing, J. (1998): A Summary of Industry MDO Applications and Needs. *AIAA Paper.*

[3] Pan, S.; Qian, Z.; Xue, C. (2001): FEA Agent for Multidisciplinary Design Optimization. *Struct Multidisc Optim 22, 373-383.*

[4] Haftka, R.; Sobieszczanski-Sobieski, J. (1997): Multidisciplinary Aerospace Design Optimization: A Survey of Recent Developments. *Struct Optim 14, 1-23.*

[5] AIAA Technical Committee on Multidisciplinary Design Optimization (January 15th, 1991). http://endo.sandia.gov/AIAA_MDOTC/sponsored/aiaa_paper.html. *Accessed Dec 29th, 2005.*

[6] Chattopadhyay, A.; McCarthy, T. (1991): Multiobjective Design of Helicopter Rotor Blades with Multidisciplinary Coupling. *Structural Systems and Industrial Applications, 451-461.*

[7] Chattopadyay, A.; Rajadas, J.; Talya, S. (2002): Multidisciplinary Design Optimization for Improved Design of a Cooled Gas Turbine Blade. *Engineering Optimization 34(2), 175-194.*

[8] Wakayama, S.; Kroo, I. (1998): The Challenge and Promise of Blended Wing Body Optimization. *AIAA Paper 98-4736.* Presented at the 7th AIAA/USAF/NASA/ISSMO Symposium on Multidisciplinary Analysis and Optimization, St. Louis, MO.

[9] Tarzanin, F.; Young, D. (1998): Boeing Rotorcraft Experience with Rotor Design and Optimization. *AIAA Paper 98-4733.* Presented at the 7th AIAA/USAF/NASA/ISSMO Symposium on Multidisciplinary Analysis and Optimization, St. Louis, MO.

[10] Radovcich, N.; Layton, D. (1998): The F-22 Structural Aeroelastic Design Process with MDO Examples. *AIAA Paper 98-4732.* Presented at the 7th AIAA/USAF/NASA/ISSMO Symposium on Multidisciplinary Analysis and Optimization, St. Louis, MO.

[11] Love, M. (1998): Multidisciplinary Design Practices for the F-16 Agile Falcon. *AIAA Paper 98-4704.* Presented at the 7th AIAA/USAF/NASA/ISSMO Symposium on Multidisciplinary Analysis and Optimization, St. Louis, MO.

[12] Anderson, R.; Young, J.; Yurkovich, R. (1998): A Description of the F/A-18 E/F Design and Design Process. *AIAA Paper 98-4701.* Presented at the 7th AIAA/USAF/NASA/ISSMO Symposium on Multidisciplinary Analysis and Optimization, St. Louis, MO.

[13] Finnegan, P.; He, B.; Rohl, P. (1998): A Collaborative Optimization Environment for Turbine Engine Development. *AIAA Paper 98-4734.* Presented at the 7th AIAA/USAF/NASA/ISSMO Symposium on Multidisciplinary Analysis and Optimization, St. Louis, MO.

[14] Fitzgerald, T.; Lillie, C.; Wehner, M. (1998): Multidisciplinary Design as Applied to Space. *AIAA Paper 98-4703.* Presented at the 7th AIAA USAF NASA ISSMO Symposium on Multidisciplinary Analysis and Optimization, St. Louis, MO.

[15] Akkerman, A.; Anderson, D.; Faruque, O.; Gu, L.; Yang, R. (2000): Robustness Optimization for Vehicular Crash Simulations. *CSE in Industry, 8-13.*

[16] Marklund, P.; Nilsson, L. (2001). Optimization of a Car Body Component Subject to Side Impact. *Struct Multidic Optim 21, 383-392.*

[17] Craig, K.; Dooge, D.; Nielen, S.; Varadappa, S. (2001): Multidisciplinary Design Optimization of Automotive Crashworthiness and NVH Using Response Surface Methods. *AIAA Journal.*

[18] Kodiyalam, S.; Sobieszczanski-Sobieski, J.; Yang, R. (2001): Optimization of a Car Body Under Constraints of Noise, Vibration, and Harshness (NVH), and Crash. *Struct Multidisc Optim 22, 295-306.*

[19] Hajela, P. (1994): Multidisciplinary Structural Design Optimization. *Geometry and Optimization Techniques, 362-386.*

[20] Balabanov V.; Burgee, S.; Giunta, A.; Grossman, B.; Haftka, R.; Kaufman, M.; Mason, W.; Watson, L. (1995): Variable-Complexity Aerodynamic Structural Optimization via Response Surface Techniques. *Workshop on MDO.* Hampton, VA, March 13-16, 1995.

[21] MSC NASTRAN, MSC Software Corporation. Headquarters: Santa Ana, California, USA.

[22] LS-DYNA, Livermore Software Technology Corp (LSTC). Headquarters: Livermore, California, USA.

[23] Osyczka, A. (1985): Multicriteria Optimization for Engineering Design. *Design Optimization, 193-227.*

[24] Nariman-Zadeh, N.; Atashkari, K.; Jamal, A.; Pilechi, A.; Yao, X. (2005): Inverse Modelling of Multi-Objective Thermodynamically Optimized Turbojet Engines. *Engineering Optimization 37, 437-462.*

[25] Alexandrov, N.; Lewis, R. (2000): Algorithmic Perspectives on Problem Formulations in MDO. *AIAA Paper 2000-4719.*

[26] Renaud, J. (1997): A Concurrent Engineering Approach for Multidisciplinary Design in a Distributed Computing Environment. *Multidisciplinary Design Optimization: State of the Art, SIAM.*

[27] Braun, R.; Gage, P.; Kroo, I.; Sobieski, I. (1996): Implementation and Performance Issues in Collaborative Optimization. *Sixth AIAA/USAF NASA ISSMO Symposium on Multidisciplinary Design Analysis and Optimization.* Bellevue, Washington. AIAA Paper No. 96-4017, September 4-6, 1996.

[28] Balling, R.; Rawlings, M. (2000): Collaborative Optimization with Multidisciplinary Conceptual Design. *Struct Multidisc Optim 20, 232 241.*

[29] Altair HyperWorks website: http://www.osc.edu/hpc/statewide/altair.shtml. *Accessed February, 2006.*

[30] Topography Optimization in Optistruct: http://www.neptune.net/bev/Stopog.html. *Accessed: January, 2005.*

[31] Kilian, S.; Talke, F.; Zander, U. (2003): Suspension Modeling and Optimization Using Finite Element Analysis. *Tribology International 36, 317 – 324.*
[32] Altair HyperWorks Software Package, Altair Engineering Corporation. Headquarters: Troy, Michigan, USA.
[33] Fourie, P.; Groenwold, A. (2002): The Particle Swarm Optimization Algorithm in Size and Shape Optimization. *Struct Multidisc Optim 23, 259 – 267.*
[34] Topology Optimization theory: TopOpt.dtu.dk. *Accessed: February, 2005.*
[35] R. Kutylowski (1999): On an Effective Topology Procedure. *Structural Multidisciplinary Optimization 20, 49 – 56.*
[36] Buhl, T.; Pedersen, C.; Sigmund, O. (2000): Stiffness Design of Geometrically Non-linear Structures Using Topology Optimization. *Structural and Multidisciplinary Optimization 19, 93-104.*
[37] Shyy, Y.; Thomas, H.; Zhou, M. (2001). Checkerboard and Minimum Member Size Control in Topology Optimization. *Struct Multidisc Optim 21, 152 – 158.*
[38] LS-DYNA Environment website: http://www.arup.com/dyna/software/LS-DYNA/LS-DYNA.htm. *Accessed April 2006*
[39] Response Surface Methodology. http://www.mne.psu.edu/me82/Learning/RSM/rsm.html. *Accessed: January, 2006*
[40] Model Courtesy of Van-Rob Stampings, Inc. *June 2005.*
[41] GM Material Database, Van-Rob Stampings Inc. *Accessed April 2005.*
[42] Model courtesy of Freedom Motors, *April 2005.*
[43] Serway, R.; Beichner, R. (2000): Physics for Scientists and Engineers. *Saunders College Publishing, 255.*

Appendix A

Parameter Matrix of Constraints for

Radiator Support MDO

Parameter Matrix of Constraints

NVH Constraints

Constraint	Type of Constraint	Value of Constraint
Mode 1	Greater Than	11.8 Hz
Mode 2	Greater Than	16.1 Hz

Stress Constraints (Max Stress for Subcases 103 & 106)

Component	Type of Constraint	Value of Constraint
Condenser Bracket	Less Than	800 MPa
Condenser Plate	Less Than	800 MPa
Cross Bar	Less Than	800 MPa
Cross Brace	Less Than	800 MPa
End Cap	Less Than	800 MPa
Hood Bracket	Less Than	800 MPa
Hood Support	Less Than	800 MPa
Inner Post	Less Than	800 MPa
Lower Tie Bar 1.0	Less Than	800 MPa
Lower Tie Bar 1.2	Less Than	800 MPa
Lower Tie Bar 1.9	Less Than	800 MPa
Outer Post	Less Than	800 MPa
Reinforcement LTB	Less Than	800 MPa
Reinf. Rad. Support	Less Than	800 MPa
Reinforcement Strap	Less Than	800 MPa
Upper Tie Bar	Less Than	800 MPa

Weld Constraints (Upper)

Constraint	Type of Constraint	Value of Constraint	Part # of Welded Parts
Weld 1	Less Than	1.5	16 - 1
Weld 2	Less Than	1.5	16 - 7
Weld 3	Less Than	1.5	12 - 15
Weld 4	Less Than	1.5	12 - 5
Weld 5	Less Than	1.5	12 - 13
Weld 6	Less Than	1.5	12 - 11
Weld 7	Less Than	1.5	8 - 15
Weld 8	Less Than	1.5	8 - 5
Weld 9	Less Than	1.5	8 - 13
Weld 10	Less Than	1.5	8 - 11
Weld 11	Less Than	1.5	8 - 14
Weld 12	Less Than	1.5	13 - 11
Weld 13	Less Than	1.5	2 - 10
Weld 14	Less Than	1.5	2 - 9
Weld 15	Less Than	1.5	14 - 11
Weld 16	Less Than	1.5	4 - 7
Weld 17	Less Than	1.5	4 - 6
Weld 18	Less Than	1.5	4 - 3
Weld 19	Less Than	1.6	11 - 10
Weld 20	Less Than	1.25	10 - 9

Weld Constraints (Lower)

Constraint	Type of Constraint	Value of Constraint	Part # of Welded Parts
Weld 1	Greater Than	0.5	16 - 1
Weld 2	Greater Than	0.5	16 - 7
Weld 3	Greater Than	0.5	12 - 15
Weld 4	Greater Than	0.5	12 - 5
Weld 5	Greater Than	0.5	12 - 13
Weld 6	Greater Than	0.5	12 - 11
Weld 7	Greater Than	0.5	8 - 15
Weld 8	Greater Than	0.5	8 - 5
Weld 9	Greater Than	0.5	8 - 13
Weld 10	Greater Than	0.5	8 - 11
Weld 11	Greater Than	0.5	8 - 14
Weld 12	Greater Than	0.5	13 - 11
Weld 13	Greater Than	0.5	2 - 10
Weld 14	Greater Than	0.5	2 - 9
Weld 15	Greater Than	0.5	14 - 11
Weld 16	Greater Than	0.5	4 - 7
Weld 17	Greater Than	0.5	4 - 6
Weld 18	Greater Than	0.5	4 - 3
Weld 19	Greater Than	0.6	11 - 10
Weld 20	Greater Than	0.8	10 - 9

Material Ratio Constraints (for subcases 103 & 106)

Constraint*	Type of Constraint	Value of Constraint
Condenser Bracket	Greater Than	1.0
Condenser Plate	Greater Than	1.0
Cross Bar	Greater Than	1.0
Cross Brace	Greater Than	1.0
End Cap	Greater Than	1.0
Hood Bracket	Greater Than	1.0
Hood Support	Greater Than	1.0
Inner Post	Greater Than	1.0
Lower Tie Bar 1.0	Greater Than	1.0
Lower Tie Bar 1.2	Greater Than	1.0
Lower Tie Bar 1.9	Greater Than	1.0
Outer Post	Greater Than	1.0
Reinforcement LTB	Greater Than	1.0
Reinf. Rad. Support	Greater Than	1.0
Reinforcement Strap	Greater Than	1.0
Upper Tie Bar	Greater Than	1.0

* Constraint is: (part material yield (Mpa))/(part maximum stress (Mpa))

Appendix B

MDO of Radiator Support Design Parameter

Matrices

Parameter Matrix for Radiator Support (Original Model)

Part Name	Part Number	Material Yield Strength (Mpa)	Part Gauge (mm)	Part Area (mm^2)	Part Volume (mm^3)	Part Mass (kg)
Condenser Bracket	1	270	1.000	16914.000	16914.000	0.132
Condenser Plate	2	270	1.200	7422.000	8906.400	0.070
Cross Bar	3	270	1.500	27540.000	41310.000	0.323
Cross Brace	4	180	1.200	130445.000	156534.000	1.226
End Cap	5	550	1.500	52191.000	78286.500	0.613
Hood Bracket	6	550	1.200	33431.000	40117.200	0.314
Hood Support	7	550	1.200	31946.000	38335.200	0.300
Inner Post	8	550	1.000	243905.000	243905.000	1.910
Lower Tie Bar 1.0	9	420	1.000	163148.000	163148.000	1.277
Lower Tie Bar 1.2	10	420	1.200	42795.000	51354.000	0.402
Lower Tie Bar 1.9	11	420	1.900	111626.000	212089.400	1.661
Outer Post	12	550	1.100	111698.000	122867.800	0.962
Reinforcement LTB	13	550	1.200	29537.000	35444.400	0.278
Reinf. Rad. Support	14	550	1.200	15781.000	18937.200	0.148
Reinforcement Strap	15	550	1.500	10934.000	16401.000	0.128
Upper Tie Bar	16	420	1.000	272477.000	272477.000	2.133
TOTAL				1301790.000	1517027.100	11.630

Part Name	Part Max Stress Case 103 (MPa)	Element # With Max Stress (Case 103)	Part Max Stress Case 106 (MPa)	Element # With Max Stress (Case 106)	Part Cost ($)
Condenser Bracket	38	163	30	509	
Condenser Plate	54	1178	41	1199	0.12
Cross Bar	43	2039	33	1524	0.07
Cross Brace	204	8940	160	3897	0.31
End Cap	676	10045	420	10399	1.11
Hood Bracket	447	12905	374	12905	0.65
Hood Support	295	14525	252	13431	0.33
Inner Post	548	14698	570	21312	0.32
Lower Tie Bar 1.0	229	28956	167	28794	2.01
Lower Tie Bar 1.2	283	32727	201	33513	1.28
Lower Tie Bar 1.9	584	36812	513	36413	0.40
Outer Post	573	39569	505	41838	1.67
Reinforcement LTB	459	46064	450	46004	1.01
Reinf. Rad. Support	286	46658	252	46166	0.29
Reinforcement Strap	535	46802	494	47006	0.16
Upper Tie Bar	714	47429	682	59505	0.14
TOTAL					9.86

HyperStudy MDO Results (Trial 1)

Part Name	Part Number	Initial Gauge (mm)	Initial Material (MPa)	HyperOpt Gauge (mm)	HyperOpt Material (MPa)	User Gauge (mm)	User Material (MPa)	True "Altered" Material (MPa)
Condenser Bracket	1	1.000	270	0.800	520	0.80	520	270
Condenser Plate	2	1.200	270	0.877	520	0.90	520	270
Cross Bar	3	1.500	270	0.889	520	0.90	520	270
Cross Brace	4	1.200	180	0.800	520	0.80	520	270
End Cap	5	1.500	550	2.004	520	2.00	520	270
Hood Bracket	6	1.200	550	1.049	569	1.05	590	340
Hood Support	7	1.200	550	0.801	576	0.80	590	340
Inner Post	8	1.000	550	1.004	594	1.00	630	380
Lower Tie Bar 1.0	9	1.000	420	0.934	520	0.95	520	270
Lower Tie Bar 1.2	10	1.200	420	1.167	520	1.20	520	270
Lower Tie Bar 1.9	11	1.900	420	1.862	610	1.90	630	380
Outer Post	12	1.100	550	1.079	706	1.10	750	500
Reinforcement LTB	13	1.200	550	1.373	560	1.40	590	340
Reinf. Rad. Support	14	1.200	550	0.977	520	1.00	520	270
Reinforcement Strap	15	1.500	550	2.009	520	2.00	520	270
Upper Tie Bar	16	1.000	420	0.982	639	1.00	670	420

		Topology Opt	HyperOpt		User		% Change wrt Initial
Mass (kg)	11.957	11.630	11.024		11.362		4.98
Delta Mass (kg)			0.933		0.595		
Cost ($)	$9.86		$8.99		9.00		8.72
Max Stress 103 (MPa)	714		707		696		2.52
Max Stress 106 (MPa)	682		680		672		1.47
Mode 1 (Hz)	11.83		11.85		11.86		-0.25
Mode 2 (Hz)	16.18		16.19		16.19		-0.06

Parameter Matrix for Radiator Support (Trial 1)

Part Name	Part Number	Material Yield Strength (Mpa)	Part Gauge (mm)	Part Area (mm^2)	Part Volume (mm^3)	Part Mass (kg)
Condenser Bracket	1	270	0.80	16914.000	13531.200	0.106
Condenser Plate	2	270	0.90	7422.000	6679.800	0.052
Cross Bar	3	270	0.90	27540.000	24786.000	0.194
Cross Brace	4	270	0.80	130445.000	104356.000	0.817
End Cap	5	340	2.00	52191.000	104382.000	0.817
Hood Bracket	6	340	1.05	33431.000	35102.550	0.275
Hood Support	7	340	0.80	31946.000	25556.800	0.200
Inner Post	8	380	1.00	243905.000	243905.000	1.910
Lower Tie Bar 1.0	9	270	0.95	163148.000	154990.600	1.214
Lower Tie Bar 1.2	10	270	1.20	42795.000	51354.000	0.402
Lower Tie Bar 1.9	11	380	1.90	111626.000	212089.400	1.661
Outer Post	12	500	1.10	111698.000	122867.800	0.962
Reinforcement LTB	13	340	1.40	29537.000	41351.800	0.324
Reinf. Rad. Support	14	270	1.00	15781.000	15781.000	0.124
Reinforcement Strap	15	270	2.00	10934.000	21868.000	0.171
Upper Tie Bar	16	420	1.00	272477.000	272477.000	2.133
TOTAL				1301790.000	1451078.950	11.362

Part Name	Part Max Stress Case 103 (Mpa)	Element # With Max Stress (Case 103)	Part Max Stress Case 106 (Mpa)	Element # With Max Stress (Case 106)	Part Cost ($)
Condenser Bracket	48	163	34	509	0.01
Condenser Plate	61	1178	46	1199	0.10
Cross Bar	69	2039	49	1524	0.05
Cross Brace	331	8940	242	3897	0.18
End Cap	460	10045	344	10399	0.77
Hood Bracket	557	12905	478	12905	0.79
Hood Support	556	14525	369	13431	0.27
Inner Post	545	14698	564	21312	0.19
Lower Tie Bar 1.0	215	28956	155	28794	1.88
Lower Tie Bar 1.2	322	32727	205	33513	1.14
Lower Tie Bar 1.9	614	36812	492	36413	0.38
Outer Post	581	39569	494	41838	1.64
Reinforcement LTB	386	46064	379	46004	1.00
Reinf. Rad. Support	304	46658	250	46166	0.31
Reinforcement Strap	411	46802	390	47006	0.12
Upper Tie Bar	696	47429	672	59505	0.16
TOTAL					9.00

HyperStudy MDO Results (Trial 2)

Part Name	Part Number	Initial Gauge (mm)	Initial Material (MPa)	HyperOpt Gauge (mm)	HyperOpt Material (MPa)	User Gauge (mm)	User Material (MPa)	True "Altered" Material (MPa)
Condenser Bracket	1	1.000	270	0.800	520	0.80	520	270
Condenser Plate	2	1.200	270	1.062	520	1.10	520	270
Cross Bar	3	1.500	270	0.800	520	0.80	520	270
Cross Brace	4	1.200	180	0.800	520	0.80	520	270
End Cap	5	1.500	550	1.966	520	2.00	520	270
Hood Bracket	6	1.200	550	1.089	543	1.10	590	340
Hood Support	7	1.200	550	0.800	598	0.80	630	380
Inner Post	8	1.000	550	0.992	520	1.00	520	270
Lower Tie Bar 1.0	9	1.000	420	0.957	520	1.00	520	270
Lower Tie Bar 1.2	10	1.200	420	1.192	520	1.20	520	270
Lower Tie Bar 1.9	11	1.900	420	1.899	618	1.90	630	380
Outer Post	12	1.100	550	1.302	614	1.30	630	380
Reinforcement LTB	13	1.200	550	1.399	520	1.40	590	340
Reinf. Rad. Support	14	1.200	550	1.000	520	1.00	520	270
Reinforcement Strap	15	1.500	550	1.985	520	2.00	520	270
Upper Tie Bar	16	1.000	420	0.809	728	0.85	750	500

		Topology Opt	HyperOpt		User		% Change wrt Initial
Mass (kg)	11.957	11.630	10.889		11.284		5.63
Delta Mass (kg)			1.068		0.673		
Cost ($)	$9.86		$8.89		$9.25		6.19
Max Stress 103 (MPa)	714		796		689		3.50
Max Stress 106 (MPa)	682		726		750		-9.97
Mode 1 (Hz)	11.83		11.837		11.837		0.00
Mode 2 (Hz)	16.18		16.115		16.155		0.00

Parameter Matrix for Radiator Support (Trial 2)

Part Name	Part Number	Material Yield Strength (Mpa)	Part Gauge (mm)	Part Area (mm^2)	Part Volume (mm^3)	Part Mass (kg)
Condenser Bracket	1	270	0.80	16914.000	13531.200	0.106
Condenser Plate	2	270	1.10	7422.000	8164.200	0.064
Cross Bar	3	270	0.80	27540.000	22032.000	0.173
Cross Brace	4	270	0.80	130445.000	104356.000	0.817
End Cap	5	340	2.00	52191.000	104382.000	0.817
Hood Bracket	6	340	1.10	33431.000	36774.100	0.288
Hood Support	7	340	0.80	31946.000	25556.800	0.200
Inner Post	8	380	1.00	243905.000	243905.000	1.910
Lower Tie Bar 1.0	9	270	1.00	163148.000	163148.000	1.277
Lower Tie Bar 1.2	10	270	1.20	42795.000	51354.000	0.402
Lower Tie Bar 1.9	11	380	1.90	111626.000	212089.400	1.661
Outer Post	12	500	1.30	111698.000	145207.400	1.137
Reinforcement LTB	13	340	1.40	29537.000	41351.800	0.324
Reinf. Rad. Support	14	270	1.00	15781.000	15781.000	0.124
Reinforcement Strap	15	270	2.00	10934.000	21868.000	0.171
Upper Tie Bar	16	420	0.85	272477.000	231605.450	1.813
TOTAL				1301790.000	1441106.350	11.284

Part Name	Part Max Stress Case 103 (Mpa)	Element # With Max Stress (Case 103)	Part Max Stress Case 106 (Mpa)	Element # With Max Stress (Case 106)	Part Cost ($)
Condenser Bracket	47	163	33	509	0.01
Condenser Plate	58	1178	43	1199	0.10
Cross Bar	68	2039	52	1524	0.06
Cross Brace	332	8940	243	3897	0.16
End Cap	455	10045	378	10399	0.77
Hood Bracket	520	12905	448	12905	0.79
Hood Support	571	14525	364	13431	0.28
Inner Post	531	14698	568	21312	0.19
Lower Tie Bar 1.0	230	28956	161	28794	1.88
Lower Tie Bar 1.2	324	32727	198	33513	1.20
Lower Tie Bar 1.9	606	36812	482	36413	0.38
Outer Post	514	39569	421	41838	1.64
Reinforcement LTB	400	46064	392	46004	1.18
Reinf. Rad. Support	304	46658	246	46166	0.31
Reinforcement Strap	414	46802	393	47006	0.12
Upper Tie Bar	750	47429	689	59505	0.16
TOTAL					9.25

HyperStudy MDO Results (Trial 3)

Part Name	Part Number	Initial Gauge (mm)	Initial Material (MPa)	HyperOpt Gauge (mm)	HyperOpt Material (MPa)	User Gauge (mm)	User Material (MPa)	True "Altered" Material (MPa)
Condenser Bracket	1	1.000	270	0.800	520	0.80	520	270
Condenser Plate	2	1.200	270	1.062	520	1.10	520	270
Cross Bar	3	1.500	270	0.800	520	1.00	520	270
Cross Brace	4	1.200	180	0.800	520	0.80	520	270
End Cap	5	1.500	550	1.966	557	1.90	520	270
Hood Bracket	6	1.200	550	1.089	552	1.10	590	340
Hood Support	7	1.200	550	0.800	520	0.90	630	380
Inner Post	8	1.000	550	0.992	574	1.00	520	270
Lower Tie Bar 1.0	9	1.000	420	0.957	520	1.00	520	270
Lower Tie Bar 1.2	10	1.200	420	1.192	520	1.20	520	270
Lower Tie Bar 1.9	11	1.900	420	1.899	520	1.90	630	380
Outer Post	12	1.100	550	1.302	690	1.10	630	380
Reinforcement LTB	13	1.200	550	1.399	545	1.30	590	340
Reinf. Rad. Support	14	1.200	550	1.000	520	1.10	520	270
Reinforcement Strap	15	1.500	550	1.985	520	1.90	520	270
Upper Tie Bar	16	1.000	420	0.809	750	0.90	750	500

		Topology Opt	HyperOpt		User		% Change wrt Initial
Mass (kg)	11.957	11.630	11.713		11.903		0.45
Delta Mass (kg)			0.244		0.054		
Cost ($)	$9.86		$8.92		$7.94		19.47
Max Stress 103 (MPa)	714		756		743		-4.06
Max Stress 106 (MPa)	682		710		674		1.17
Mode 1 (Hz)	11.83		11.837		11.837		0.00
Mode 2 (Hz)	16.18		16.115		16.155		0.00

Parameter Matrix for Radiator Support (Trial 3)

Part Name	Part Number	Material Yield Strength (Mpa)	Part Gauge (mm)	Part Area (mm^2)	Part Volume (mm^3)	Part Mass (kg)
Condenser Bracket	1	270	0.80	16914.000	13531.200	0.106
Condenser Plate	2	270	1.10	7422.000	8164.200	0.064
Cross Bar	3	270	1.00	27540.000	27540.000	0.216
Cross Brace	4	270	0.80	130445.000	104356.000	0.817
End Cap	5	270	1.90	52191.000	99162.900	0.776
Hood Bracket	6	270	1.10	33431.000	36774.100	0.288
Hood Support	7	270	0.90	31946.000	28751.400	0.225
Inner Post	8	340	1.00	243905.000	243905.000	1.910
Lower Tie Bar 1.0	9	270	1.00	163148.000	163148.000	1.277
Lower Tie Bar 1.2	10	270	1.20	42795.000	51354.000	0.402
Lower Tie Bar 1.9	11	380	1.90	111626.000	212089.400	1.661
Outer Post	12	340	1.10	111698.000	122867.800	0.962
Reinforcement LTB	13	270	1.30	29537.000	38398.100	0.301
Reinf. Rad. Support	14	270	1.10	15781.000	17359.100	0.136
Reinforcement Strap	15	270	1.90	10934.000	20774.600	0.163
Upper Tie Bar	16	500	0.90	272477.000	245229.300	1.920
TOTAL				1301790.000	1433405.100	11.224

Part Name	Part Max Stress Case 103 (Mpa)	Element # With Max Stress (Case 103)	Part Max Stress Case 106 (Mpa)	Element # With Max Stress (Case 106)	Part Cost ($)
Condenser Bracket	47	163	33	509	0.01
Condenser Plate	58	1178	41	1199	0.10
Cross Bar	61	2039	49	1524	0.06
Cross Brace	308	8940	238	3897	0.20
End Cap	499	10045	355	10399	0.64
Hood Bracket	516	12905	439	12905	0.73
Hood Support	474	14525	315	13431	0.27
Inner Post	526	14698	565	21312	0.21
Lower Tie Bar 1.0	224	28956	153	28794	1.85
Lower Tie Bar 1.2	270	32727	191	33513	1.20
Lower Tie Bar 1.9	597	36812	468	36413	0.20
Outer Post	584	39569	469	41838	1.64
Reinforcement LTB	395	46064	385	46004	0.25
Reinf. Rad. Support	281	46658	244	46166	0.28
Reinforcement Strap	445	46802	397	47006	0.13
Upper Tie Bar	743	47429	674	59505	0.15
TOTAL					7.94

Appendix C

Cost Model Information

Material: CQ [CR-1] Cold Rolled - 600 x 800 mm sheet - High Strength Low Alloy

Yield Strength (MPa)	Altered Yield (MPa)	Price for Specific Yield ($/Ckg)	Average Base Price ($/Ckg)	Final Cost ($/Ckg)	Final Cost ($/kg)
270	520	11.85	82.41	94.26	0.94
300	550	13.12	82.41	95.53	0.96
340	590	14.03	82.41	96.44	0.96
380	630	16.45	82.41	98.86	0.99
420	670	18.52	82.41	100.93	1.01
500	750	21.50	82.41	103.91	1.04
550	800	22.38	82.41	104.79	1.05

Material: CQ [HR-1] Hot Rolled Pickled and Oiled - 600 x 800 mm sheet - High Strength Low Alloy

Yield Strength (MPa)	Altered Yield (MPa)	Price for Specific Yield ($/Ckg)	Average Base Price ($/Ckg)	Final Cost ($/Ckg)	Final Cost ($/kg)
270	520	6.95	72.24	79.19	0.79
300	550	7.74	72.24	79.98	0.80
340	590	8.11	72.24	80.35	0.80
380	630	8.7	72.24	80.94	0.81
420	670	9.59	72.24	81.83	0.82
500	750	14.83	72.24	87.07	0.87
550	800	15.45	72.24	87.69	0.88

Line of Best Fit Results (CR)

Yield Strength (MPa)	**Cubic Polynomial** Cost ($/kg)	**Linear*** Cost ($/kg)	Actual Cost ($/kg)
520	0.94	0.94	0.94
550	0.95	0.95	0.96
590	0.97	0.97	0.96
630	0.99	0.99	0.99
670	1.01	1.00	1.01
750	1.04	1.03	1.04
800	1.05	1.05	1.05

Line of Best Fit Results (HR)

Yield Strength (MPa)	4th Order Poly* Cost ($/kg)	Linear Cost ($/kg)	Actual Cost ($/kg)
520	0.79	0.78	0.79
550	0.80	0.79	0.80
590	0.80	0.81	0.80
630	0.81	0.82	0.81
670	0.82	0.83	0.82
750	0.87	0.86	0.87
800	0.88	0.87	0.88

* Best Choice Used

Cost vs. Thickness

Thickness (mm)	HR Price ($/kg)	CR Price ($/kg)
0.49 & under	7.44	9.28
0.5 - 0.69	7.44	8.55
0.7 - 1.49	7.44	8.12
1.50 & over	7.04	8.08

Material Yield Strength vs. Cost (Hot Rolled)

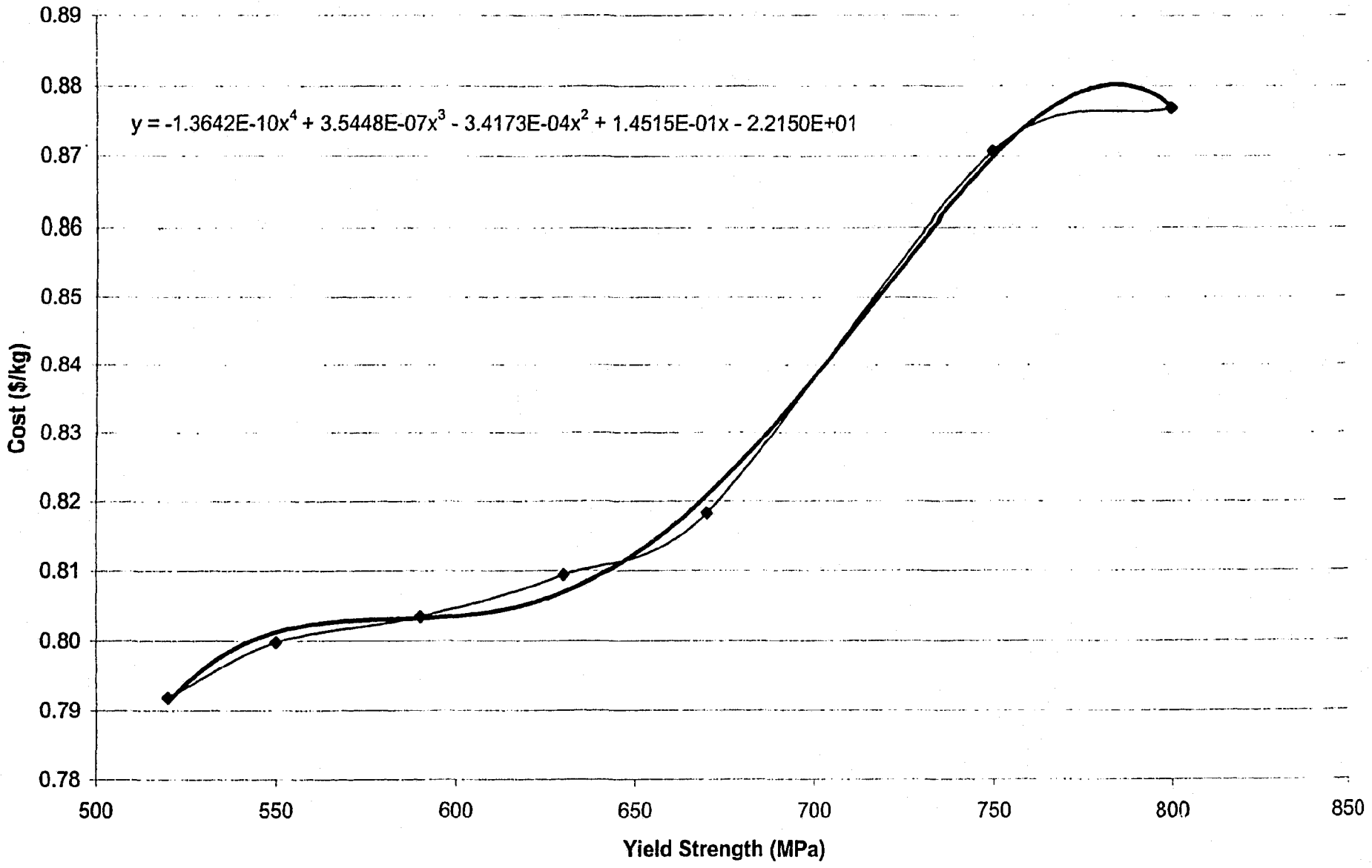

Material Yield Strength vs. Cost (Cold Rolled) - Polynomial

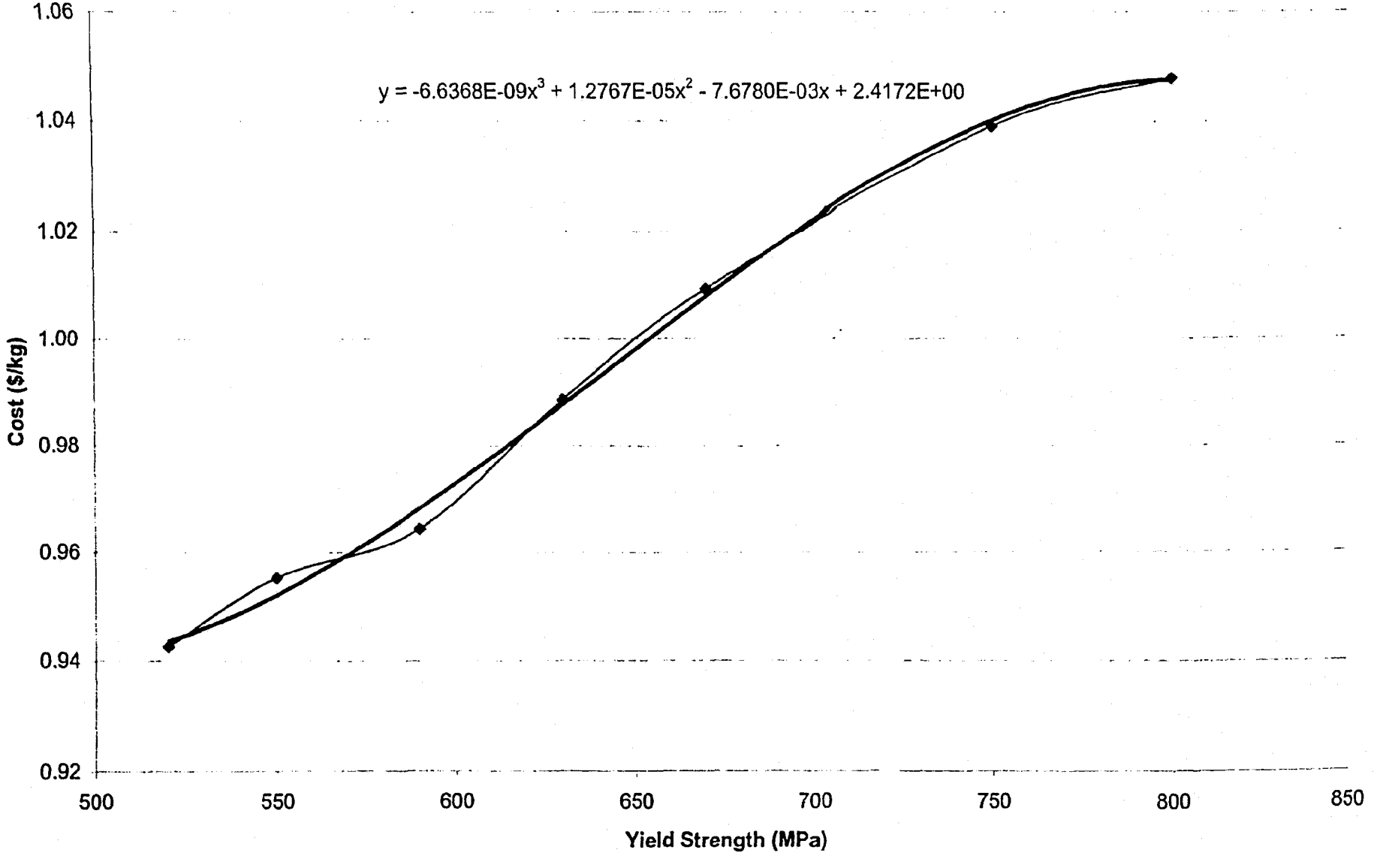

Material Yield Strength vs. Cost (Cold Rolled) - Linear

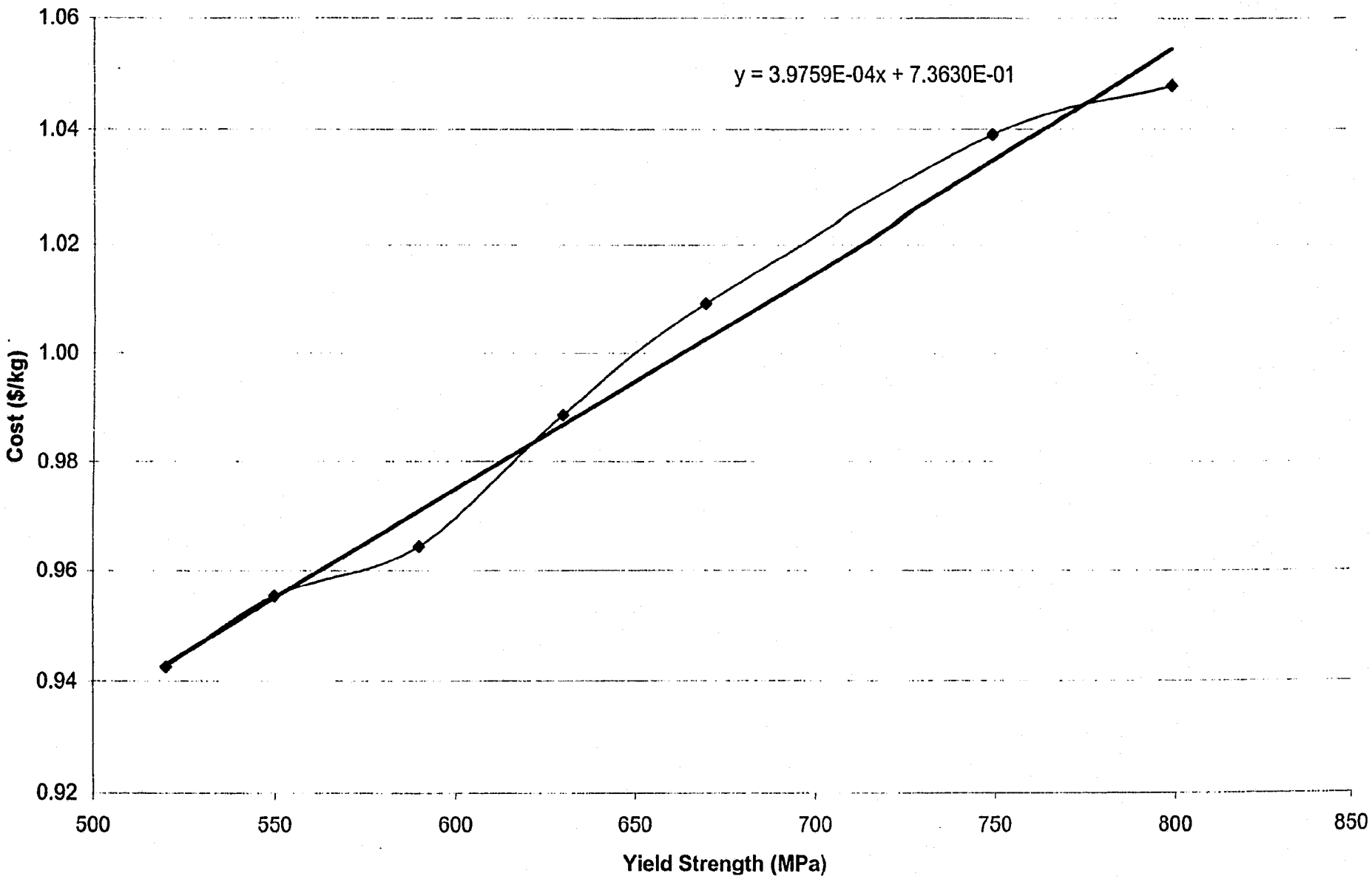

Appendix D

MATLAB Program Code and Results

```
%function read_stress()

function A = read_stress(A);

fid = fopen('stress_106.f06', 'r');
status = fseek(fid, 20000000, -1);
%read in elements to be checked

elements{1,1} = '0     509';
elements{2,1} = '0    1199';
elements{3,1} = '0    1524';
elements{4,1} = '0    8316';
elements{5,1} = '0   10869';
elements{6,1} = '0   12905';
elements{7,1} = '0   13820';
elements{8,1} = '0   21312';
elements{9,1} = '0   28794';
elements{10,1} = '0   33503';
elements{11,1} = '0   36413';
elements{12,1} = '0   42345';
elements{13,1} = '0   45096';
elements{14,1} = '0   46166';
elements{15,1} = '0   47006';
elements{16,1} = '0   59505';

%elements{1,1} = '0     163';
%elements{2,1} = '0     164';
%elements{3,1} = '0    1138';
%elements{4,1} = '0    1139';
%elements{5,1} = '0    2039';
%elements{6,1} = '0    2040';
%elements{7,1} = '0    1179';
%elements{8,1} = '0    1180';

match = 0;
%status = fseek(fid, 25160000, -1);

%find the element's data in the file
%re-read from beginning if EOF is reached

for i = 1:1:16

    while feof(fid) == 0
        tline = fgetl(fid);
        match = strmatch(elements{i,1}, tline);
       if match > 0
           tline
         break
       elseif feof(fid) == 1
           fprintf(1, '%s', 're-reading from beginning of file')
           status = fseek(fid, 20000000, -1);
       end
```

```
    end

%read element data and take the proper information

    D = textscan(tline, '%f%f%f%f%f%f%f%f%f%f', 1)
    E = textscan(fid, '%f%f%f%f%f%f%f%f', 1);
    A{i,3} = D(2);

%take the highest Von Mises stress: Z1 or Z2

    if cell2mat(E(8)) > cell2mat(D(10))
        max_elem_stress = E(8);
    else max_elem_stress = D(10);
    end

    A(i,4) = max_elem_stress;
    match = 0;

end
A
fclose(fid);
```

```
%function read_thickness()

%open file and find PSHELL cards

fid = fopen('stress_106.dat', 'r+');
status = fseek(fid, 18000000, -1);

while feof(fid) == 0
   tline = fgetl(fid);
   match = findstr(tline, 'PSHELL Data');
   if match >= 0
       break
   end
end

%read contents of one PSHELL card, keep thickness in its own matrix
%repeat for 15 PSHELL cards

for i = 1:1:16

    C(1,1) = textscan(fid, '%s', 1);
    C(2,1) = textscan(fid, '%s', 1);
    C(2,2) = textscan(fid, '%s', 1);
    C(2,3) = textscan(fid, '%f', 1);
    A(i,1) = textscan(fid, '%q', 1);
    C(3,1) = textscan(fid, '%s', 1);
    C(3,2) = textscan(fid, '%s', 1);
    C(3,3) = textscan(fid, '%f', 1);
    C(3,4) = textscan(fid, '%f', 1);
    C(4,1) = textscan(fid, '%s', 1);
    C(4,2) = textscan(fid, '%f', 1);
    C(4,3) = textscan(fid, '%f', 1);
    A(i,2) = textscan(fid, '%3f', 1);

%round off the thickness

    round_off = textscan(fid, '%f', 1);
    round_off = cell2mat(round_off);

    if (round_off >= 500) & (round_off < 5000)
        round_off = 0.05000;
    elseif round_off > 5000
        round_off = 0.1;
    else
        round_off = 0;
    end

    A(i,2) = num2cell(cell2mat(A(i,2)) + round_off);


%write the new thickness in the proper spot of the card
```

```
    fseek(fid, -9, 'cof');
    fprintf(fid, '%1.5f', cell2mat(A(i,2)));

    C(4,5) = textscan(fid, '%f', 1);
    C(4,6) = textscan(fid, '%f', 1);

end
A
fclose(fid);

A = read_stress(A);
A = read_yields(A);
A
```

```
%function read_yields()

function A = read_yields(A);

fid = fopen('opt_1.hyperopt', 'r');

% read in the list of yield strengths

yield_list(1) = 520;
yield_list(2) = 550;
yield_list(3) = 590;
yield_list(4) = 630;
yield_list(5) = 670;
yield_list(6) = 750;
yield_list(7) = 800;

str = '                          ********** DESIGN #  53 **********';

%read in the design variables to be checked

d_var{1} = 'DESIGN   VARIABLE   17';
d_var{2} = 'DESIGN   VARIABLE   18';
d_var{3} = 'DESIGN   VARIABLE   19';
d_var{4} = 'DESIGN   VARIABLE   20';
d_var{5} = 'DESIGN   VARIABLE   21';
d_var{6} = 'DESIGN   VARIABLE   22';
d_var{7} = 'DESIGN   VARIABLE   23';
d_var{8} = 'DESIGN   VARIABLE   24';
d_var{9} = 'DESIGN   VARIABLE   25';
d_var{10} = 'DESIGN   VARIABLE   26';
d_var{11} = 'DESIGN   VARIABLE   27';
d_var{12} = 'DESIGN   VARIABLE   28';
d_var{13} = 'DESIGN   VARIABLE   29';
d_var{14} = 'DESIGN   VARIABLE   30';
d_var{15} = 'DESIGN   VARIABLE   31';
d_var{16} = 'DESIGN   VARIABLE   32';

match = 0;

%search for the last run (RUN 53)

while feof(fid) == 0
        tline = fgetl(fid);
        match = strmatch(str, tline, 'exact');
       if match > 0
          break
       end
end

%search for the proper Design Variables
%and reads their values
```

```
for i = 1:1:16

  match = 0;

    while feof(fid) == 0
            tline = fgetl(fid);
            match = findstr(d_var{i}, tline);
        if match > 0
            break
        end
    end

    A(i,5) = textscan(tline, '%*s%*s%*s%*s%f', 1);

%round off design variables and determine actual yield

    if A{i,4} <= 520
       A{i,6} = 520;
       A(i,7) = num2cell(cell2mat(A(i,6)) - 250);
    end

    for j = 1:1:6

        if ((A{i,4} > yield_list(j)) & (A{i,4} <= yield_list(j+1)))
            A{i,6} = yield_list(j+1);
            A(i,7) = num2cell(cell2mat(A(i,6)) - 250);
        else
            j = j+1;
        end

    end

end

fclose(fid);
```

Example of a PSHELL card

```
$$--------------------------------------------------------------------$
$$   Property Definition for Surface and Volume Elements
$$--------------------------------------------------------------------$
$$
$$  PSHELL Data
$
$HMNAME COMP              91"cond_bkt"
$HMCOLOR COMP              91     12
PSHELL      91  109065 0.8         65109.0       65       0.0
$
$HMNAME COMP          84632089"cond_plt"
$HMCOLOR COMP          84632089      1
PSHELL  84632089  109065 0.9         65109.0       65       0.0
```

Example of MSC-Nastran Output File

S T R E S S E S I N Q U A D R I L A T E R A L E L E M E N T S
(Q U A D 4)

ELEMENT FIBER STRESSES IN ELEMENT COORD SYSTEM PRINCIPAL STRESSES
(ZERO SHEAR)

	ID.	DISTANCE	NORMAL-X	NORMAL-Y	SHEAR-XY
0	4994	-6.000000E-01	7.347092E+00	1.671746E+01	-1.770289E+00
		6.000000E-01	-8.033156E+00	1.286837E+01	-1.044494E-01

ANGLE	MAJOR	MINOR	VON MISES
-79.6505	1.704076E+01	7.023796E+00	1.483342E+01
-89.7137	1.286889E+01	-8.033678E+00	1.826288E+01

Example of a HyperStudy Output File

********** DESIGN # 53 **********

OBJECTIVE FUNCTION: 8.964E+00 % change = -0.80
MAXIMUM CONTRAINT STATUS: 0.1% feasible

DESIGN VARIABLE 1 = 8.000E-01

DESIGN VARIABLE 2 = 1.077E+00

DESIGN VARIABLE 3 = 1.002E+00

DESIGN VARIABLE 4 = 8.000E-01

DESIGN VARIABLE 5 = 1.925E+00

DESIGN VARIABLE 6 = 1.071E+00

DESIGN VARIABLE 7 = 8.561E-01

DESIGN VARIABLE 8 = 9.698E-01

DESIGN VARIABLE 9 = 9.771E-01

Matrix A - Subcase 103

Part Name	Part Number	New Gauge Thickness (mm)	Max Stress Element Number	Maximum Stress (MPa)	HyperOpt Yield Strength (MPa)	MATLAB Yield Strength (MPa)	Actual Yield Strength (MPa)
Condenser Bracket	1	0.80	163	47	520	520	270
Condenser Plate	2	1.10	1178	58	520	520	270
Cross Bar	3	1.00	2039	61	520	520	270
Cross Brace	4	0.80	8940	308	520	520	270
End Cap	5	1.90	10045	499	557	520	270
Hood Bracket	6	1.10	12905	516	552	520	270
Hood Support	7	0.90	14525	474	520	520	270
Inner Post	8	1.00	14698	526	574	550	300
Lower Tie Bar 1.0	9	1.00	28956	224	520	520	270
Lower Tie Bar 1.2	10	1.20	32727	270	520	520	270
Lower Tie Bar 1.9	11	1.90	36812	597	520	630	380
Outer Post	12	1.10	39569	584	690	590	340
Reinforcement LTB	13	1.30	46064	395	545	520	270
Reinf. Rad. Support	14	1.10	46658	281	520	520	270
Reinforcement Strap	15	1.90	46802	445	520	520	270
Upper Tie Bar	16	0.90	47427	743	589	750	500

Matrix A - Subcase 106

Part Name	Part Number	New Gauge Thickness (mm)	Max Stress Element Number	Maximum Stress (MPa)	HyperOpt Yield Strength (MPa)	MATLAB Yield Strength (MPa)	Actual Yield Strength (MPa)
Condenser Bracket	1	0.80	509	33	520	520	270
Condenser Plate	2	1.10	1199	41	520	520	270
Cross Bar	3	1.00	1524	49	520	520	270
Cross Brace	4	0.80	8316	238	520	520	270
End Cap	5	1.90	10869	355	520	520	270
Hood Bracket	6	1.10	12905	439	520	520	270
Hood Support	7	0.90	13820	315	520	520	270
Inner Post	8	1.00	21312	565	574	590	340
Lower Tie Bar 1.0	9	1.00	28794	153	520	520	270
Lower Tie Bar 1.2	10	1.20	33503	191	520	520	270
Lower Tie Bar 1.9	11	1.90	36413	468	520	520	270
Outer Post	12	1.10	42349	469	520	520	270
Reinforcement LTB	13	1.30	45096	385	520	520	270
Reinf. Rad. Support	14	1.10	46166	244	520	520	270
Reinforcement Strap	15	1.90	47006	297	520	520	270
Upper Tie Bar	16	0.90	59505	674	709	690	440

Appendix E

MDO of Wheel Chair Ramp Constraints and Results

Wheel Chair Ramp Model Runs

	Wall Speed (mm/s)	Max Von Mises Stress (MPa)
	100.00	83.99
	200.00	102.90
	235.00	123.20
	310.00	139.80
	500.00	153.60
	550.00	209.60
	600.00	303.70
	650.00	400.00
	700.00	506.00
	1000.00	714.50
	1500.00	919.70
	2000.00	1192.00
Run File:	*675.00*	*448.00*

Wheel Chair Ramp Crash Model - Parameter Matrix of Constraints

NVH Constraints

Constraint	Type of Constraint	Value of Constraint
Mode 1	Greater Than	6.67 Hz
Mode 2	Greater Than	9.85 Hz

Stress Constraints (Max Stress for Subcases 103 & 106)

Part #	Component	Type of Constraint	Value of Constraint
1	Side Rails	Less Than	200 MPa
2	Cross Mem 1	Less Than	200 MPa
3	Flanges	Less Than	200 MPa
4	Rear Floor	Less Than	200 MPa
5	Front Floor	Less Than	200 MPa
6	Cross Mem 2	Less Than	200 MPa
7	Cross Mem 3	Less Than	200 MPa
8	Cross Mem 4	Less Than	200 MPa
9	Cross Mem 5	Less Than	200 MPa
10	Cross Mem 6	Less Than	200 MPa
11	Cross Mem 7	Less Than	200 MPa

Weld Constraints (Upper)

Constraint	Type of Constraint	Value of Constraint	Part # of Welded Parts
Weld 1	Less Than	2.0	1 - 2
Weld 2	Less Than	2.0	1 - 3
Weld 3	Less Than	2.0	1 - 6
Weld 4	Less Than	2.0	1 - 7
Weld 5	Less Than	2.0	1 - 8
Weld 6	Less Than	2.0	1 - 9
Weld 7	Less Than	2.0	1 - 10
Weld 8	Less Than	2.0	5 - 4
Weld 9	Less Than	2.0	5 - 2
Weld 10	Less Than	2.0	5 - 6
Weld 11	Less Than	2.0	5 - 7
Weld 12	Less Than	2.0	5 - 8
Weld 13	Less Than	2.0	4 - 9
Weld 14	Less Than	2.0	4 - 10
Weld 15	Less Than	2.0	4 - 11

Weld Constraints (Lower)

Constraint	Type of Constraint	Value of Constraint	Part # of Welded Parts
Weld 1	Less Than	0.5	1 - 2
Weld 2	Less Than	0.5	1 - 3
Weld 3	Less Than	0.5	1 - 6
Weld 4	Less Than	0.5	1 - 7
Weld 5	Less Than	0.5	1 - 8
Weld 6	Less Than	0.5	1 - 9
Weld 7	Less Than	0.5	1 - 10
Weld 8	Less Than	0.5	5 - 4
Weld 9	Less Than	0.5	5 - 2
Weld 10	Less Than	0.5	5 - 6
Weld 11	Less Than	0.5	5 - 7
Weld 12	Less Than	0.5	5 - 8
Weld 13	Less Than	0.5	4 - 9
Weld 14	Less Than	0.5	4 - 10
Weld 15	Less Than	0.5	4 - 11

Wheel Chair Ramp MDO Results - Gauges

Part Name	Part Number	Initial Gauge (mm)	HyperOpt Gauge (mm)	User Gauge (mm)	User Gauge (preferred) (mm)
Side Rails	1	4.7500	4.7458	4.7630	4.7630
Cross Mem 1	2	4.7500	5.2842	5.5560	6.3500
Flanges	3	4.7500	4.9207	5.1590	6.3500
Rear Floor	4	4.7500	3.0780	3.1750	3.1750
Front Floor	5	4.7500	3.2328	3.5720	4.7630
Cross Mem 2	6	4.7500	4.5452	4.7630	4.7630
Cross Mem 3	7	4.7500	4.2157	4.3660	4.7630
Cross Mem 4	8	4.7500	4.1425	4.3660	4.7630
Cross Mem 5	9	4.7500	4.1425	4.3660	4.7630
Cross Mem 6	10	4.7500	4.2064	4.3660	4.7630
Cross Mem 7	11	4.7500	4.4024	4.7630	4.7630

Wheel Chair Ramp MDO Results - Masses

Part Name	Part Number	Initial Mass (kg)	HyperOpt Mass (kg)	User Mass (kg)	User Mass (preferred) (kg)
Side Rails	1	28.5000	28.4800	28.5800	28.5800
Cross Mem 1	2	2.1540	2.3970	2.5200	2.8800
Flanges	3	1.3110	1.3580	1.4240	1.7520
Rear Floor	4	45.1200	29.2400	30.1060	30.1060
Front Floor	5	69.9680	46.4380	52.6159	70.1428
Cross Mem 2	6	6.1890	5.9220	6.2060	6.2060
Cross Mem 3	7	5.7630	5.1150	5.2970	5.7790
Cross Mem 4	8	6.1890	5.3980	5.6890	6.2060
Cross Mem 5	9	6.1890	5.3980	5.6890	6.2060
Cross Mem 6	10	5.7630	5.1040	5.2970	5.7790
Cross Mem 7	11	4.4440	4.1900	4.4560	4.4560

	Initial	HyperOpt	User	User Preferred
Mass (kg)	181.59	139.04	147.88	168.09
% Change	0	0.23	0.19	0.07
Max Stress (MPa)	394.00	384.00	398.00	399.00
Mode 1 (Hz)	7.16	7.17	7.17	7.17
Mode 2 (Hz)	10.53	10.56	10.56	10.55

Sheet Metal Gauges

No:	Size (inches)	Decimal (inches)	Metric (mm)
0	5/16	0.3125	7.938
1	9/32	0.28125	7.144
2	17/64	0.265625	6.747
3	1/4	0.25	6.350
4	15/64	0.234375	5.953
5	7/32	0.21875	5.556
6	13/64	0.203125	5.159
7	3/16	0.1875	4.763
8	11/64	0.171875	4.366
9	5/32	0.15625	3.969
10	9/64	0.140625	3.572
11	1/8	0.125	3.175
12	7/64	0.109375	2.778
13	3/32	0.09375	2.381
14	5/64	0.078125	1.984
15	5/71	0.0703125	1.786
16	1/16	0.0625	1.588